7-054
HTSA-86-2

Vehicle Component Characterization
Vol. I: Project Results

David J. Segal
Leonard R. Kamholz
Davis G. Griffith

MGA Research Corporation
12790 Main Road
P.O. Box 71
Akron, NY 14001-0071

January 1987
Final Report

U.S. Department of Transportation
National Highway Traffic Safety Administration

Office of Research and Development
Office of Crashworthiness Research
Washington DC 20590

Technical Report Documentation Page

1. Report No.	2. Government Accession No.	3. Recipient's Catalog No.
DOT-HS-807-054		

4. Title and Subtitle	5. Report Date
VEHICLE COMPONENT CHARACTERIZATION, VOL. I: PROJECT RESULTS	January 1987
	6. Performing Organization Code: DTS-44
	8. Performing Organization Report No.: DOT-TSC-NHTSA-86-2

7. Author(s)	
David J. Segal, Leonard R. Kamholz, and Davis G. Griffith	

9. Performing Organization Name and Address	10. Work Unit No. (TRAIS)
MGA Research Corporation* 12790 Main Road P.O. Box 71 Akron, N.Y. 14001-0071	HS676/S6511
	11. Contract or Grant No.: DTRS-57-84-C-00003
	13. Type of Report and Period Covered: Final Report July 1984 - January 1986
12. Sponsoring Agency Name and Address U.S. Department of Transportation National Highway Traffic Safety Administration Office of Research and Development Washington, DC 20590	14. Sponsoring Agency Code: NRD-11

15. Supplementary Notes

U.S. Department of Transportation
Research and Special Programs Administration
*Under contract to: Transportation Systems Center
Cambridge, MA 02142

16. Abstract

MGA Research Corporation has undertaken a project sponsored by the Transportation Systems Center of the U.S. Department of Transportation which involved the quasi-static and dynamic testing of automobile instrument panels and windshields. During the instrument panel testing phase of this project, the instrument panels of 19 vehicles were tested for their stiffness characteristics using procedures developed under a previous study. (This testing attempted to simulate loadings which occur during frontal collisions and includes contacts of knees to lower instrument panel sections, torso to mid-section and head to upper section.) Also included in the instrument panel testing were parametric tests investigating the effects of different loading geometry. The windshield testing portion of this project included developing a procedure for the testing of windshields as they would be loaded under frontal collision conditions (head/windshield contact) through static and dynamic testing of the windshields of the 19 vehicles used in the instrument panel testing. During the procedural study, it was determined that only dynamic impacts properly duplicate the loading conditions found during an accident. Also carried out during the windshield testing was a parametric study into the effects of different loading and physical conditions.

The purpose of this testing was to develop a set of data which could be used in computer crash occupant simulation models in order to study automobile crashworthiness. The data generated by this testing has been used to develop a data base on the National Highway Traffic Safety Administration's VAX 11/780 computer. The data presented in this report are directly available to anyone having access to the NHTSA computer.

This report is presented in two volumes: Volume I Project Results
Volume II Data Appendices

17. Key Words	18. Distribution Statement
Instrument Panel Stiffness Characteristics Windshield Stiffness Characteristics Computer Simulation Computer Database Crashworthiness	DOCUMENT IS AVAILABLE TO THE PUBLIC THROUGH THE NATIONAL TECHNICAL INFORMATION SERVICE, SPRINGFIELD, VIRGINIA 22161

19. Security Classif. (of this report)	20. Security Classif. (of this page)	21. No. of Pages	22. Price
Unclassified	Unclassified	120	

Form DOT F 1700.7 (8-72) Reproduction of completed page authorized

METRIC CONVERSION FACTORS

Approximate Conversions to Metric Measures

Symbol	When You Know	Multiply by	To Find	Symbol
		LENGTH		
in	inches	*2.5	centimeters	cm
ft	feet	30	centimeters	cm
yd	yards	0.9	meters	m
mi	miles	1.6	kilometers	km
		AREA		
in^2	square inches	6.5	square centimeters	cm^2
ft^2	square feet	0.09	square meters	m^2
yd^2	square yards	0.8	square meters	m^2
mi^2	square miles	2.6	square kilometers	km^2
	acres	0.4	hectares	he
		MASS (weight)		
oz	ounces	28	grams	g
lb	pounds	0.45	kilograms	kg
	short tons (2000 lb)	0.9	tonnes	t
		VOLUME		
tsp	teaspoons	5	milliliters	ml
Tbsp	tablespoons	15	milliliters	ml
fl oz	fluid ounces	30	milliliters	ml
c	cups	0.24	liters	l
pt	pints	0.47	liters	l
qt	quarts	0.95	liters	l
gal	gallons	3.8	liters	l
ft^3	cubic feet	0.03	cubic meters	m^3
yd^3	cubic yards	0.76	cubic meters	m^3
		TEMPERATURE (exact)		
°F	Fahrenheit temperature	5/9 (after subtracting 32)	Celsius temperature	°C

*1 in. = 2.54 cm (exactly). For other exact conversions and more detail tables see NBS Misc. Publ. 286, Units of Weight and Measures. Price $2.25 SD Catalog No. C13 10 286.

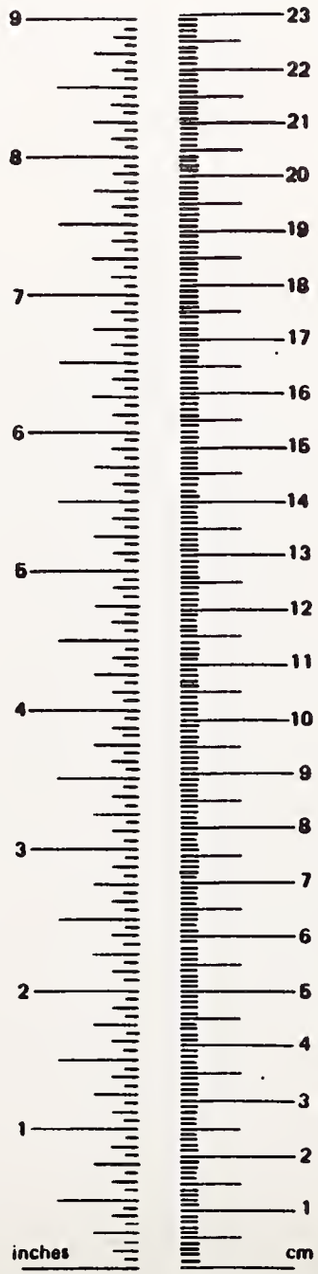

Approximate Conversions from Metric Measures

Symbol	When You Know	Multiply by	To Find	Symbol
		LENGTH		
mm	millimeters	0.04	inches	in
cm	centimeters	0.4	inches	in
m	meters	3.3	feet	ft
m	meters	1.1	yards	yd
km	kilometers	0.6	miles	mi
		AREA		
cm^2	square centimeters	0.16	square inches	in^2
m^2	square meters	1.2	square yards	yd^2
km^2	square kilometers	0.4	square miles	mi^2
he	hectares (10,000 m^2)	2.5	acres	
		MASS (weight)		
g	grams	0.035	ounces	oz
kg	kilograms	2.2	pounds	lb
t	tonnes (1000 kg)	1.1	short tons	
		VOLUME		
ml	milliliters	0.03	fluid ounces	fl oz
l	liters	2.1	pints	pt
l	liters	1.06	quarts	qt
l	liters	0.26	gallons	gal
m^3	cubic meters	36	cubic feet	ft^3
m^3	cubic meters	1.3	cubic yards	yd^3
		TEMPERATURE (exact)		
°C	Celsius temperature	9/5 (then add 32)	Fahrenheit temperature	°F

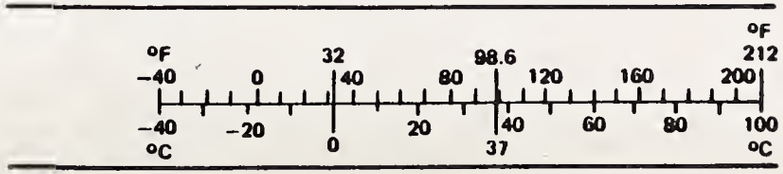

CONTENTS

LIST OF ILLUSTRATIONS

LIST OF ILLUSTRATIONS (CONT.)

LIST OF ILLUSTRATIONS (CONT.)

LIST OF ILLUSTRATIONS (CONT.)

LIST OF TABLES

1. INTRODUCTION

In support of the National Highway Traffic Safety Administration's study of frontal crashworthiness protection, the Transportation Systems Center has been charged with the responsibility of providing input data for computer simulations for the study of occupant crash protection. In support of that activity, MGA Research Corporation has undertaken testing activities to determine physical characteristics of a number of automobiles under Contract No. DTRS-57-84-C-00003.

Testing activities under two Technical Task Directives (TTD's) are covered in this report. The first Technical Task Directive, No. 6, involved determining force-deflection characteristics of various areas of the interior surfaces of some nineteen different automobiles. This task included both static and dynamic testing of instrument panels as well as investigation of the consequences of changes in test conditions. Static and dynamic tests on windshields were also conducted. The second Technical Task Directive, No. 7, covered a parametric study of windshield test conditions and an evaluation of instrument panel friction characteristics.

The test procedures employed in the project were developed on a pilot testing effort in which static and dynamic test procedures were developed and a series of tests were conducted on a Cheverolet Citation. The basic testing effort included static tests on the following areas of instrument panels of the nineteen vehicles covered in this effort:

- Passenger side femur-to-lower panel
- Passenger side torso-to-center panel
- Passenger side head-to-upper panel
- Driver side femur-to-lower panel

Dynamic tests were conducted on the passenger side on the lower and center panel areas, and in a limited number of cases, on the driver side lower panel. Tests were conducted utilizing appropriate body parts from a Part 572 anthropomorphic dummy with the exception of the dynamic torso test which utilized a rigid body form in the shape of the dummy torso.

In all cases, data were processed to obtain force-deflection information. In the static tests, force and deflection were measured and recorded directly on an analog X-Y plotter. For the dynamic tests, axial deceleration of the body part, impact velocity and maximum penetration were measured. The acceleration signal was then filtered and integrated to obtain a deflection time history. The acceleration was also multiplied by the mass of the impactor to obtain a force time history. Cross plotting then provided force-displacement data. Subsequent processing included development of G, R, and K values - the ratio of permanent to maximum deflection, the ratio of conserved energy to maximum absorbed energy and the unloading slope, respectively. In addition, the geometry of the vehicle interior surfaces was measured. An effective average damping factor was also computed based on difference in absorbed energy between static and dynamic tests.

All data were reported on a special data summary form developed specifically for that purpose. Data was also installed on a data base created on the NHTSA VAX computer system for direct access by interested parties.

Although this testing project has developed the first comprehensive set of vehicle interior force-deflection characteristics on a substantial number of automobiles, it was not a research effort per se. Rather, it was structured as a routine data gathering effort. As test results became available, however, it became apparent that much more extensive analysis of the data would be necessary to understand and properly interpret some of the results. This detailed analysis was not a part of the original scope of the effort and therefore was not undertaken. However, conclusions resulting from a brief review of the data collected and experience with the testing approaches, and recommendations for subsequent activities are provided in the next section.

This is followed by a detailed description of the test procedures used during the study. The last section of this volume presents discussions of the various test results obtained in the effort. Six appendices are provided in a separate volume containing results from static instrument panel tests, dynamic instrument panel tests, static windshield tests, dynamic windshield tests, instrument panel parametric tests and windshield parametric tests.

2. CONCLUSIONS AND RECOMMENDATIONS

This section summarizes conclusions and recommendations resulting from the reported testing project. It should be emphasized that the project undertaken was not a research project and a detailed analysis of the data was therefore not considered within the project scope. Nevertheless, significant findings resulting from a brief review of the test data are noted below.

2.1 CONCLUSIONS

Static Instrument Panel Tests - The static instrument panel tests undertaken on some nineteen cars exhibited a wide range of stiffness. By characterizing the overall envelope of crush data by a minimum stiffness and a maximum stiffness, ratios of maximum to minimum stiffness of between 5 to 1 and 12 to 1, depending on the type of test conducted and the point of load application, were observed. The driver femur area stiffness was typically significantly higher than the passenger femur data due to the influence of steering column brackets.

Dynamic Instrument Panel Tests - The dynamic instrument panel test results also exhibited a broad range of characteristics. Comparisons of dynamic to corresponding static test results indicated an inconsistent pattern. That is, in most cases, dynamic forces were higher than corresponding static forces. However, in other cases, the levels were about the same or static force levels were higher than dynamic. The reasons for this behavior is uncertain but differences in failure modes of the instrument panel materials have been suggested as a possible explanation of lower dynamic force levels. Additional testing is needed in this area to gain a better understanding of these observed results.

Instrument Panel Parametric Tests - The results of the instrument panel parametric test effort, in which loading directions and locations were changed from the baseline condition, indicate that both of these variations can have a significant effect on the measured force-deflection properties. As the location changed laterally towards the center of the car, different component or construction on or behind the panel resulted in different force levels. As loading direction changes, particularly for the torso, a different deformation pattern resulted in different force levels.

Windshield Tests - The repeatability of the windshield impact tests conducted on the Chevrolet Citation was as indicated in Section 4.7. A distinct inertia spike was evident on initial contact. By varying the location of the impact relative to the windshield edge, some variation in the apparent stiffness of the windshield was observed; but this was not felt to be a strong effect. Pre-stressing the windshield by bending the mounting frame produced a more noticeable increase in stiffness than did the variation in impact location. Securiflex windshields produce a noticeably different inertia spike (i.e., it is longer) and higher force levels on penetration than do standard windshields. These also appear to produce higher plowing forces at high penetration levels than standard windshields.

Instrument Panel Friction - Tests on one instrument panel indicated a relatively constant friction coefficient (about 0.9) that was largely independent of normal force. However, extreme deflections (where pocketing or plowing may occur) were not tested.

2.2 RECOMMENDATIONS

Additional dynamic instrument panel tests should be undertaken in an effort to better understand the relationship between static and dynamic characteristics. Such an effort should include repeat tests for evaluation of force-deflection repeatability over a number of different vehicles and should include high-speed film coverage for evaluation of failure modes.

Additional windshield impacts should also be undertaken to evaluate dynamic rate effects. Malfunctions in the impactor system used for this project precluded the collection of data from different velocity tests at similar test conditions. Consequently, adequate evaluation of rate sensitivity could not be undertaken.

An improved impactor system should be used on subsequent efforts that would allow collection of dynamic displacement as a means of confirming acceleration measurements.

3. TEST PROCEDURES

This section describes the test procedures and data processing procedures that were employed in the instrument panel and windshield testing undertaken on the project. Both static and dynamic testing was undertaken; hence the following material includes brief discussions of both general types of tests. Before proceeding to those descriptions, an overview of all tests conducted is helpful.

Tests were generally categorized as production (or standard) tests and parameter study tests. This standard test matrix is presented in Table 3-1 indicating those tests that were conducted on each vehicle. Note that in all cases, static instrument panel tests were conducted. Dynamic tests on the passenger side instrument panel were conducted on eleven vehicles. Dynamic windshield tests were conducted on all vehicles with a limited number of static windshield tests also being conducted.

The parameter test matrix is shown in Table 3-2. Note that parametric instrument panel tests were conducted on four vehicles while parametric windshield tests were conducted only on the Citation.

Discussions of procedures used in conducting these tests follow.

3.1 INSTRUMENT PANEL TEST PROCEDURES

This section describes test procedures utilized for both static and dynamic instrument panel tests and procedures for documenting certain dimensional information on instrument panels necessary for computer simulation purposes.

3.1.1 Static Instrument Panel Test Procedures

The test procedures for the static instrument panel testing are described in this section. First the general procedures for performing a static test are discussed, then the difference between the four different static tests are presented.

The static testing was performed in a load frame that acted as a support for both the vehicle cowl section (or clip) being tested and also supported the equipment used to test the instrument panel (see Figure 3-1). The clip was welded and bolted to the load frame. The static crush equipment was bolted to an adjustable frame which allowed positioning of the body form to the angle and target for the specific test undertaken.

TABLE 3-1. STANDARD TEST MATRIX FOR INSTRUMENT PANELS AND WINDSHIELDS

No.	Vehicle	Model Year	Instrument Panels							Windshields		
			Static				Dynamic				Dynamic	
			Passenger Femur	Passenger Torso	Passenger Head	Driver Femur	Passenger Femur	Passenger Torso	Driver Femur	Static	Normal	Horizontal*
1	Volare	1977	x	x	x	x	x	x		x		x
2	Honda	1975	x	x	x	x	x	x		x		x
3	Chevette	1979	x	x	x	x	x	x		x		x
4	LTD	1979	x	x	x	x	x	x		x		x
5	Monza	1976	x	x	x	x	x	x		x		x
6	Mustang	1979	x	x	x	x	x	x		x		x
7	Pinto	1977	x	x	x	x	x	x		x		x
8	Omni	1980	x	x	x	x	x	x				x
9	Fairmont	1978	x	x	x	x						
10	Firebird	1975	x	x	x	x					x	
11	Celebrity	1983	x	x	x	x	x	x	x		x	
12	Datsun 210	1980	x	x	x	x					x	
13	Lemans	1978	x	x	x	x					x	
14	Nova	1979	x	x	x	x					x	
15	Granda	1979	x	x	x	x					x	
16	Cordoba	1978	x	x	x	x					x	
17	LeSabre	1978	x	x	x	x	x	x	x		x	
18	Rabbit	1980	x	x	x	x					x	
19	Citation	1980	x	x	x	x	x	x		x	x**	x**

*See Section 4.4 for comments
**See Table 3-2

TABLE 3-2. PARAMETERIC TEST MATRIX FOR INSTRUMENT PANELS AND WINDSHIELD

INSTRUMENT PANEL TESTS								WINDSHIELD TESTS									
								SECURIFLEX		CITATION							
STATIC								20 MPH		Static		20 MPH				25 MPH	
No.	Vehicle	POSITION/ANGLE*						Normal	Horizontal	Normal	Horizontal	Normal	Horizontal	Edge Effects	Pre-Stress	Normal	
		1	2	3	4	5	6										
1	Volare	x	x	x	x	x	x										
2	Honda	x	x	x	x	x	x										
3	LTD	x	x	x	x	x	x										
4	Monza	x	x	x	x	x	x										
5	Citation							x	x	x	x	x	x	x	x	x	

*1. Passenger Femur 3-inches to left of standard loading point. Angle between 20 and 30 degrees up from the horizontal.

2. Passenger Femur, standard loading point. Angle at zero degrees (horizontal).

3. Passenger Torso 3-inches to left of standard loading point. Angle at zero degrees (horizontal).

4. Passenger Torso at standard loading point. Angle 30 degrees down from the horizontal.

5. Passenger Head 3-inches to left of standard loading point. Angle 30 degrees down from horizontal.

6. Passenger Head at standard loading point. Angle at zero degrees (horizontal).

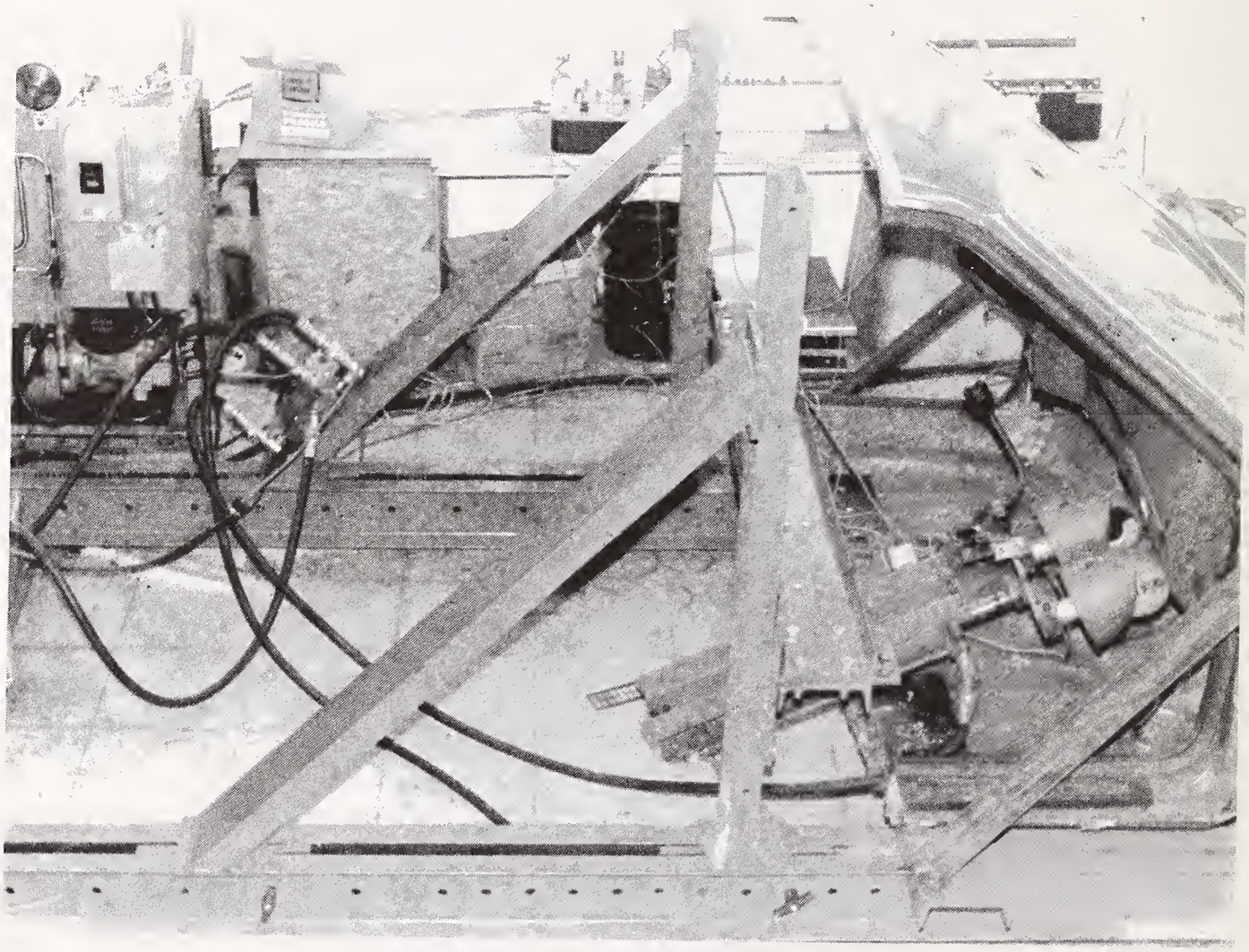

FIGURE 3-1. STATIC INSTRUMENT PANEL TESTING LOAD FRAME

The static crush equipment consisted of a hydraulic cylinder, three different body forms, one hydraulic pump, a servovalve and a servocontroller to control motion of the hydraulic cylinder (see Figure 3-2). The body forms were attached to the end of the hydraulic cylinder shaft. This allowed the body forms to be forced into the instrument panel. Before the static crush equipment was positioned, the profile of the instrument panel was taken using a piece of lead wire. This profile was then transferred to a piece of paper by tracing. The mechanical setup was completed with the positioning of the static crush equipment to the desired target and angle.

The instrumentation for the static crush testing consisted of load sensors, displacement sensor, signal conditioning, a servocontroller, and X-Y plotters. The displacement sensor and load cell positions are shown in Figures 3-2 and 3-3. The servocontroller used displacement feedback for control. The sensor signals went to a signal conditioner which amplified the signal levels to be acceptable for use on the X-Y plotter. The plotter was configured to produce a force vs. deflection plot. Once the instrumentation was setup the dummy body form was positioned against the panel to give the starting position for the test. After positioning of the body form, photos and measurements were taken to fully document the positions of all major components in the static crush system. The test was then performed by displacing the body form into the instrument panel at a rate of about 2 inches per minute. The load was applied until the body form bottomed out (as indicated by a sudden force increase) or until the hydraulic cylinder was fully extended to its 16 inch maximum stroke. At this point, photos and measurements were taken just as they were prior to the test. The instrument panel was now unloaded and post-load photos and measurements were taken. Finally the crushed instrument panel profile was recorded. The output of these tests was force vs. deflection plots that were transferred to a computer for data processing.

There were four different static crush tests performed. They were: passenger femur, passenger torso, passenger head, and driver femur tests. Tests were performed in that order for each vehicle tested. The test procedures were designed to approximate loading that would occur during a frontal collision with an unrestrained occupant. The difference between the tests included body part, panel location, and load angle for initial penetration.

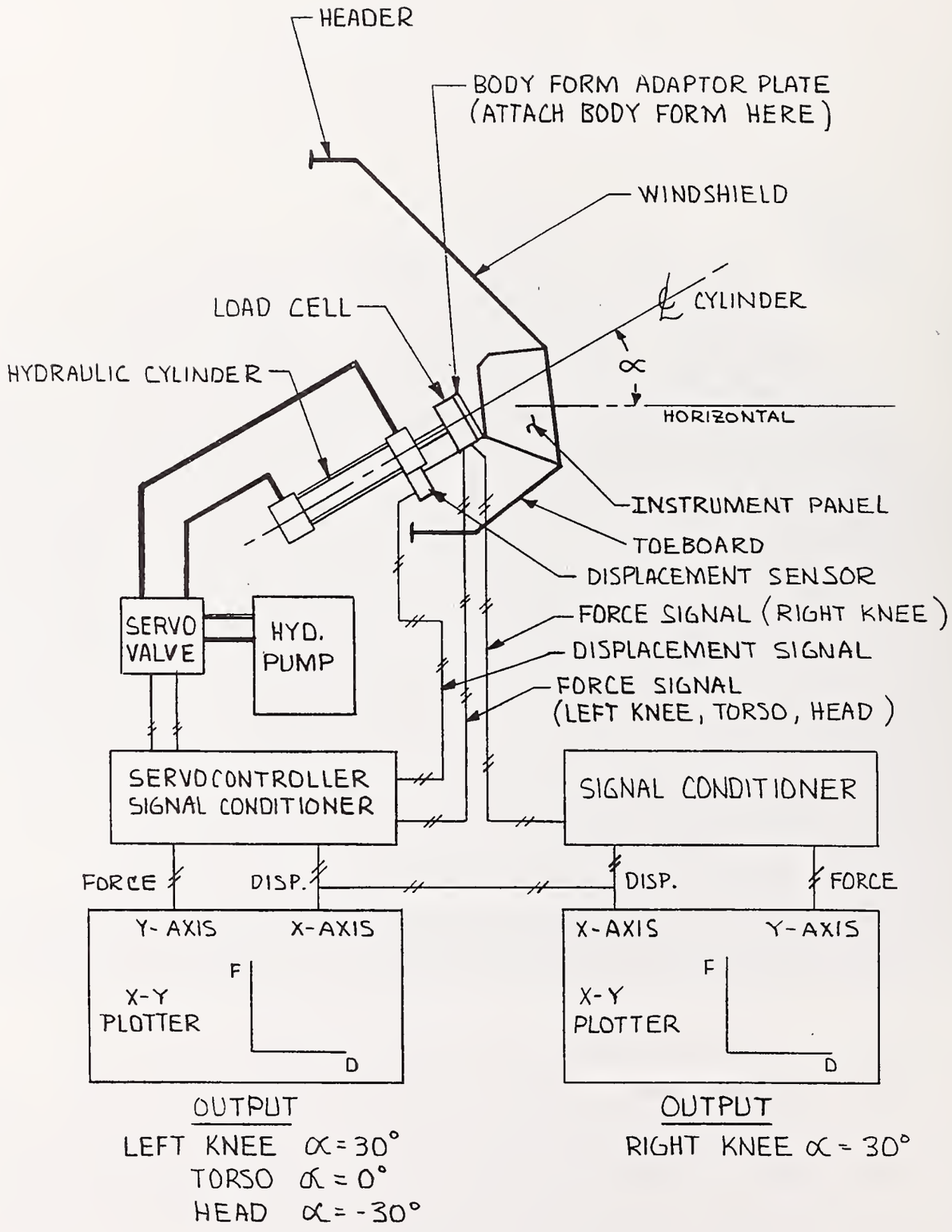

FIGURE 3-2. STATIC INSTRUMENT PANEL TEST SYSTEM

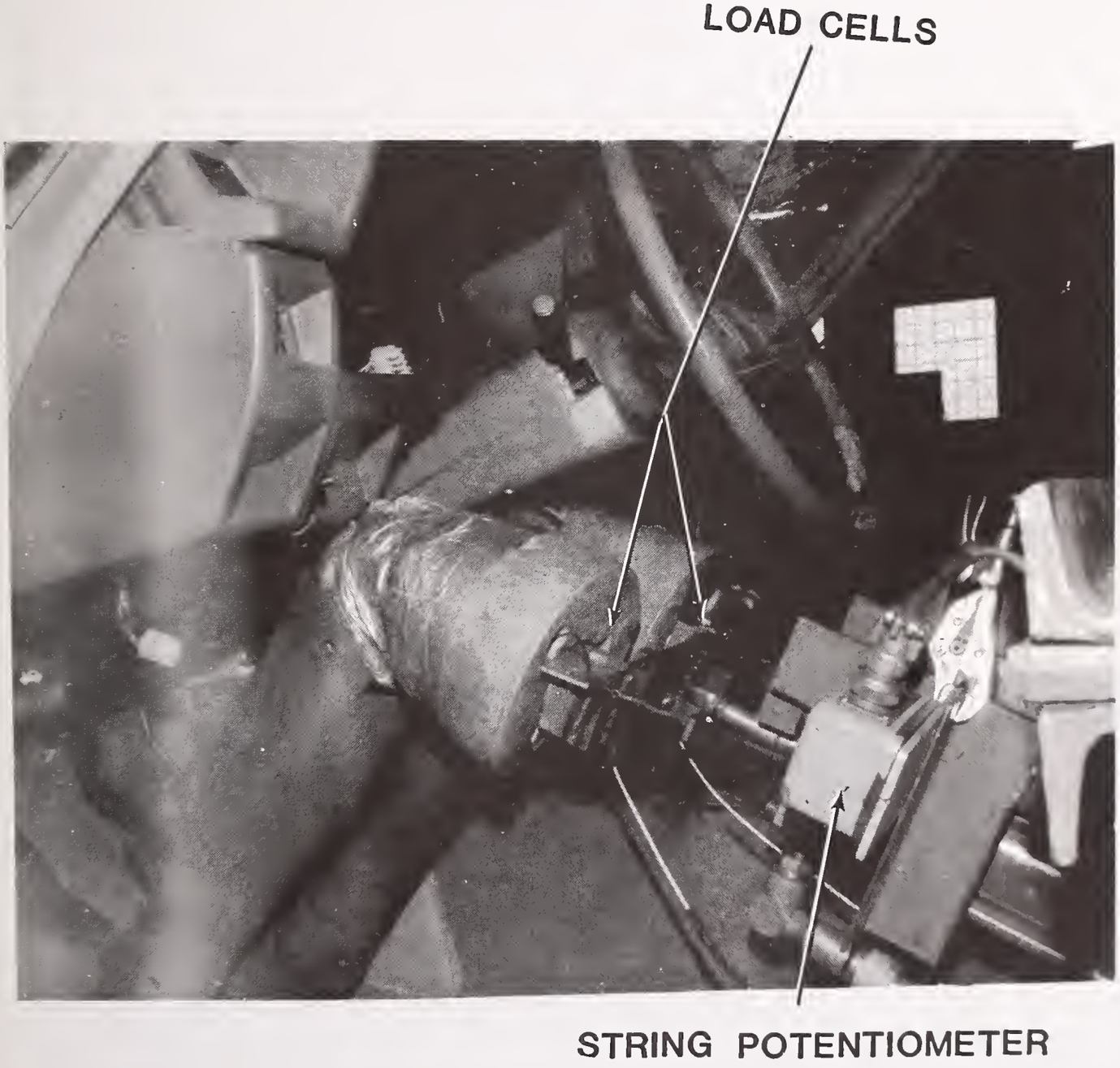

FIGURE 3-3. FORCE AND DISPLACEMENT SENSORS

The hydraulic cylinder mount was allowed to pivot for the femur tests to allow for proper kinematics whereas the cylinder was rigidly mounted for the torso and head tests. The knees were placed in the center of the passenger position and usually penetrated into the glove box (see Figure 3-4). The orientation and initial contact position was determined by placing the dummy heels at the floorboard-toeboard intersection with the passenger femurs at an angle of about 20 degrees (Figure 3-1). The same positioning was used on the driver's side with the femurs centered around the steering column (see Figure 3-5). The passenger torso was constrained to horizontal travel during penetration. The torso was in the center of the passenger position vertically located to minimize neck or shoulder area contact with the windshield (see Figure 3-6). During torso tests, the knees were put back to a position simulating maximum load. Care was taken to prevent the torso from striking the knees. The orientation of the head was about 30° downward (see Figure 3-7) and was such that the head would not contact the windshield at maximum load. Travel was approximately parallel to the windshield of the vehicle (see Figure 3-7). The head was also in the center of the passenger position and normally struck the top of the instrument panel. It should be noted that all static tests in this sequence were performed on the same instrument panel, thus torso and head tests involved testing in a previously damaged area.

3.1.2 Dynamic Instrument Panel Test Procedure

The test procedures for the dynamic instrument panel testing are described in this section. First the general procedure for performing a dynamic test is discussed, then the difference between each of the three dynamic instrument panel tests are presented.

The dynamic testing was performed in the same load frame as the static testing. The mounting of the vehicle clip was identical to the static testing clip mounting (see Figure 3-8). The difference was the dynamic test equipment used during dynamic testing. A pneumatically actuated impactor was used to dynamically penetrate instrument panels with body forms. The dynamic test equipment was bolted to an adjustable frame that was positioned to the angle and impact location on the panel desired.

The dynamic crush equipment consisted of a 3 inch diameter piston cylinder arrangement, three different forms, a pneumatic fire valve, and a high pressure nitrogen source (see Figure 3-9). The body forms were attached to the end of the

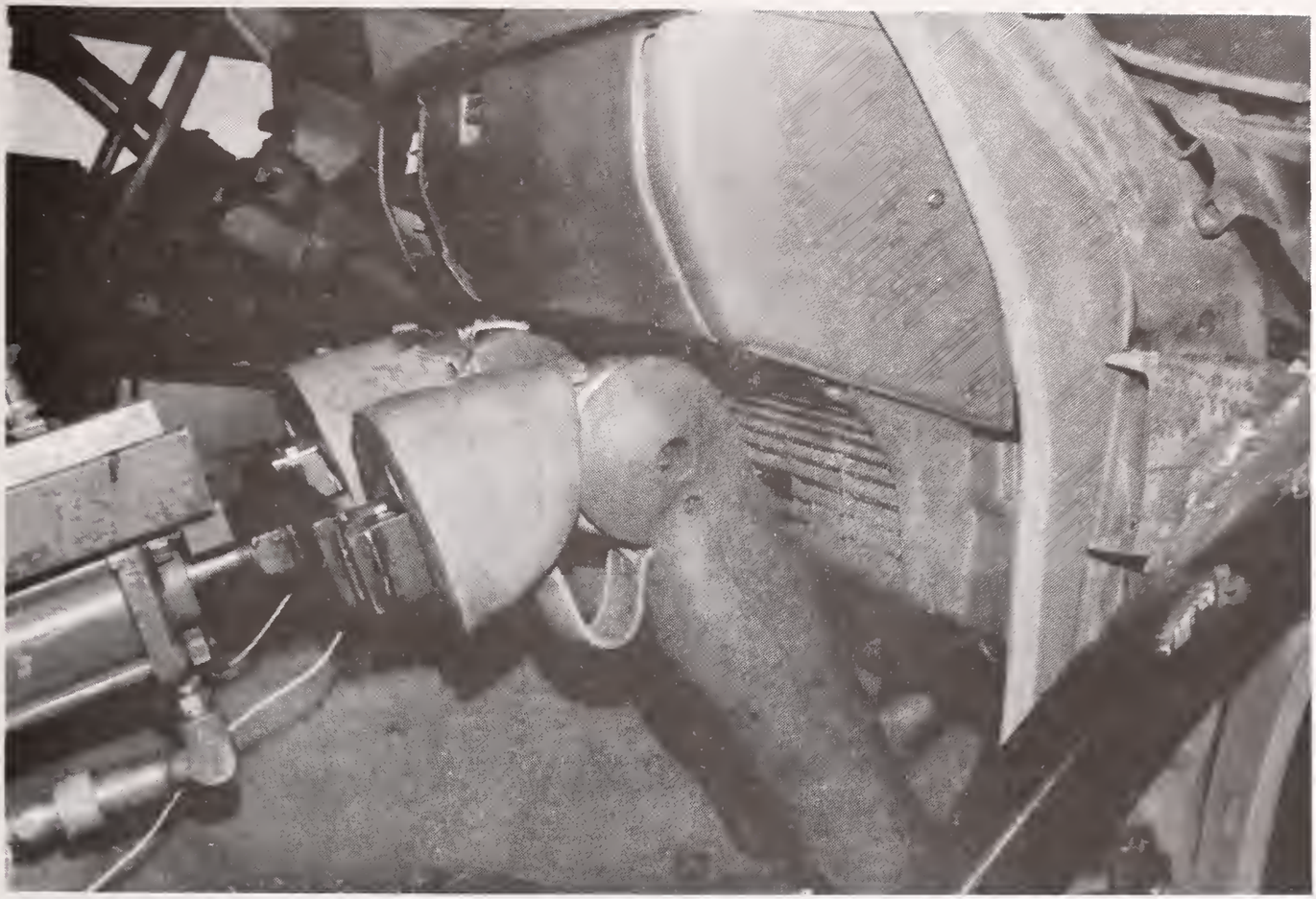

FIGURE 3-4. PASSENGER FEMUR SET-UP

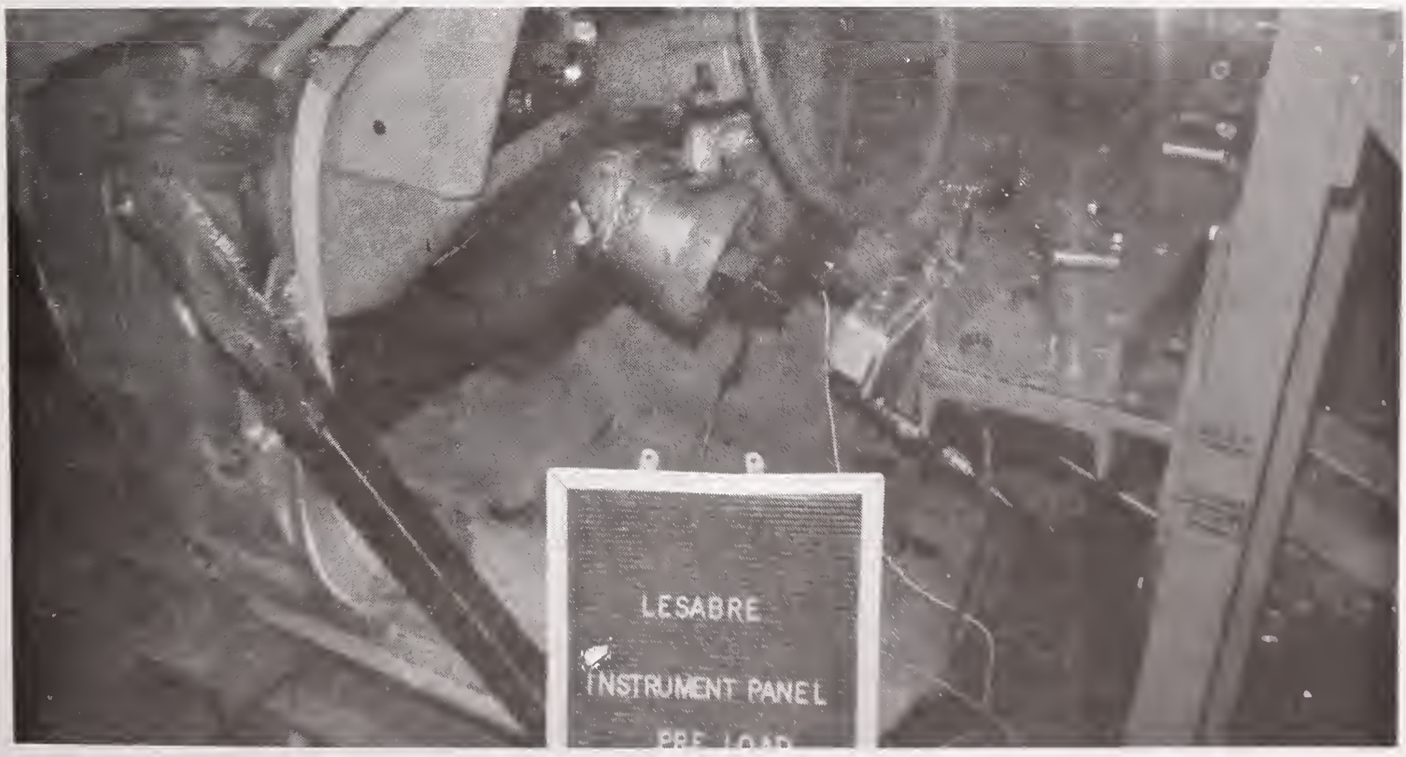

FIGURE 3-5. DRIVER FEMUR SET-UP

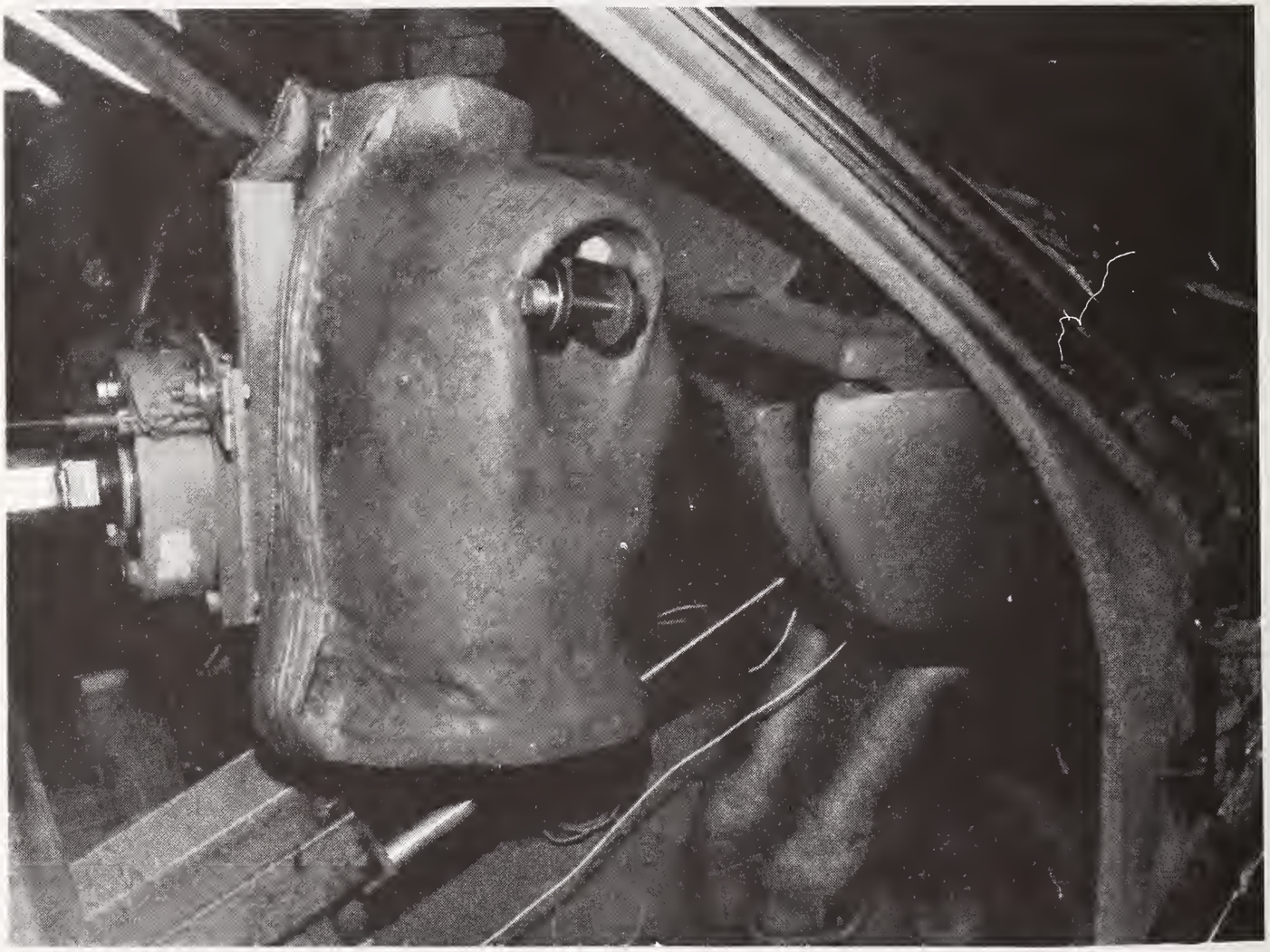

FIGURE 3-6. PASSENGER TORSO SET-UP

FIGURE 3-7. PASSENGER HEAD SET-UP

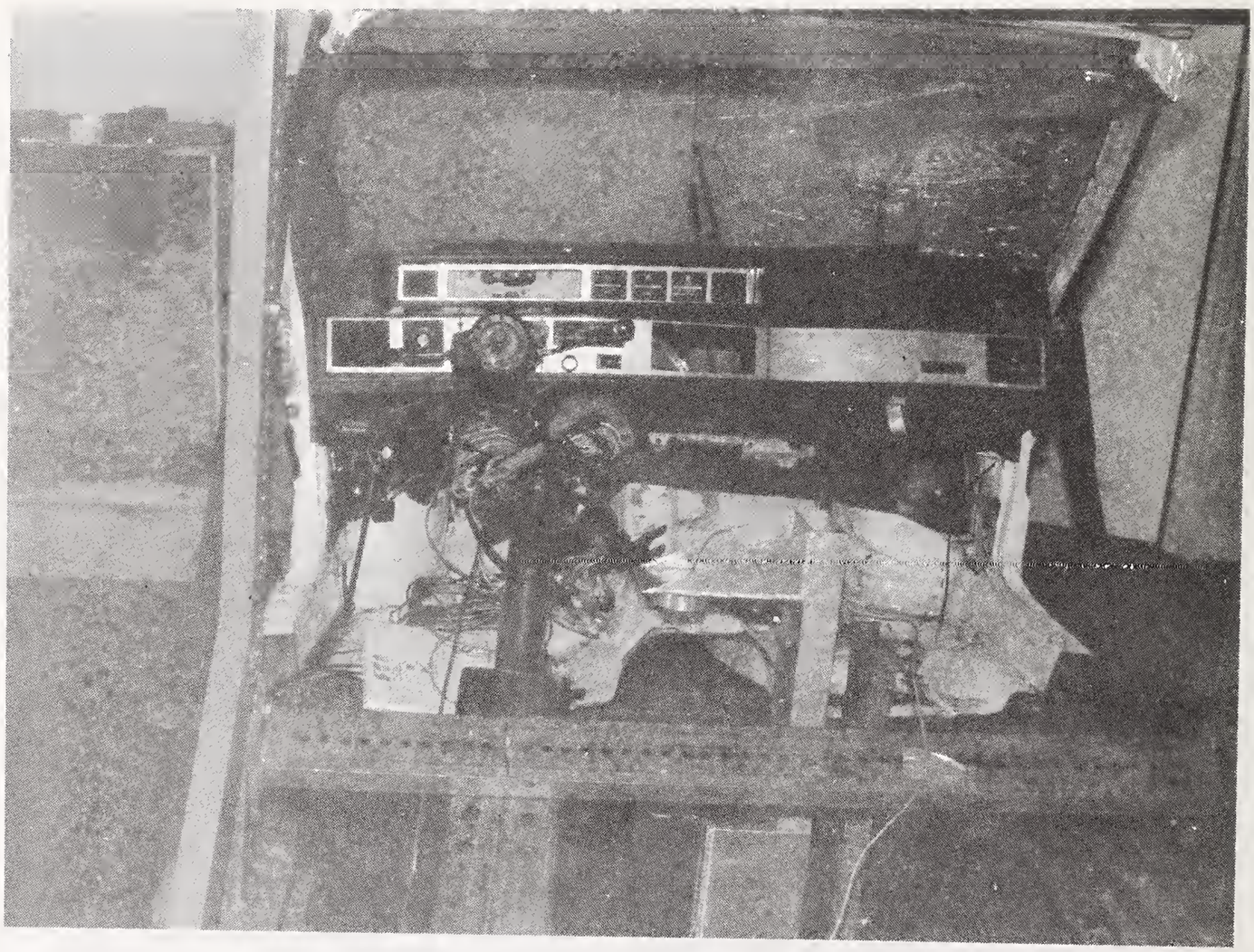

FIGURE 3-8. DYNAMIC TESTING LOAD FRAME

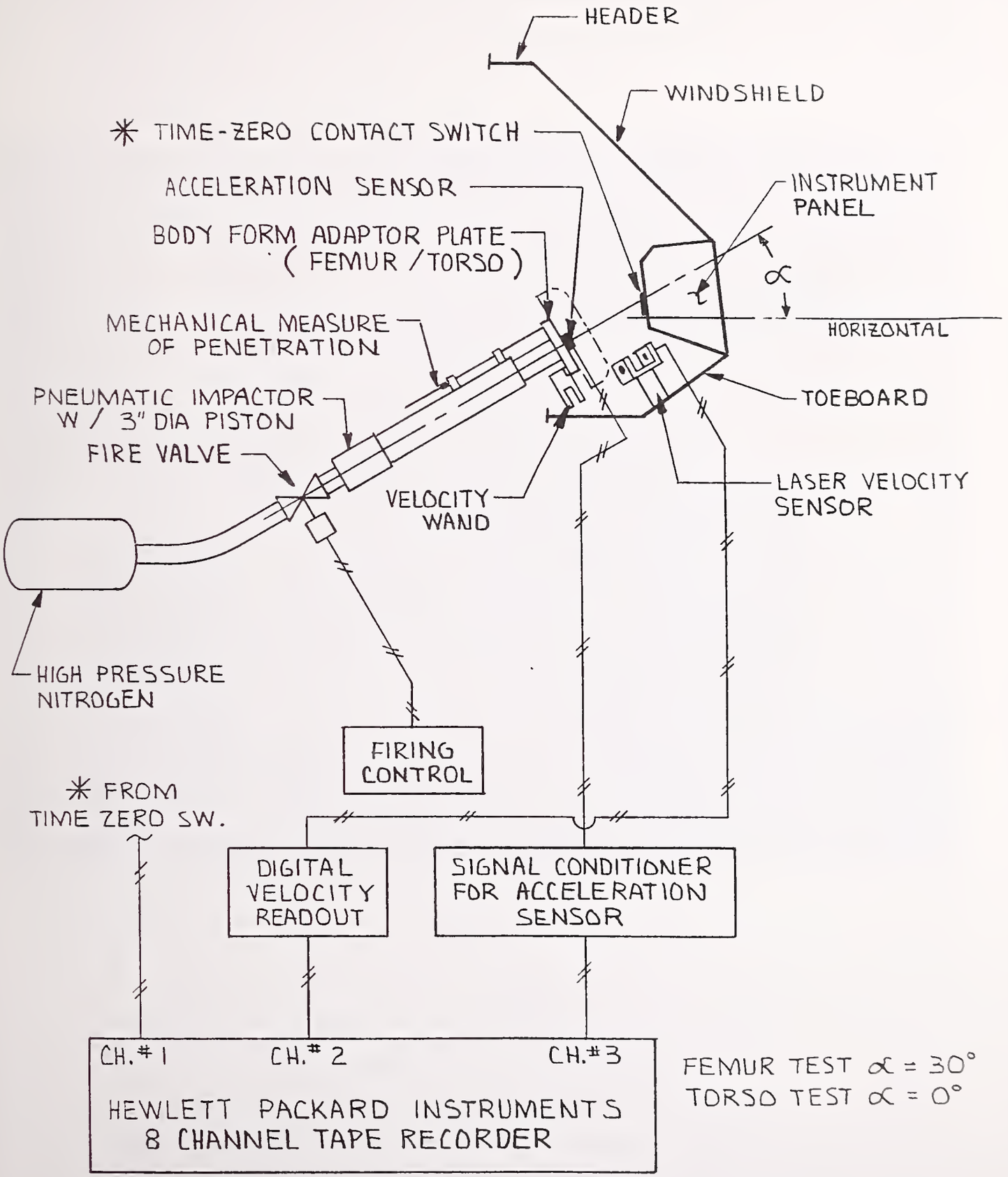

FIGURE 3-9 DYNAMIC INSTRUMENT PANEL TEST SYSTEM

impactor shaft. Before the impactor was placed in the final position, the profile of the instrument panel was recorded in the same manner as was done in the static testing. Next the impactor was positioned to its correct angle and target. The body form was allowed 12" of travel before contact with the instrument panel to insure a constant speed was achieved. Maximum penetration was measured using mechanical rod and tube assembly (see Figure 3-10).

The instrumentation used during dynamic instrument panel testing consisted of acceleration sensors, a time-of-contact switch (time zero), a velocity sensor, an electrical firing system, and signal conditioning. All signals were recorded on a Hewlett Packard Instrumentation Tape Recorder. The tape recorder was set up to record time traces of acceleration, contact time, and velocity before impact. The accelerometers were mounted on the impactor shaft as close to its centerline as possible. Impact velocity was measured using a laser-wand which produced digital readout of elapsed time for the wand to pass through the beam and a signal to be recorded on the tape recorder. The time zero switch was placed on the instrument panel so that the body form would contact it first. Once the instrumentation was setup, photos and measurements were taken to document the position of the major components prior to impact. The setup distance was verified, maximum penetration assembly was measured and the target location verified. The targets for all dynamic testing were identical to the static instrument panel testing for each respective body form (see Figures 3-11, 3-12, and 3-13).

After pre-test photos and measurements were taken, the tape recorder was setup to receive the sensor signals. Zero levels and calibration levels were recorded first. At this point the system was ready for a test. The impactor was then pressurized to the desired pressure to produce the speed that was required. The safety pin in the impactor was then removed and then the tape recorder was started. Once recording began, the fire button was pressed and the body form penetrated the instrument panel. The tape recorder was then turned off and post test photos and measurements were taken. The recorded data - acceleration, time of contact, and velocity at contact was then ready to be digitized and processed.

The differences between the dynamic tests were the position of impact, body form used and the impact velocity. The three tests were passenger femur, passenger torso, and driver's femur. These tests were performed in that order in each vehicle clip. The impact velocity for the femur tests was 15 mph and 20 mph

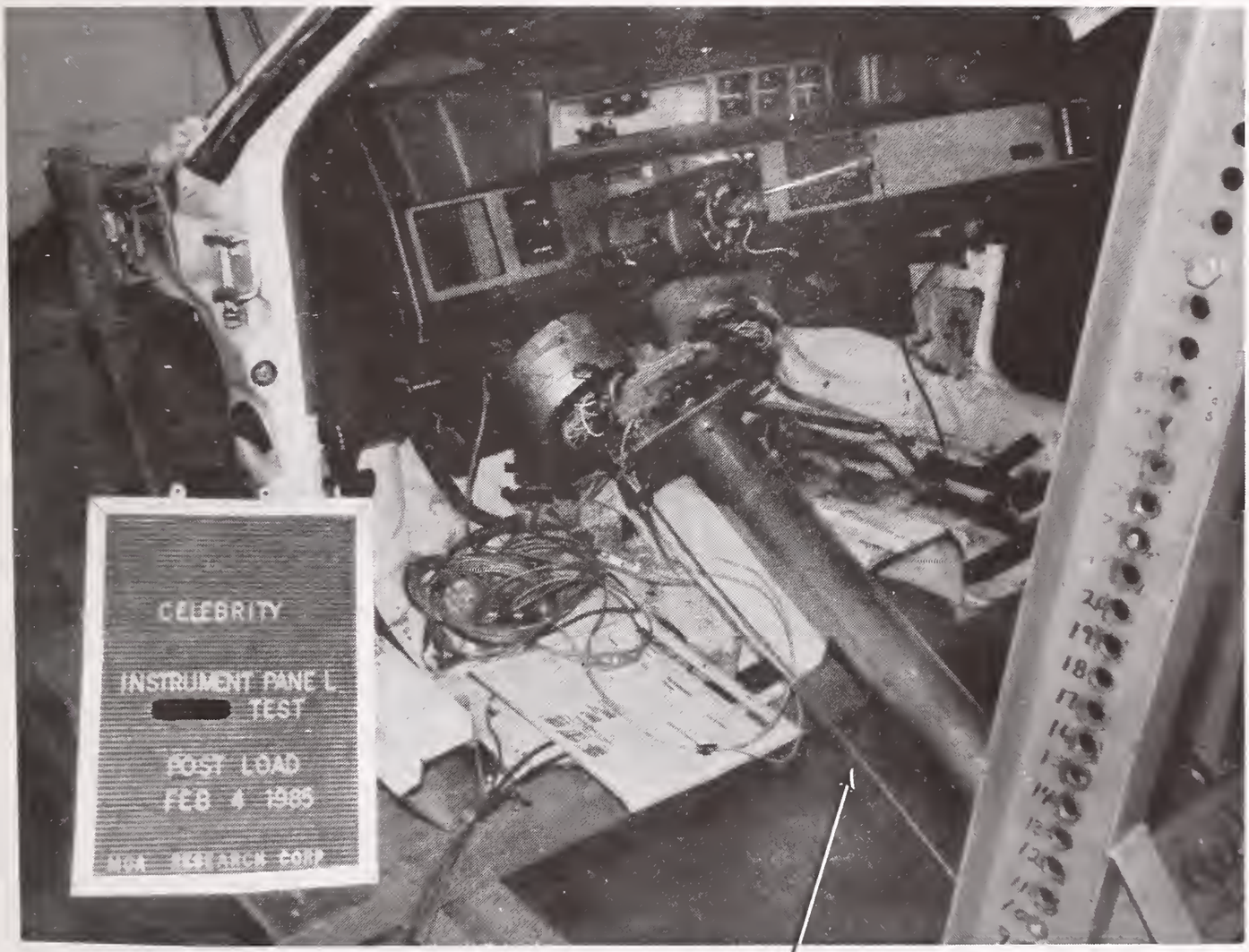

MAXIMUM
PENETRATION
MEASUREMENT
ASSEMBLY

FIGURE 3-10. MAXIMUM PENETRATION MEASUREMENT ASSEMBLY

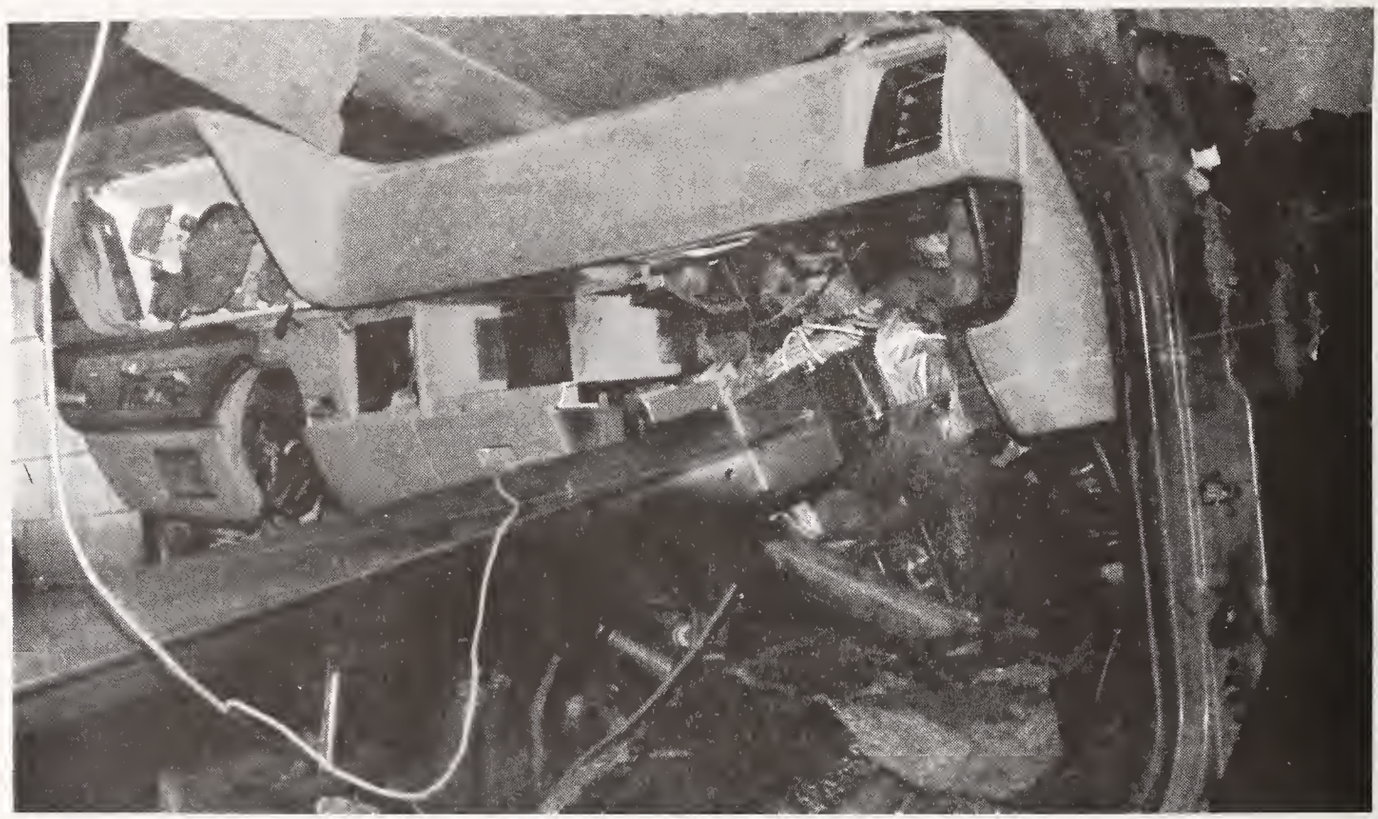

FIGURE 3-11. DYNAMIC PASSENGER FEMUR

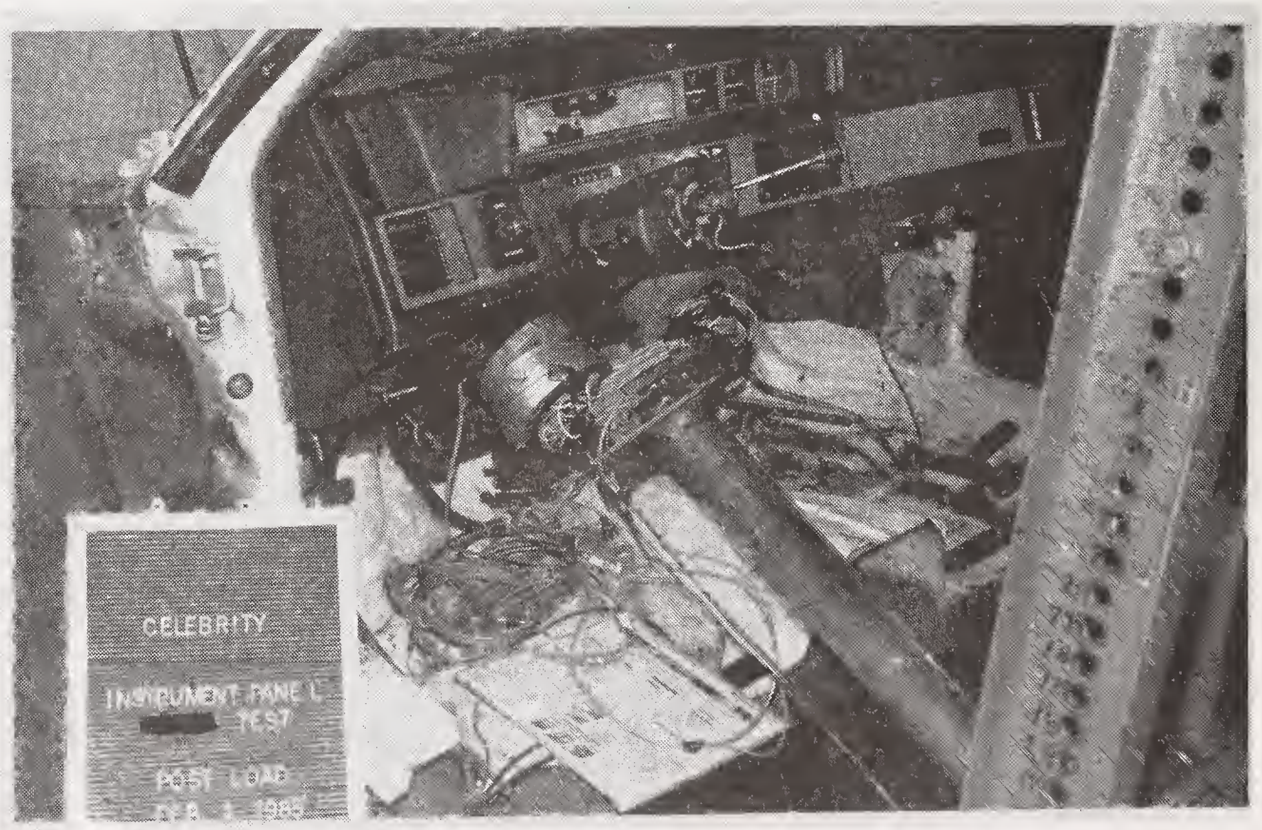

FIGURE 3-12. DYNAMIC DRIVER'S FEMUR

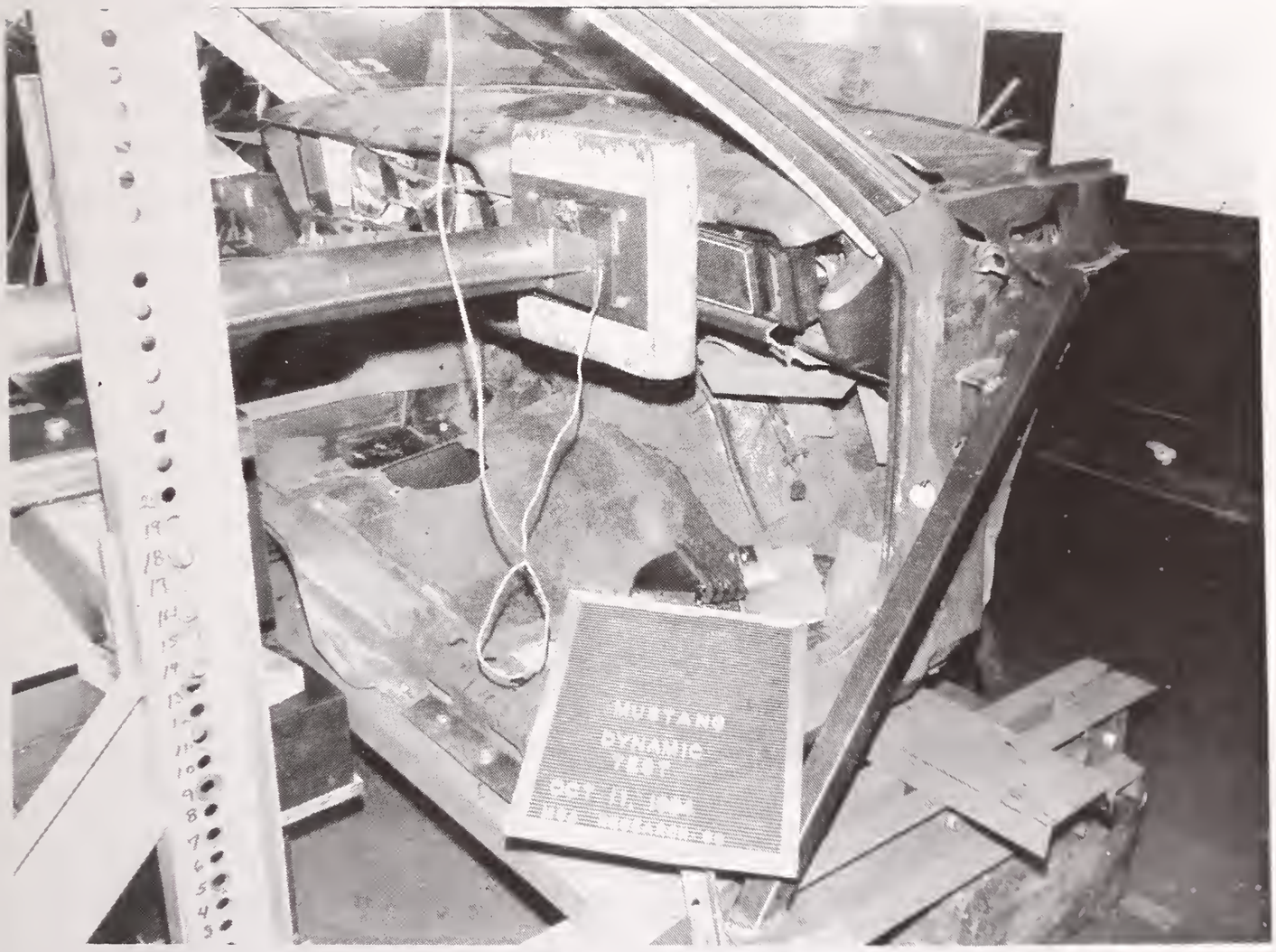

FIGURE 3-13. DYNAMIC PASSENGER TORSO

for the torso. The position and angles were identical to the positions and angles used in the static instrument panel testing. During the passenger torso tests, the passenger femurs were held at maximum penetration by bolting a body form into proper position.

3.1.3 Dimensional Properties of Instrument Panels

In addition to the force-deflection characteristics of the instrument panels, data was gathered for some physical dimensions. The dimensions of special interest were those to specify the shape and location of the instrument panel within the vehicle. In order to obtain the instrument panel shape, a piece of heavy solder was bent around the surface of the area of interest (i.e. the area of impact). The shape specified by the solder was then traced onto a piece of paper and manually digitized using a desk-top computer. In order to assure proper sizing and orientation of the shape (curve), pre-determined points were measured from a fixed reference point. These measurements were then used to locate the instrument panel shape with respect to the intersection of the vehicle's floorboard and toeboard. This point serves as a common reference point for all vehicles and allows transportation of the data to any coordinate system used in crash victim simulation programs.

3.2 DATA PROCESSING

Static Tests

Electronic data that was acquired during the quasi-static instrument Panel testing consisted of forces measured by load cells and displacements measured by string potentiometers. These data were plotted directly as force-deflection curves for both loading and unloading on analog X-Y plotters. Processing of these measurement data consisted primarily of manually digitizing the analog force-deflection curves to store the information in digital form on a desk-top computer and manipulating the data for presentation and comparison purposes.

In addition to overplotting repeat tests, data for the head-upper instrument panel were resolved to obtain force and deflection components normal to the impact surface.

All force-deflection measurements made represented the combined compliance for both the instrument panel surfaces and anthropomorphic dummy body parts. Since the head and knee forms had the standard vinyl skin of minimal thickness (about one-quarter inch or less), the body part compliance for these two measurements was negligible and was ignored. Thus the measured force-deflection characteristics were assumed to represent the instrument panel surface characteristics alone.

This is not the case, however, when considering the torso force-deflection measurement. In this case significant compliance of the torso relative to the measured deflection was expected. Hence, an independent measurement of the torso force-deflection characteristics was also made. This measurement was performed by forcing the anthropomorphic dummy torso against a rigid surface. The resulting force-deflection curve allowed subtracting the compliance of the torso from the measured deflection of the test to obtain a true measure of instrument panel deflection.

Dynamic Testing

The processing of the dynamic data was carried out on the desk-top computer as well. The acceleration data, which was stored on the tape recorder in analog form, was digitized through an analog-to-digital converter at 3,360 samples per second and stored on the computer. A computer program was then used to digitally filter the acceleration. An example of the effect of filtering a raw acceleration time history trace at two different corner frequencies is shown in Figure 3-14. The filtered data was then integrated twice to produce a displacement-time plot. The acceleration data was also multipled by the mass of the impactor and then cross plotted with the displacement data to give a force-deflection relationship. There was no need to remove any torso compliance effect from the torso tests since a solid wood body form was used.

Processing Common to Static and Dynamic Tests

Once the force-deflection data was obtained for the tests, the data was further processed to obtain certain values which were used in various vehicle occupant computer simulation models. The values determined were for G (the ratio of the deflection occurring at the time when the force returns to zero upon unloading to the maximum deflection achieved during the test), R (the ratio of conserved energy to the maximum energy absorbed during the test), and K (the

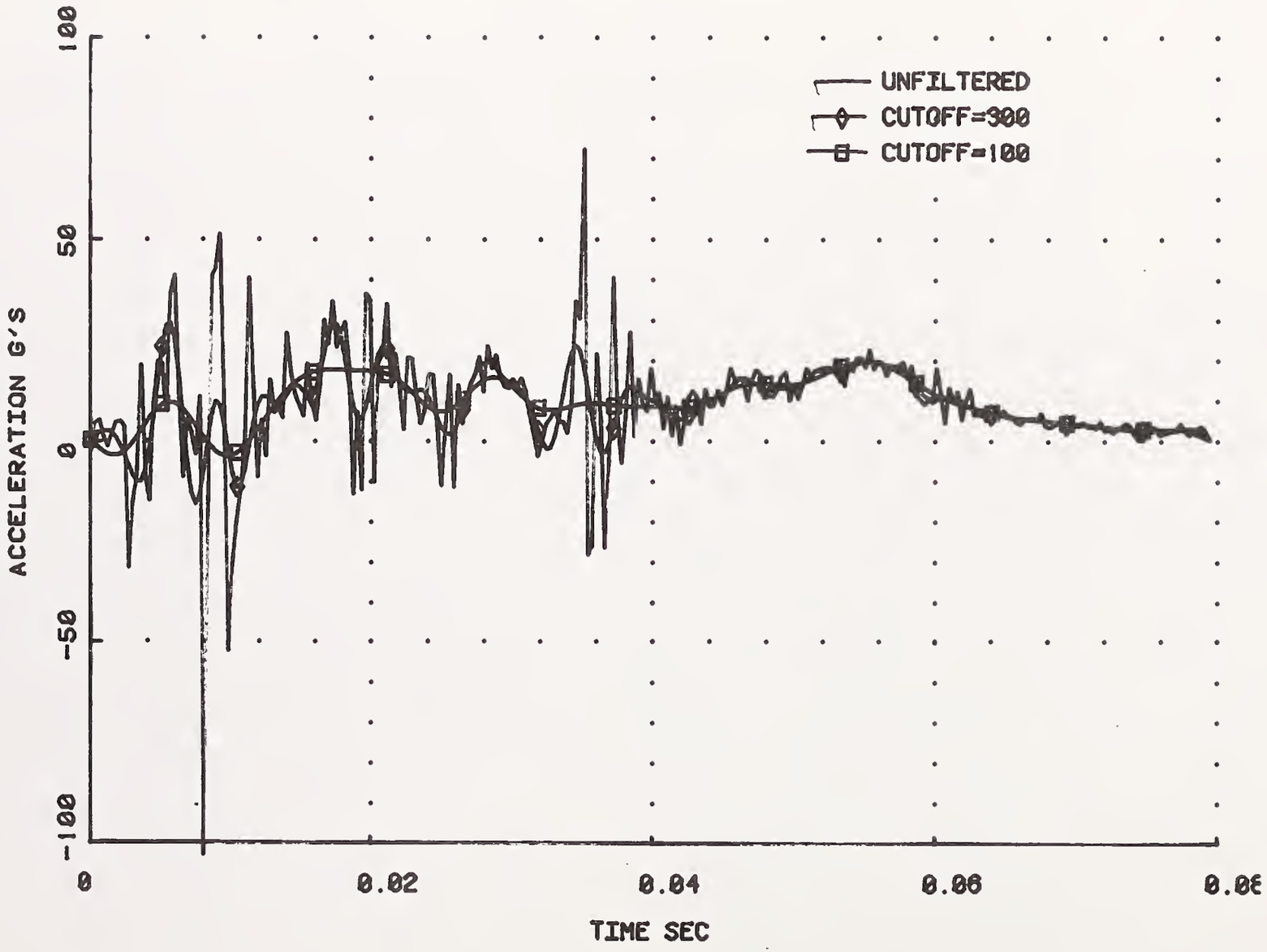

FIGURE 3-14. EXAMPLE OF DIGITAL FILTERING RESULTS

unloading slope). In addition to these values, multiple tests were processed together to obtain values for such variables as viscous damping and friction. The steps taken in determining these values will be discussed fully later in this report.

Instrument Panel Data-Base

The data from all the individual instrument panel tests were then reduced to simplified piecewise linear curves so that the number of points defining the curve would not exceed the limit in the PADS2 computer program. The points which were used to define the simplified curves were those which allowed the general loading force-deflection pattern to be maintained while also maintaining approximately the same area under the curve. These force-deflection data pairs were then put on the NHTSA VAX-11/780 computer along with the values of G, R, K, the viscous damping coefficient, the friction coefficients (μ_1, μ_2, μ_3 defined in the MVMA-2D Computer Simulation Model User's Manual), and the values of δ_A, δ_B, δ_C, δ_D, and δ_F which are deflection at specific points in the force-deflection characteristics (these are also defined in the MVMA-2D User's Manual). Most of the data are stored on the NHTSA VAX in the format described in Table 3-3.

Instrument Panel Physical Dimensions

The data obtained from the measurement and shape of the instrument panel was reduced to three straight line segments in order to agree with the PADS2 definition for vehicle interior description. The line segments were oriented to produce an approximation of the actual instrument panel shape for determining contact with the occupant. Description of these line segments are given by describing the physical position of a reference point (with respect to the vehicle's floorboard-toeboard intersection), the angle the line segment makes with a horizontal (positive counter-clockwise), and the line segment's length. These data were included on data sheets and entered onto the NHTSA VAX computer. (These data sheets have been included as Appendix F.) The format for the vehicle description files on the VAX is shown in Table 3-4.

Also included on the instrument panel profiles are the location descriptions for the windshield and header. The location measurement for these two sections are taken from the same origin point that was used for the instrument panel. The orientations for these sections were obtained by actual physical measurement using an inclinometer.

TABLE 3-3. VAX FORCE-DEFLECTION DATA FILE FORMAT

The static force-deflection data is located in files which are identified by the vehicle model followed by the extension ".FD*" where the * represents a number from 1 to 5. This number specifies which test the data is from: 1 indicates the head; 2 indicates the torso; 3 indicates the passenger side total femur; 4 indicates the driver side total femur; and 5 indicates the windshield (not all vehicles had windshield tests performed on them). These files take the following format:

Line No.	Position in Line	Description
1	1	vehicle make, model and year (if available)
2	1	test description
3	1	occupant type (1 for driver, 2 for passenger, 3 for both (windshield tests)
	2	contact plane involved (PADS2 basis)
	3	number of data points (N)
	4	value of damping coefficients
	5	zeroeth order value of friction coefficient
	6	first order value of friction coefficient
	7	second order value of friction coefficient
4	1	first deflection value
	2	first force value
.		
.		
.		
N+3	1	last deflection value
	2	last force value
N+4	1	value of G
	2	value of R
	3	value of K
N+5	1	value of DELTA - A
	2	value of DELTA - B
	3	value of DELTA - C
	4	value of DELTA - D
	5	value of DELTA - F

(DELTA - A thru DELTA - F are the values needed for card 402 in the MVMA-2D input deck.)

N+6, N+7	1	intermediate unloading occurrence identifier (= 1 for first intermediate unload, = 2 for second intermediate unload)

TABLE 3-3. VAX FORCE-DEFLECTION DATA FILE FORMAT (CONT.)

2	maximum deflection obtained before indicated unload initiated
3	value of G of indicated intermediate unloading
4	value of R of indicated intermediate unloading
5	value of K of indicated intermediate unloading

(Lines N+6 and N+7 will not be present if no intermediate unloads were carried out.)

The dynamic force-deflection data has the same format as the static force-deflection data. The files containing the dynamic test data will use the same file names as the static test data but with different extensions. The extensions for the dynamic test data will be ".F*0", where the * represents the numbers 2, 3, or 5. The single number carries the same meaning as it does for the static test data.

Notes:

1. In the case of the Chevy Citation files, file names will be CIT*.ext where the * indicates some additional test description. This is due to the multiplicity of tests done on the Citation. Explanation of the additional description will be put in the summary table of test data available that will be updated and re-issued as more data files are added.

2. Special test cases which fall outside the format standard described above will have file extensions outside of the range given above. Reason(s) for the departure from the standard will be given in test description (line 2) of the data set.

TABLE 3-4. VAX VEHICLE GEOMETRY DESCRIPTION FILE FORMAT

The plane descriptions are located in files which are identified by the vehicle model (VOLARE, CHEVETTE, etc.) followed by the extension ".VDD".

These files take the following format:

Line No.	Position in Line	Description
1	1	vehicle make, model, and year (if available)
2-4	1	further vehicle description (0 = no further description)
5-14	1	contact plane reference number (PADS2 basis)
	2	occupant type (1 for driver, 2 for passenger)
	3	plane's X reference point location
	4	plane's Y reference point location
	5	angle of plane (PADS2 standard)
	6	length of plane

3.3 WINDSHIELD TEST PROCEDURES

Described in this section are the test procedures utilized during the windshield tests conducted. Two types of tests were conducted; static and dynamic. The vehicles that were subjected to each particular test are indicated in the test matrix of Table 3-2. Discussions of each test procedure follow.

3.3.1 Static Windshield Test

The static windshield tests were conducted using most of the same equipment and procedures as the static instrument panel tests. The vehicle section was mounted on the test fixture in the same manner as for the static instrument panel tests. A hydraulic cylinder was used to force a headform into the windshield. The same headform from the instrument panel tests was used for the windshield tests.

Shown in Figure 3-15 is the hydraulic cylinder and headform positioned for a test. As shown in the photo, the headform was forced into the windshield in a horizontal direction. The cylinder was positioned such that the line of action of the cylinder was parallel to the longitudinal axis of the vehicle and through the center of gravity of an occupant when normally seated in the vehicle. The height of the headform was adjusted such that the line of action went through the vertical center line of windshield.

The instrumentation and servocontrol system used for the windshield tests were the same as used for the instrument panel tests. A load cell was positioned between the cylinder rod and the headform to measure force in the direction of travel as shown in Figure 3-15. A string potentiometer was used to measure displacement as well as control the position of the cylinder through the servcontroller. The test consisted of slowly displacing the headform into the windshield using the manual servocontroller and recording the analog force and deflection signals on an X-Y plotter.

Static tests were conducted on only a limited number of windshields before being discontinued. The static test procedure resulted in very low force levels and windshield fracture patterns that were not considered to be representative of dynamic impacts. A complete discussion of these results is provided in Section 4.3.

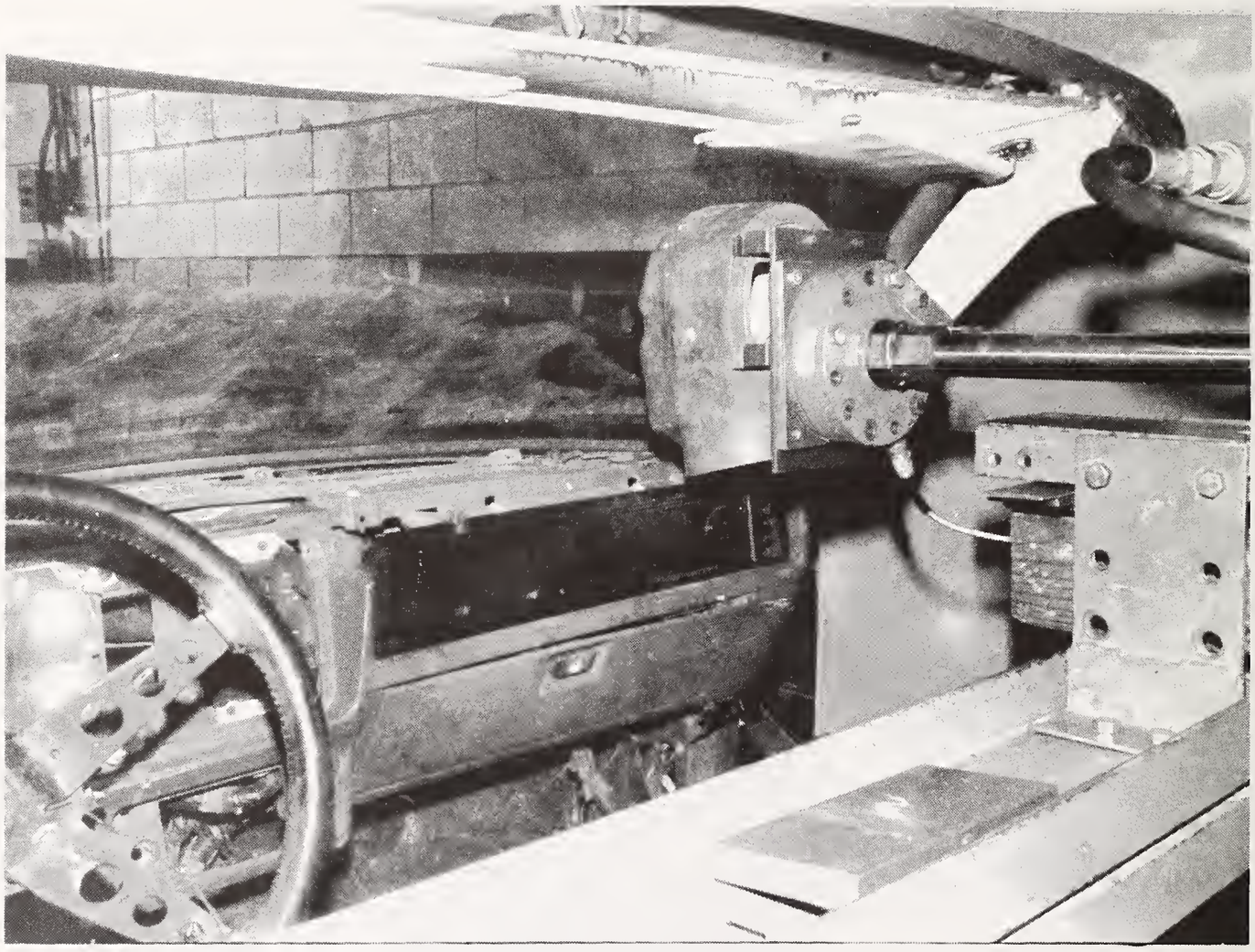

FIGURE 3-15. TYPICAL STATIC WINDSHIELD TEST SET-UP

3.3.2 Dynamic Windshield Test Procedure

The test procedure for the dynamic windshield test is discussed in this section. This test procedure is very similar to the dynamic instrument panel test procedure which will be referred to frequently.

The mechanical set-up for the dynamic windshield testing used the same load frame and vehicle cowl mounting as the dynamic instrument panel tests (see Figure 3-16). The major difference was the impactor system which used a 1-1/2" diameter piston-cylinder arrangement. A headform was attached to the impactor shaft (see Figure 3-17). The shaft centerline was positioned so that the impact was normal to the windshield. Set-up distance was 13" from the target to allow the headform to reach test speed and coast prior to impact. All sensors and the recording system were identical to the dynamic instrument panel testing. The acceleration sensors were mounted inside the headform. Photos and measurements were taken prior to impact. Temperature was recorded. The time zero contact switch was placed so that the forehead would close the switch upon contact. The speeds of the windshield tests were nominally 20 mph. The location of the windshield was the center of the Passenger position and 1/3 of the distance between the top and bottom of the windshield, down from the top of the windshield. The location was the target for the nose of the headform (see Figure 3-18).

Once the impactor was positioned, the maximum penetration assembly was measured as was the set-up distance, the angle of the windshield and the angle of the impactor. Pre-test photographs were then taken. The FM tape recorder was set-up and the system was ready to be fired. During impact, the acceleration, contact sensor, velocity and maximum penetration were monitored. After impact, photos and measurements were taken. The analog data recorded on FM tape was then available for digitizing and subsequent processing.

3.4 INSTRUMENT PANEL PARAMTERIC TEST PROCEDURE

This section describes the instrument panel parametric study that was conducted on four of the initial group of eight vehicles, as indicated in the test matrix. The purpose of this study was to determine the effect on force-deflection characteristics due to variations in the loading orientation and lateral position of the loading axis. The parametric study consisted of two additional test series performed on replaced instrument panels. While the equipment used and the

FIGURE 3-16. WINDSHIELD TEST LOAD FRAME

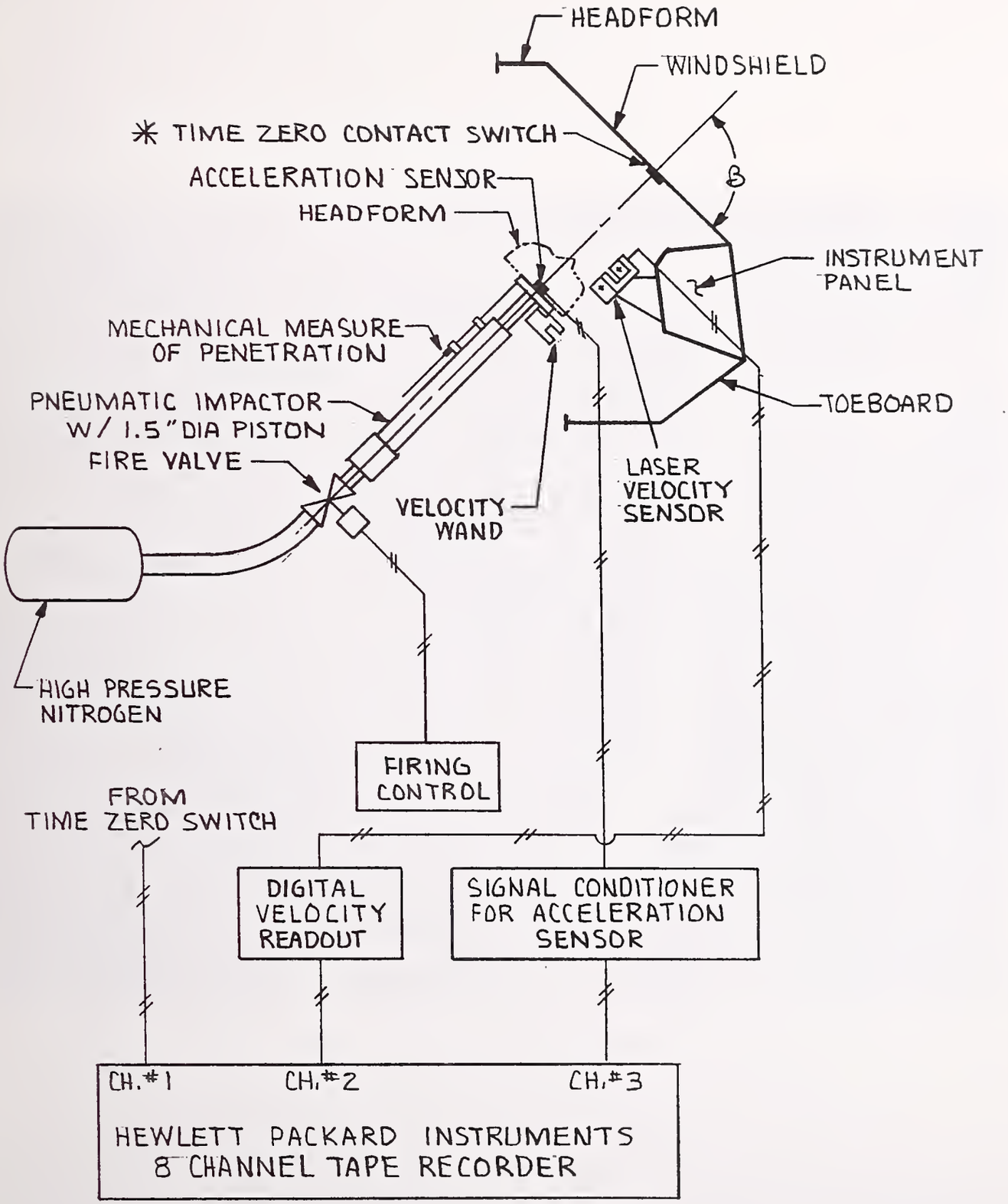

FIGURE 3-17. WINDSHIELD TEST SYSTEM

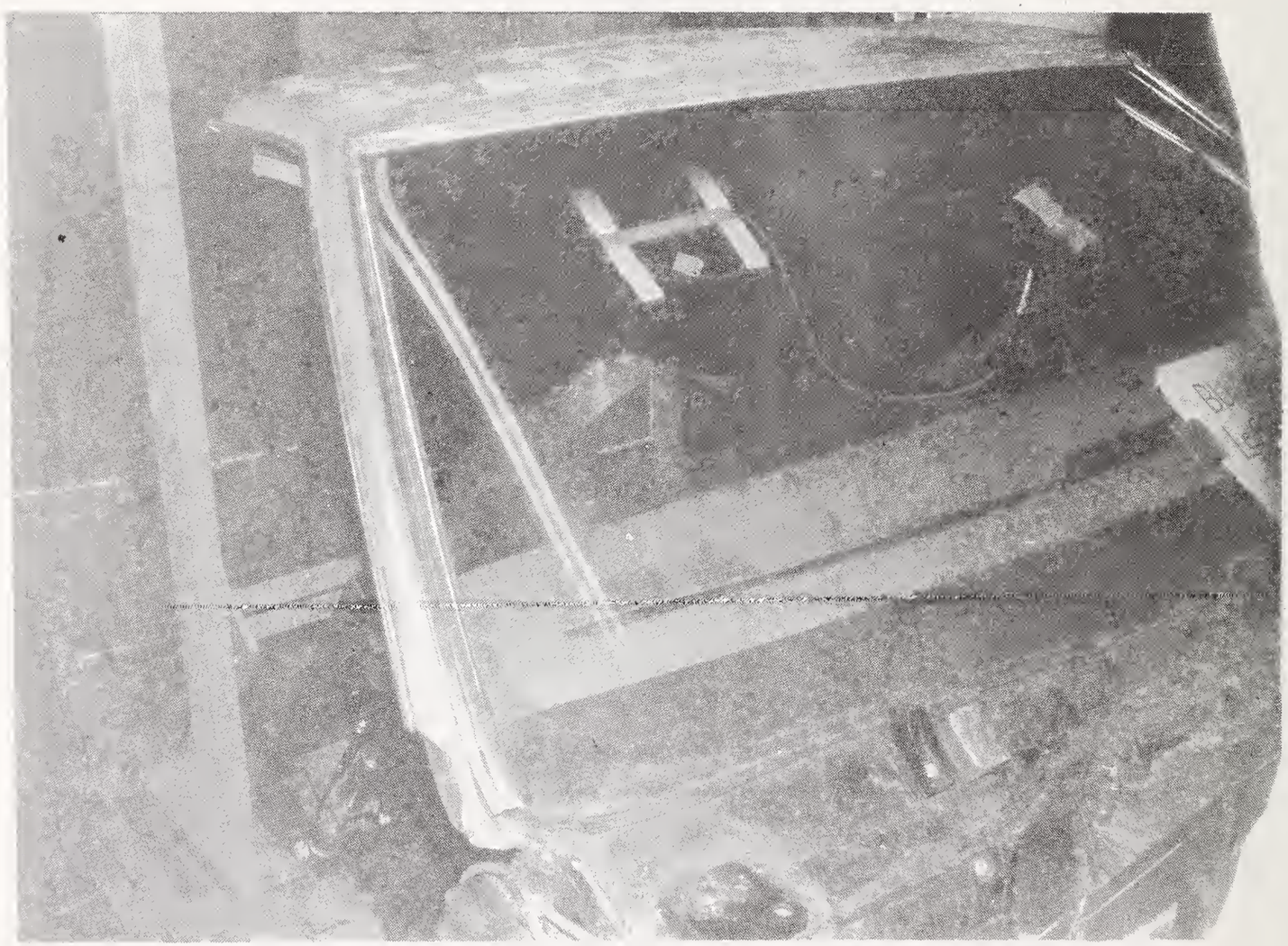

FIGURE 3-18. STANDARD WINDSHIELD TARGET

procedures followed were similar to the instrument panel production tests, the orientation and the location of the body forms were varied in the parametric tests.

The first parametric test series consisted of knee, torso, and head tests on the passenger side. The loading orientation and angles were identical to the production tests, but the hydraulic cylinder was moved towards the center of the vehicle approximately 2-3 inches. Therefore, the body forms were contacting slightly different features on the surface of the instrument panel. This test was intended to determine the sensitivity of the force-deflection relationships to small changes in locations of contact.

The second parameter test series used the same contact position on the instrument panel as used in the standard series, but the angle at which the body part contacted the instrument panel was changed. Shown in Figures 3-19, 3-20, and 3-21 are typical test set-up for the knee, torso, and head second parameteric test series. For the knee test, the hydraulic cylinder was repositioned such that it was horizontal, as opposed to angled up approximately 20 degrees as in the production tests. For the torso test, the hydraulic cylinder was angled down at 30°, instead of the horizontal direction of the production test. It should be noted, however, that the orientation of the torso was not changed from its normal vertical position. This required the fabrication of a special bracket that allowed the hydraulic cylinders and load cell to attach to the back of the torso at a 30° angle. This is pointed out in Figure 3-20. The head tests were conducted at the same location as the production test, however, the orientation was changed to horizontal. This differed from the 30 degree down orientation in the standard tests.

The same data recording and servocontrol system was used for the parametric tests as the production tests. The data was recorded on the analog X-Y plotters, digitized, and processed on a Tektronix microcomputer.

3.5 TEST PROCEDURE FOR FRICTION TESTING

The test procedure for instrument panel friction testing is described in this section. The vehicle tested was a Chevrolet Celebrity. The friction tests were performed using the load frame and vehicle cowl used during instrument panel testing. The friction test equipment consisted of a passenger kneeform,

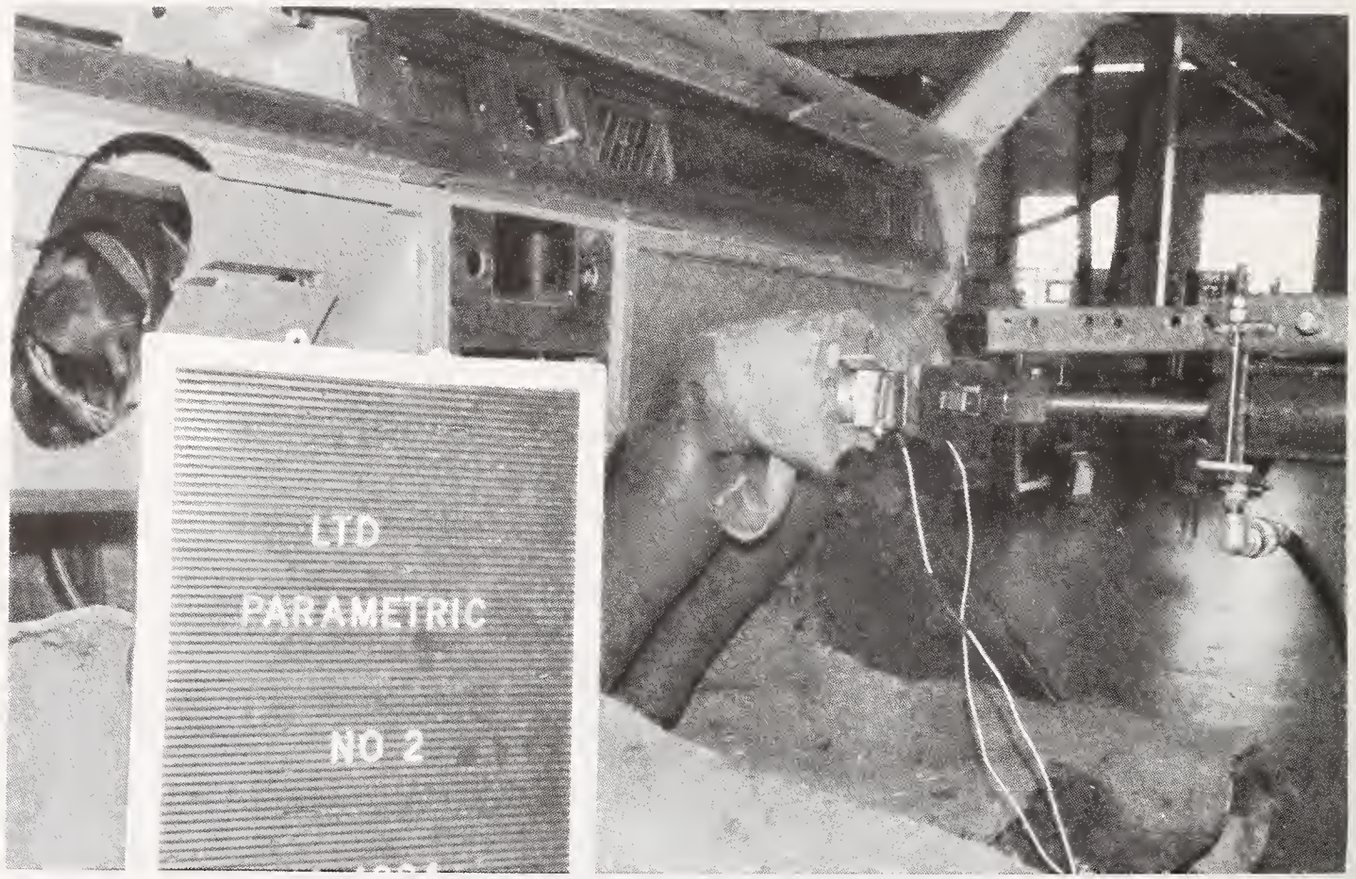

FIGURE 3-19. FEMUR PARAMETRIC TEST TYPE 2

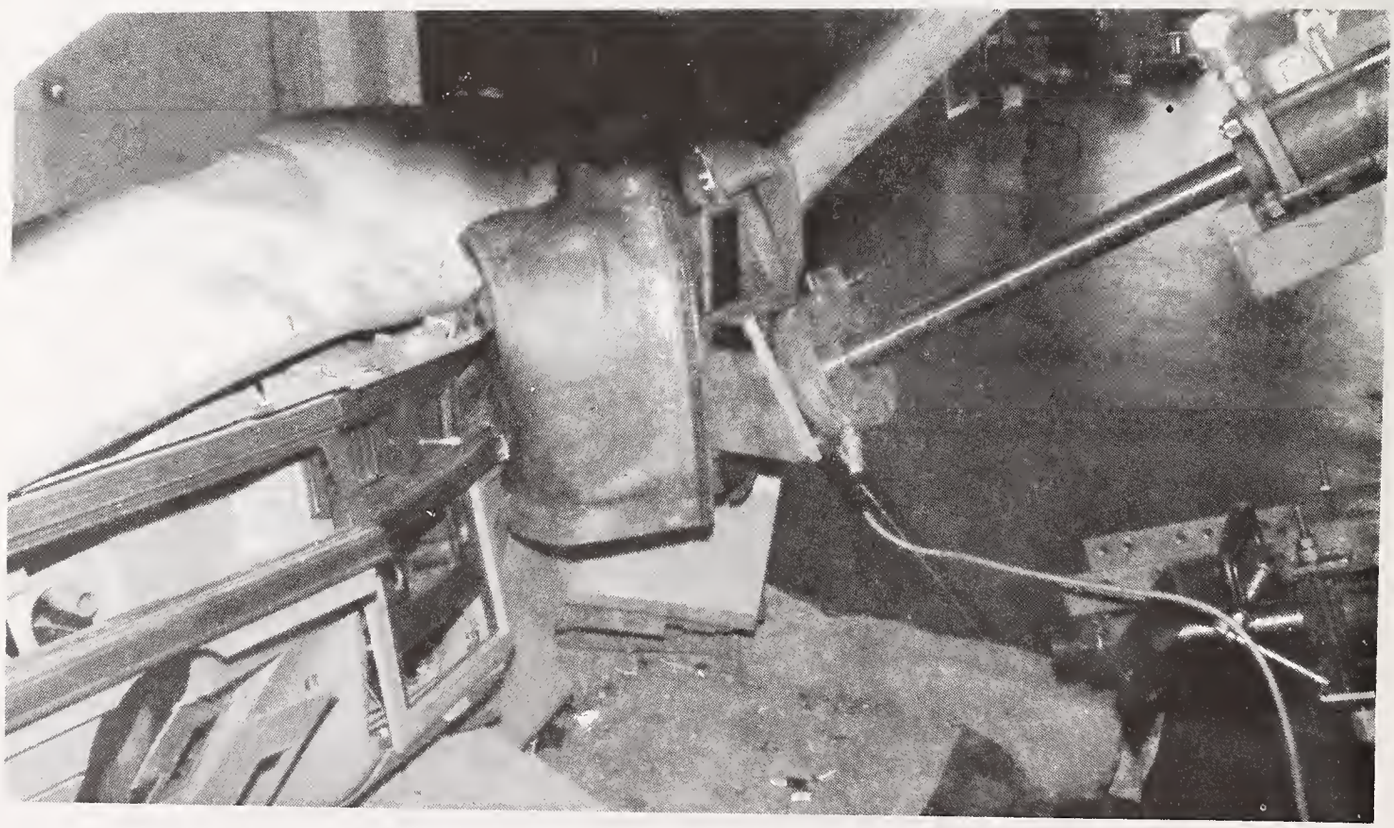

FIGURE 3-20. TORSO PARAMETER TEST TYPE 2

FIGURE 3-21. HEAD PARAMETRIC TEST TYPE 2

hydraulic cylinder servo-system, pulley system, load cells, crank mechanisms, and recording system (see Figure 3-22).

The kneeform and hydraulic cylinder servo-system was the same system used during the static instrument panel testing. The kneeform was covered with cloth that simulated a pair of pants on the occupant (see Figure 3-23).

During the tests, a normal force was created using the hydraulic cylinder. A friction force was then produced by sliding the kneeforms across the instrument panel. The sliding was possible by pivoting the kneeform and cable-crank arrangement (see Figure 3-24). Several normal force loads were used to create friction force-time traces. After the normal force was applied, the knee was pulled across the instrument panel and the force required to slide was recorded for angular sweep of about 10 degrees. Both normal and friction forces were recorded on a chart recorder as a function of time for later digitizing and processing to obtain a friction coefficient.

3.6 WINDSHIELD PARAMETRIC TEST PROCEDURE

The test procedure used in the parametric tests on Citation windshields were identical to those employed in the standard dynamic windshield tests with the exception of a number of set-up variations. The nominal target position was 7.75 inches down from the header and 11.75 inches inboard from the driver's side A-pillar. In the edge effect test, these dimensions were 4.75 and 4.0 inches respectively. Pre-stress to the windshield was applied in one test by distorting the windshield frame. This was accomplished by pulling the passenger side upper A-pillar approximately 2.5 inches rearward with a come-a-long and maintained this in distorted position during the test. Finally, in one case, a previously impacted windshield was tested on the opposite (passenger) side from the first impact.

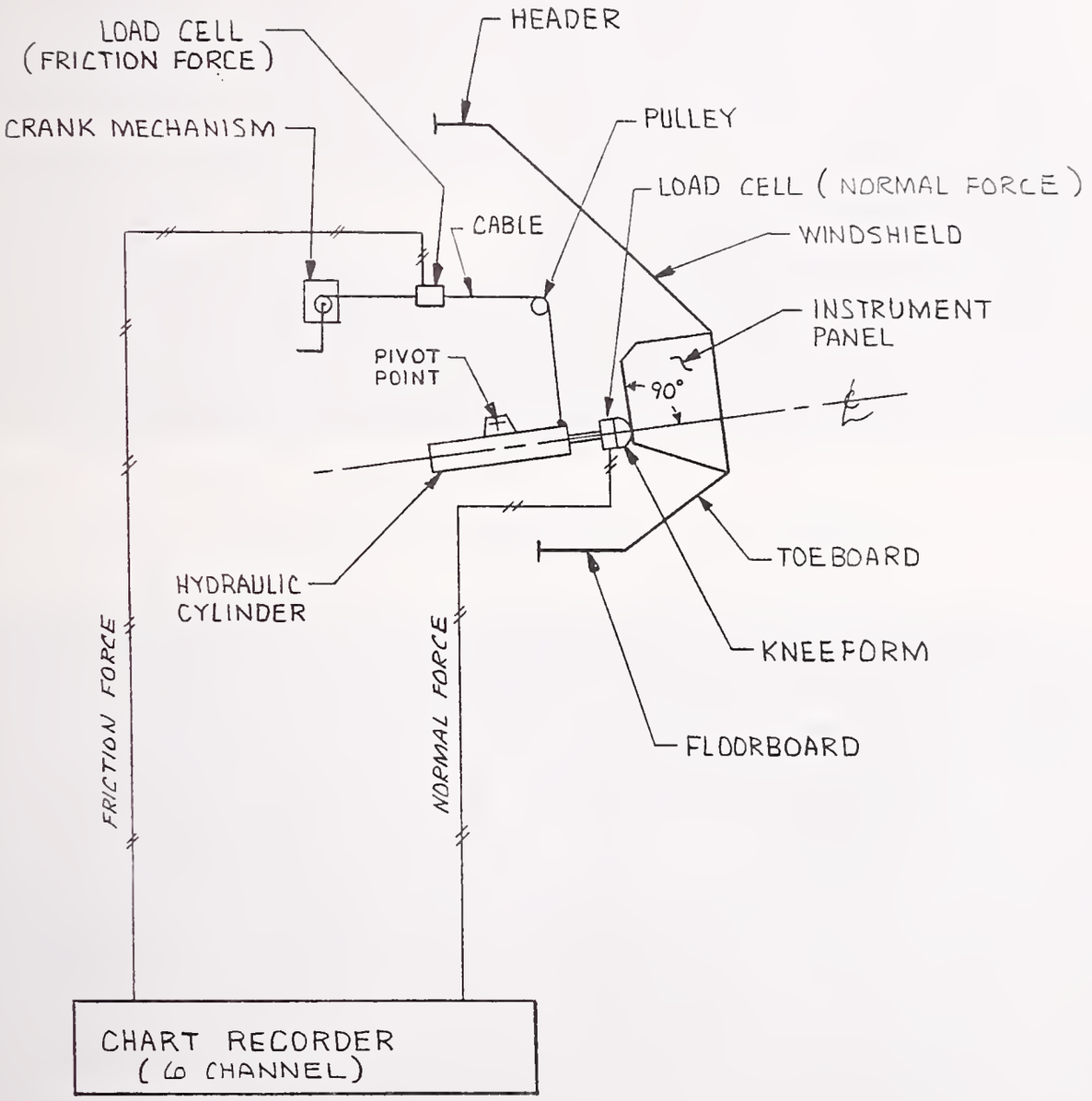

FIGURE 3-22. FRICTION TEST SYSTEM

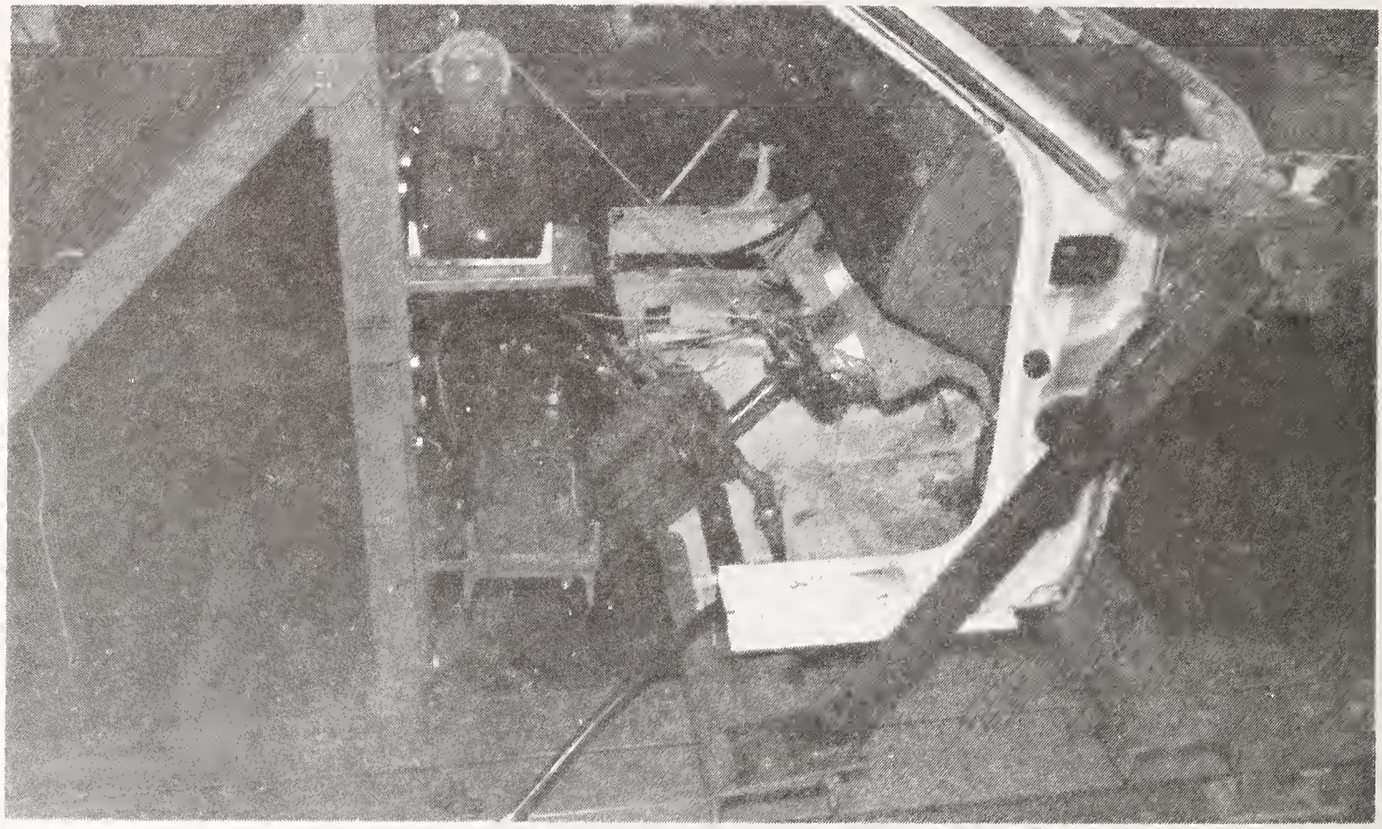

FIGURE 3-23. KNEEFORM FOR FRICTION TEST

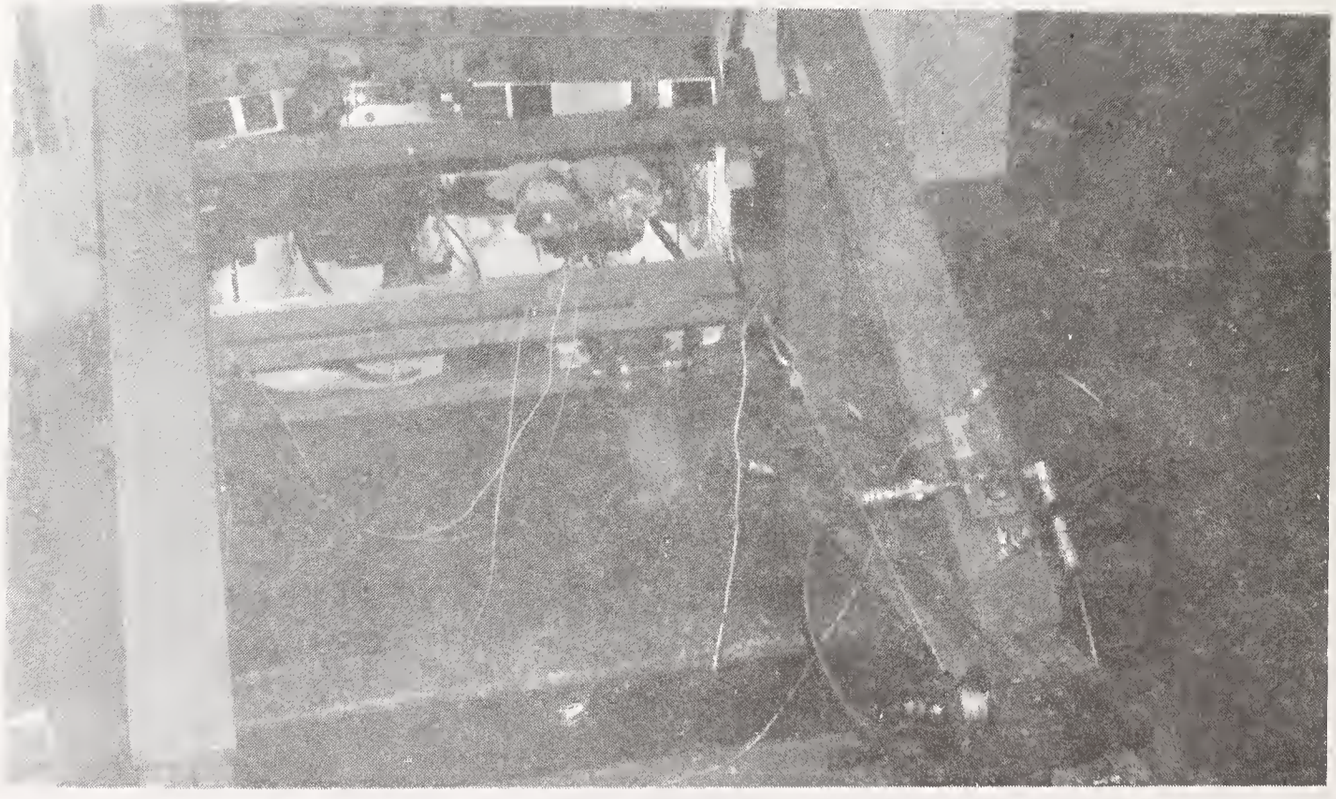

FIGURE 3-24. OVERVIEW OF FRICTION TEST

4. TEST RESULTS

This section contains discussions of the test results for each of the various tests, which were outlined in Section 3. The force-deflection data for all of static and dynamic windshield and instrument panel tests are included in Appendicies A through E. The data is presented on the standard data forms developed for this purpose and previously used to submit the data to TSC. While every test is not discussed in this section, several are referred to in order to point out various characteristics of the data that were observed.

4.1 STATIC INSTRUMENT PANEL TESTS

The static instrument panel tests indicated in the test matrix of Table 3-2 and discussed in this section consisted of displacing femur body forms into the lower instrument panel, the torso body form into the mid instrument panel, and the head form into the upper instrument panel. For all the tests, recorded data consisted of the force-deflection relationships for the instrument panel when the body form was displaced into it. Included in Appendix A are all the data recorded for these tests.

For the femur tests, a load cell measured the force on each individual femur as a function of displacement. After the test, the data was summed to produce the total femur force-deflection relationship. During several of the tests, only one of the femurs would be in contact with the instrument panel or would carry the majority of the load early in the test (first inch or two of deflection). Examples of this type of data, which resulted from shape or localized stiffness effects are shown in Figure 4-1 from the Pontiac Firebird test.

Also apparent in the data from the femur tests is that the peak deflections achieved were not consistent through-out the tests. Normally, the tests were stopped after the femurs began to bottom out, indicated by a significant rise in force levels. A typical indication of bottoming is shown in the Datsun test in Figure 4-2. However, on a few occasions, the full extensions of the hydraulic cylinder was reached before an indication of bottoming was observed. This was due primarily to the geometry of the instrument panel. The distance from the plane of the lower instrument panel (point of first contact) to the cowl or firewall

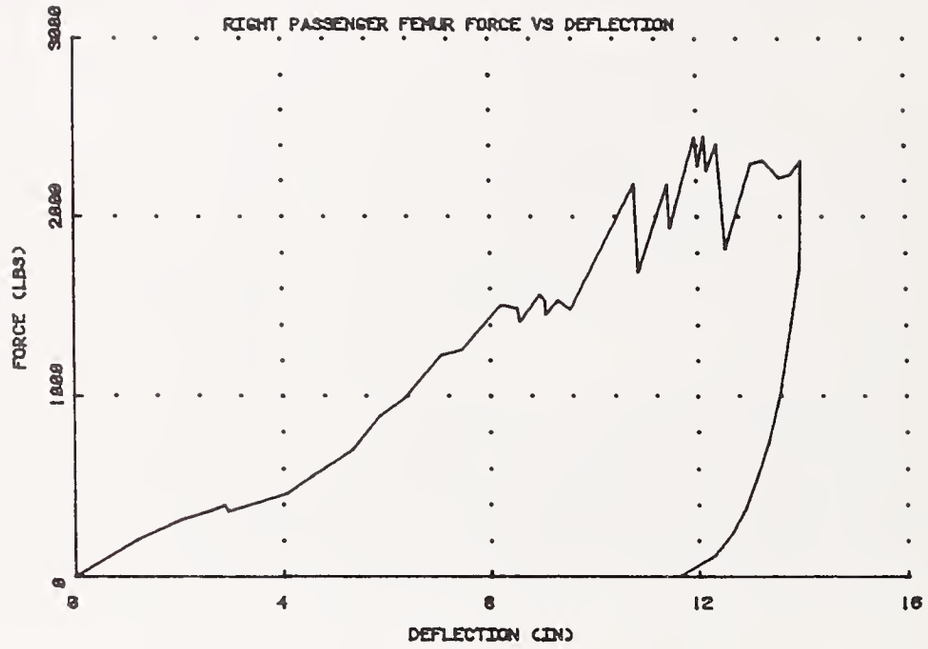

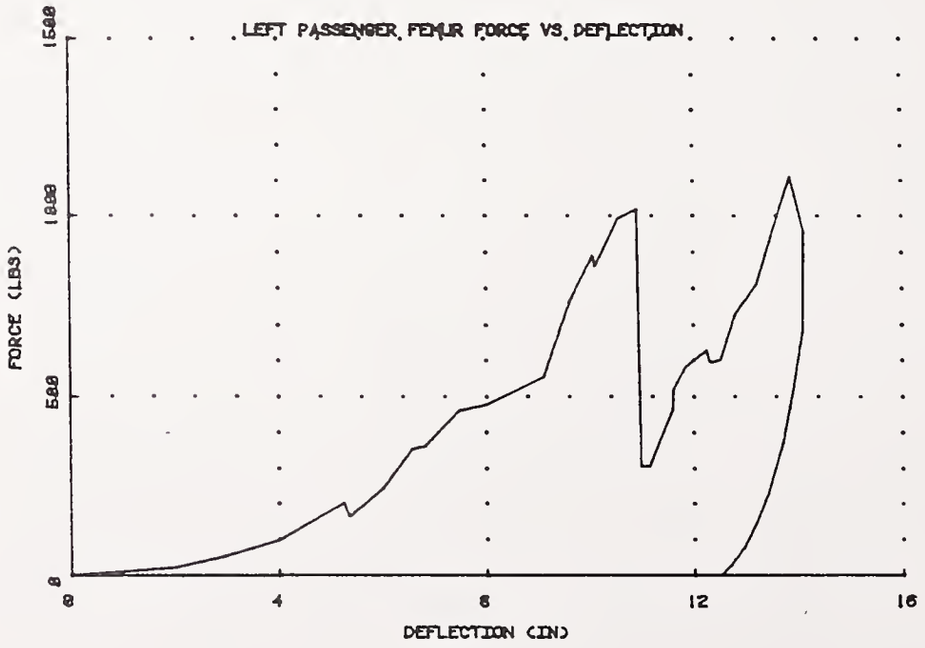

FIGURE 4-1. CONSTRASTING LEFT AND RIGHT FEMUR FORCE LEVELS LOW DISPLACEMENT (PONTIAC FIRBIRD)

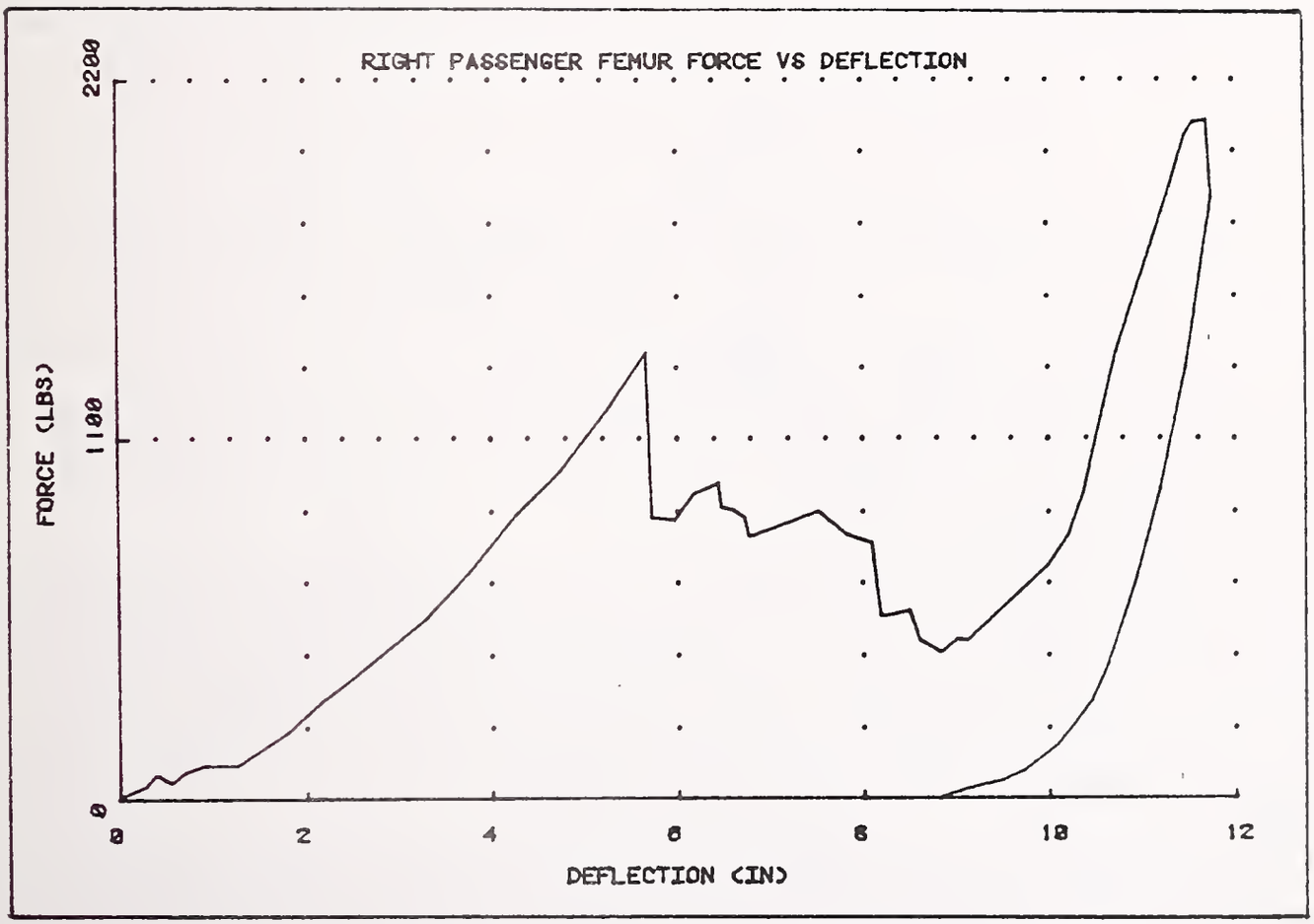

FIGURE 4-2. ILLUSTRATION OF TYPICAL BOTTOMING FORCE CHARACTERISTICS AT MAXIMUM DEFLECTION (DATSUN 210)

(typically the point of bottoming) varied from vehicle to vehicle. An example of femur data that doesn't show bottoming is the Chevy Chevette test illustrated in Figure 4-3. Other tests which did not bottom include Omni passenger knees, Firebird head and Buick head tests. For both the head tests, there was substantial damage to the lower and middle portions of the dash from the femur and torso tests. Due to this damage, the instrument panel separated from the cowl with little force during the head test. During the Omni knee test, the hydraulic cylinder was fully extended without any indication of bottoming. In this case, a total of 15 inches of deflection was recorded.

Also during the tests, the force levels would frequently drop off suddenly due to the breaking or failure of various portions or components of the instrument panel. These events were noted during the test and notations are included on the data sheets in Appendix A. An example of one of these is included in Figure 4-3.

To give an indication of the range of data recorded across all the femur tests, the data (sum of left and right femur forces) from each test was over plotted and is presented in Figure 4-4. Similar data plots for the torso, head, and driver femur are included in Figures 4-5, 4-6, and 4-7. Lines drawn through the origin of the data plots generally represent the upper and lower bounds of the data for each. Table 4-1 summarized the boundaries by listing the minimum and maximum for each set of data.

The torso data plotted in Figure 4-5 is the test data with the compliance of the body form removed. There is a substantial difference between the driver and passenger side femur data, most likely due to the steering assembly, usually supported by strong brackets, which typically resulted in a localized area of increased stiffness.

Listed in Table 4-2 are summaries of the G, R, and K values that are included on the data forms in Appendix A. For each type of test, the table includes the minimum and maximum values across the range of data, the mean, and the standard deviation.

There are several factors that influence the force deflection characteristics of each instrument panel, and therefore, contribute to the data range seen in the overplots. These factors include the geometry of the instrument panel, the material of the various components making up the instrument panel, and the method of attachment of the cowl. Some instrument panels are attached to the cowl by

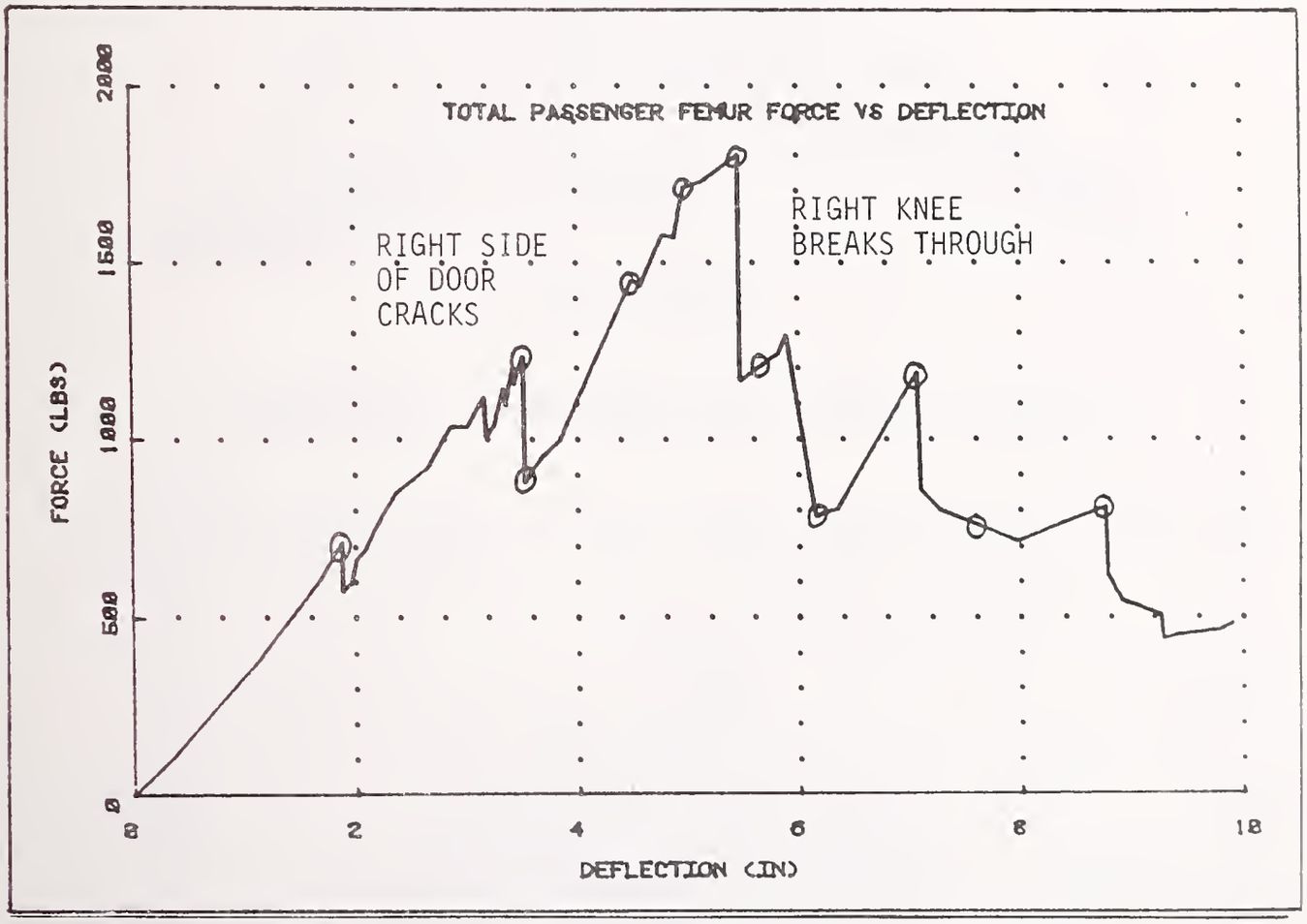

FIGURE 4-3. ILLUSTRATION OF FEMUR TEST WITH NO BOTTOMING (CHEVROLET CHEVETTE)

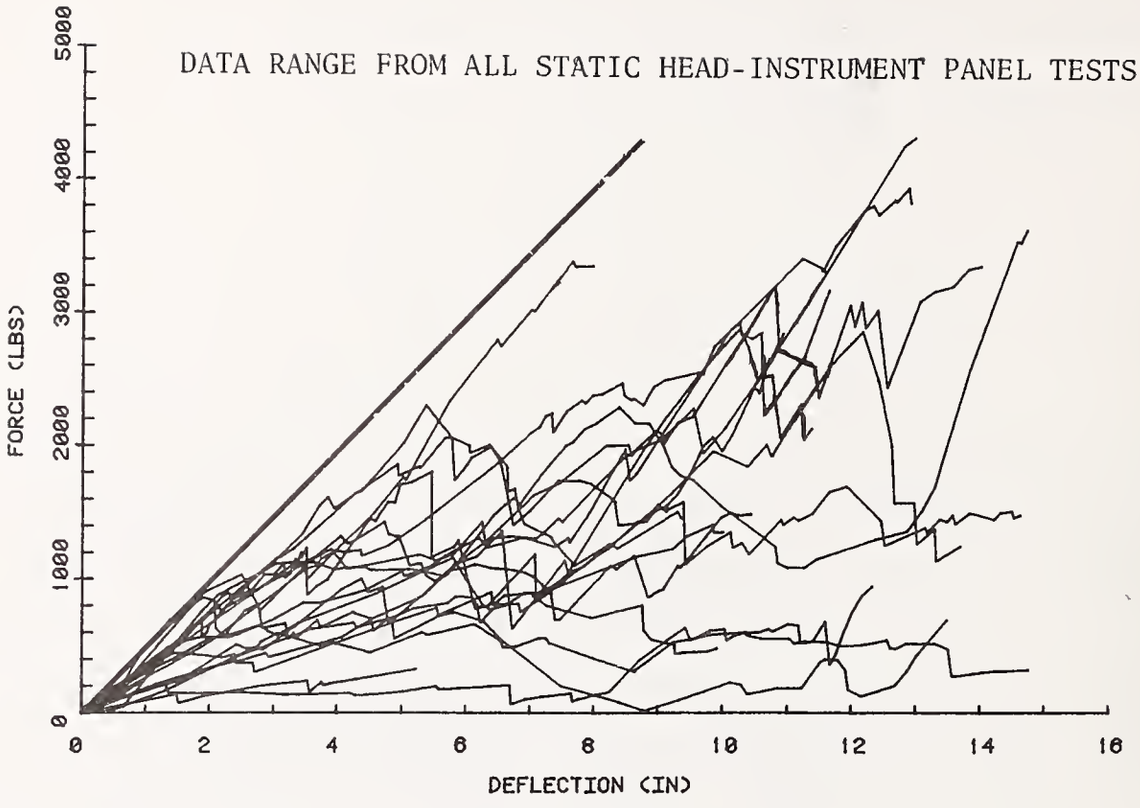

FIGURE 4-4. STATIC TOTAL FEMUR FORCE - PASSENGER SIDE

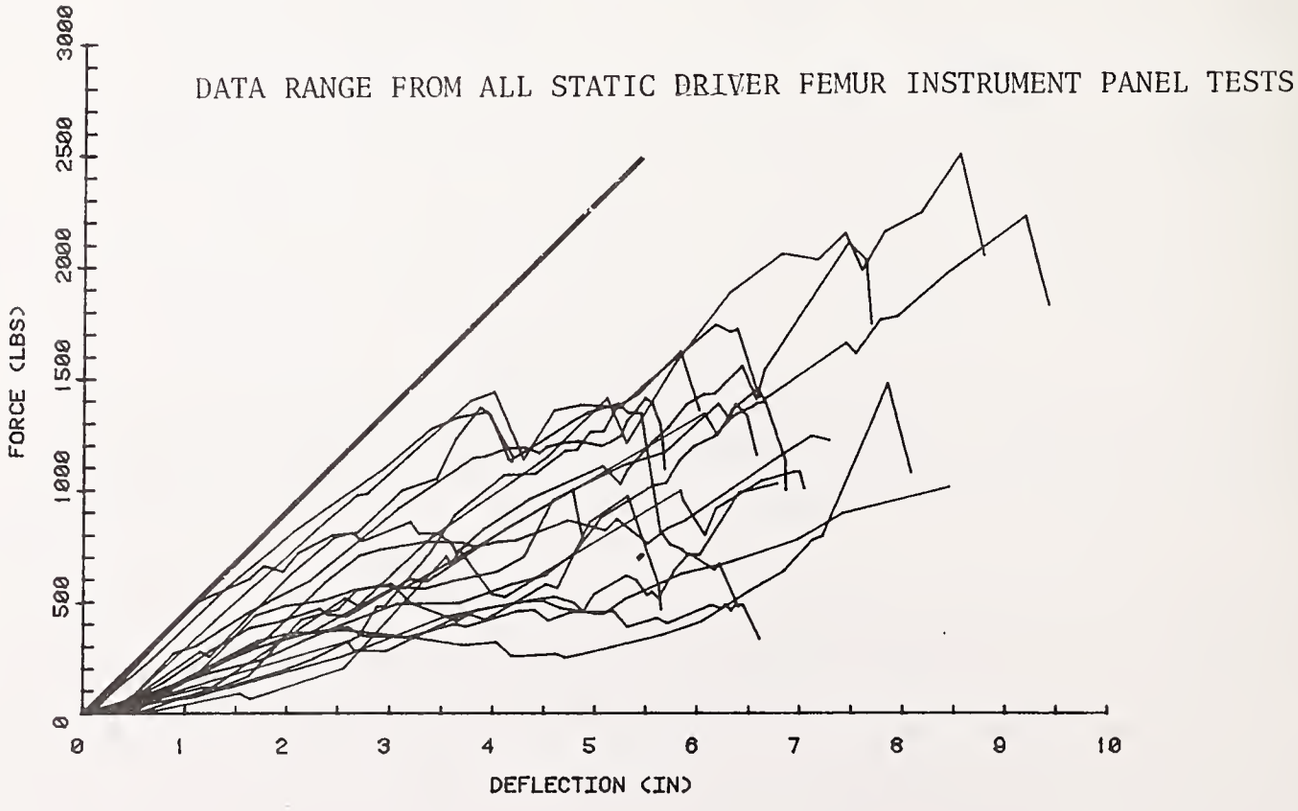

FIGURE 4-5. STATIC TORSO FORCE - PASSENGER SIDE

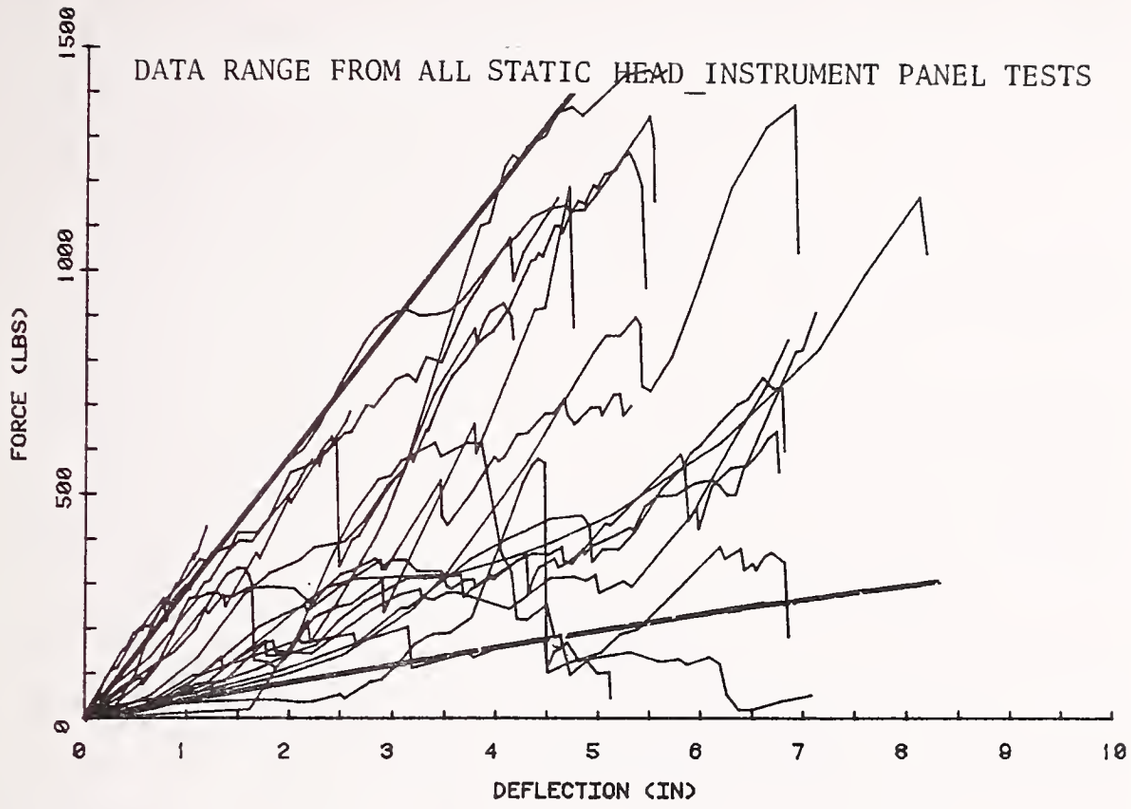

FIGURE 4-6. STATIC HEAD FORCE - PASSENGER SIDE

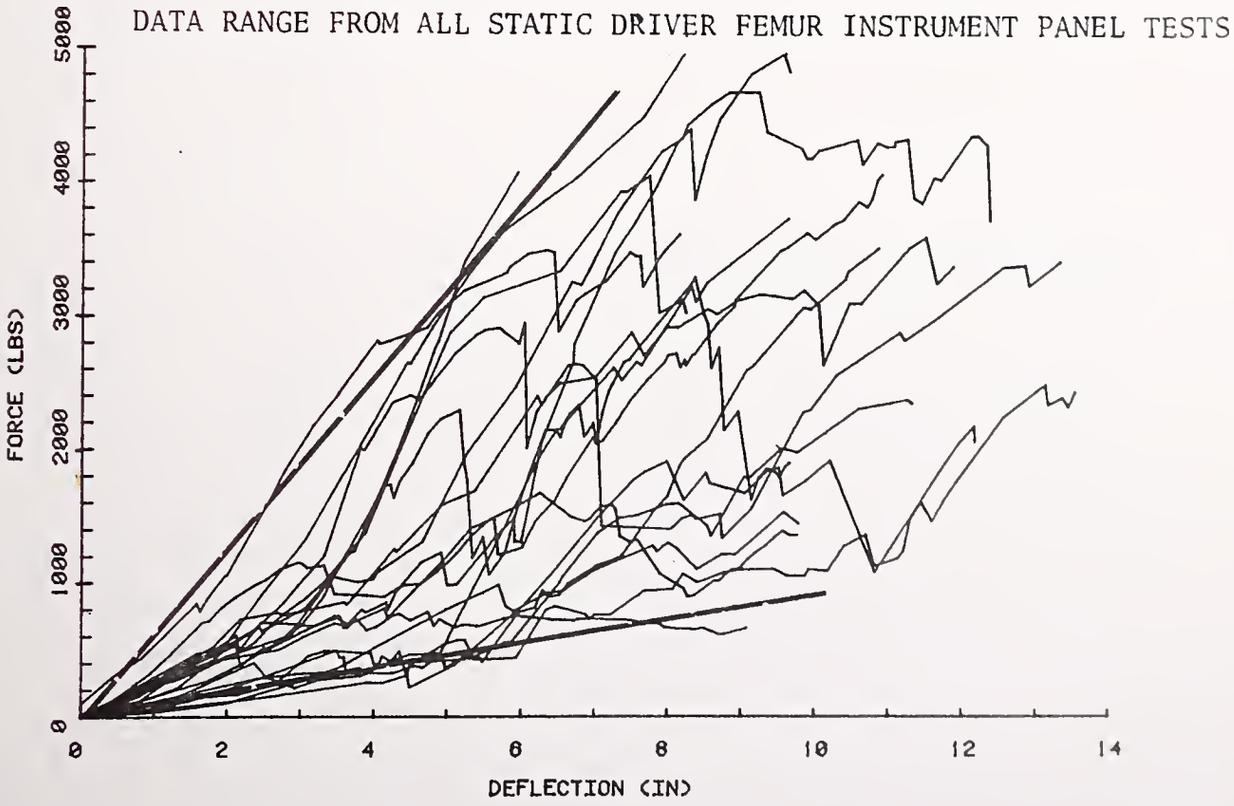

FIGURE 4-7. STATIC TOTAL FEMUR FORCE - DRIVER SIDE

TABLE 4-1. RANGE OF STATIC INSTRUMENT PANEL FORCE-DEFLECTION CHARACTERISTICS

	Minimum Slope (lb/in)	Maximum Slope (lb/in)
Passenger Femur	35	420
Driver Femur	90	640
Passenger Torso	75	375
Passenger Head	38	300

TABLE 4-2. SUMMARY OF PERMANENT SET, ABSORBED ENERGY AND UNLOADING SLOPE DATA

G Values

	Head	Torso	Passenger Femurs	Driver Femurs
Minimum Value	.385	.292	.677	.687
Maximum Value	.999	.864	.966	.929
Mean	.652	.559	.853	.793
Std. Deviation	.163	.151	.073	.070

R Values

	Head	Torso	Passenger Femurs	Driver Femurs
Minimum Value	.0001	.072	.011	.034
Maximum Value	.266	.275	.142	.292
Mean	.133	.166	.071	.127
Std. Deviation	.069	.061	.042	.067

K Values

	Head	Torso	Passenger Femurs	Driver Femurs
Minimum Value	232	273	356	309
Maximum Value	7,638	2,435	4,414	5,075
Mean	1,559	1,086	2,035	2,305
Std. Deviation	1,616	675	1,030	1,174

screws along the top and side perimeter of the panel, while others have additional attachment brackets along the bottom. The geometry of the instrument panel may influence the data due to the amount of deflection before bottoming as well as the angle of contact between the body form and the surface. Shown in Figure 4-8 are two profiles of instrument panels that illustrate quite different geometry.

Noted on the data sheets in Appendix A are the material that the instrument panel was made of. The instrument panel construction could be categorized primarily into categories of: all metal, all plastic (or synthetic material), or a combination of both. Shown in Figure 4-9 is a photo of the LTD instrument panel which is primarily of hard plastic. The photo was the post test condition and illustrates the brittle nature of failure. In contrast, Figure 4-10 shows the Pinto instrument panel which is made of metal. The photo shows the instrument panel bends rather than fractures. However, there are still items that break, such as the hinge on the glove box door. The instrument panels that were part metal and part plastic usually consisted of a plastic dash with a metal top, such that of the Omni. Shown in Figure 4-11 is a post test picture of the Omni that illustrates the metal top panel and the soft plastic front panel. The soft plastics of the Omni contrasts with the hard plastic of the LTD in that it doesn't fail in a brittle manner. In comparing the force-deflection plots in Figure 4-12 the LTD shows a more irregular force plot due to cracking of the dash compared to the Pinto.

4.2 DYNAMIC INSTRUMENT PANEL TEST

The dynamic instrument panel tests were conducted on the same vehicles as the static tests. However, only the femurs and torso tests on the passenger side were conducted. Dynamic head tests were not conducted because the femur and torso tests typically caused a great deal of damage to the instrument panel such that there was little area left to impact. Since the data collected was acceleration time histories as described in Section 3, only the total femur force could be obtained from acceleration measurements. The force-deflection data calculated from the acceleration time histories are included on the standard data forms in Appendix B.

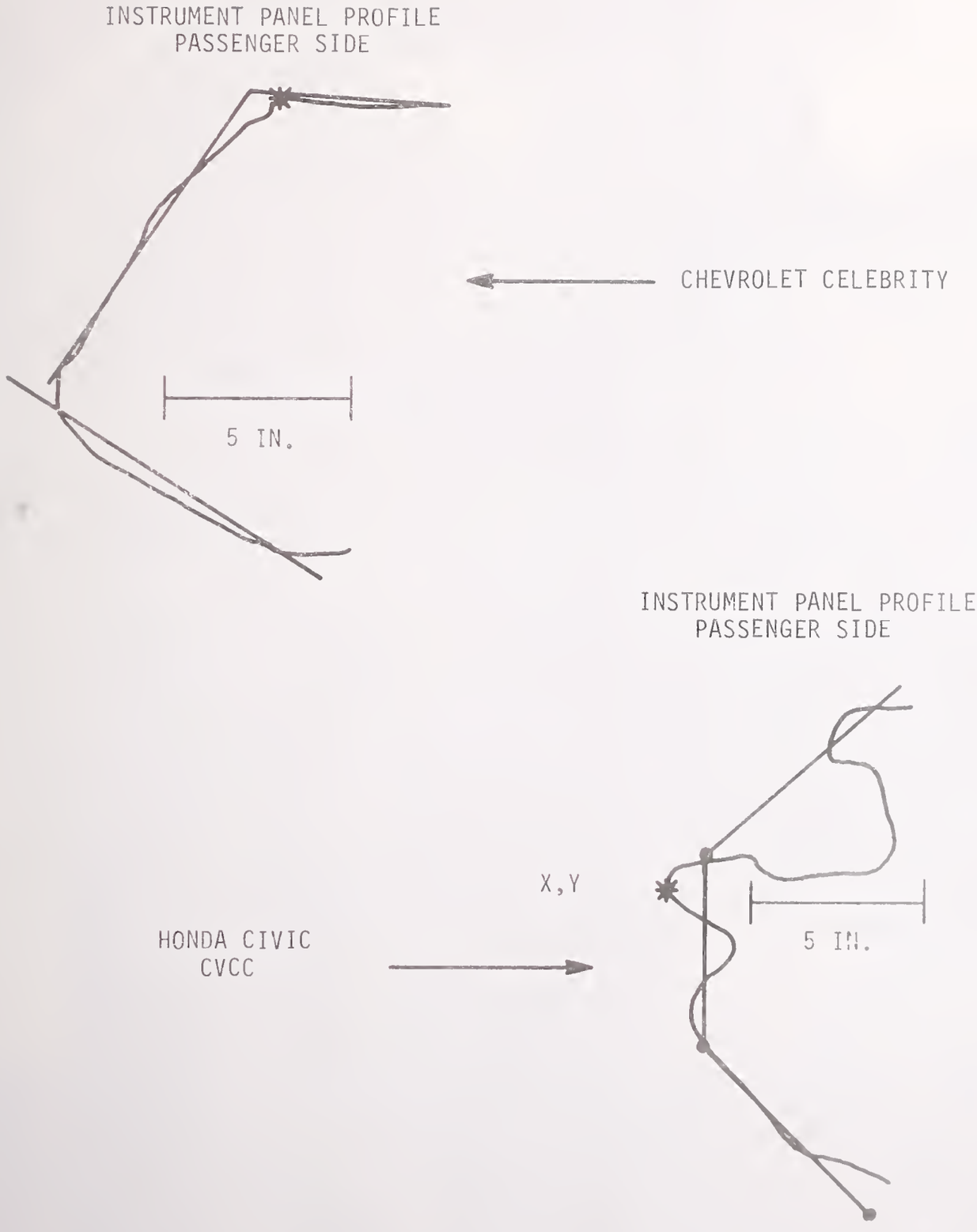

FIGURE 4-8. INSTRUMENT PANEL PROFILE COMPARISONS

FIGURE 4-9. PLASTIC INSTRUMENT PANEL (LTD)

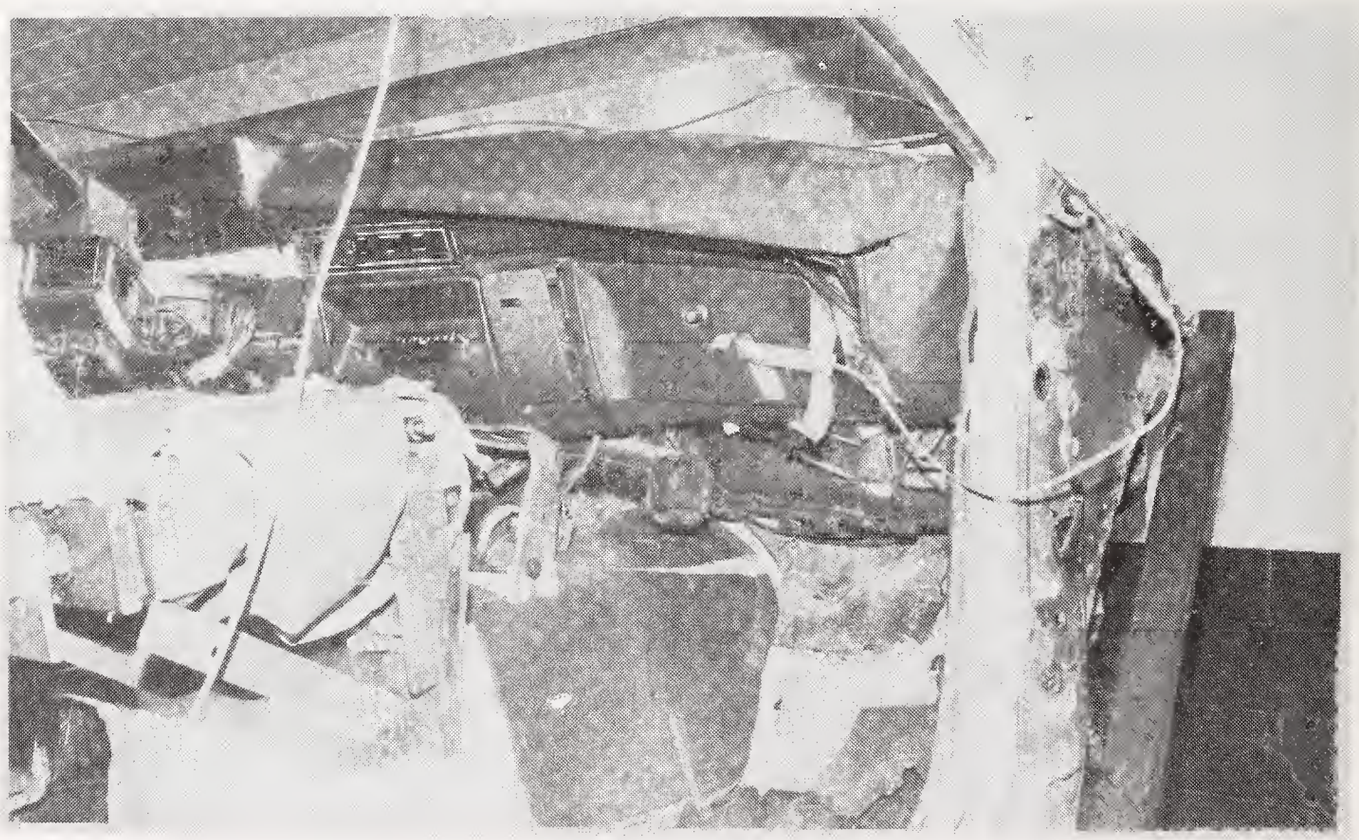

FIGURE 4-10. METAL INSTRUMENT PANEL (PINTO)

FIGURE 4-11. COMBINED PLASTIC AND METAL INSTRUMENT PANEL (OMNI)

Test: Head (static) Date: August 28, 1984

Vehicle: Ford LTD

Options: Air conditioning, radio missing

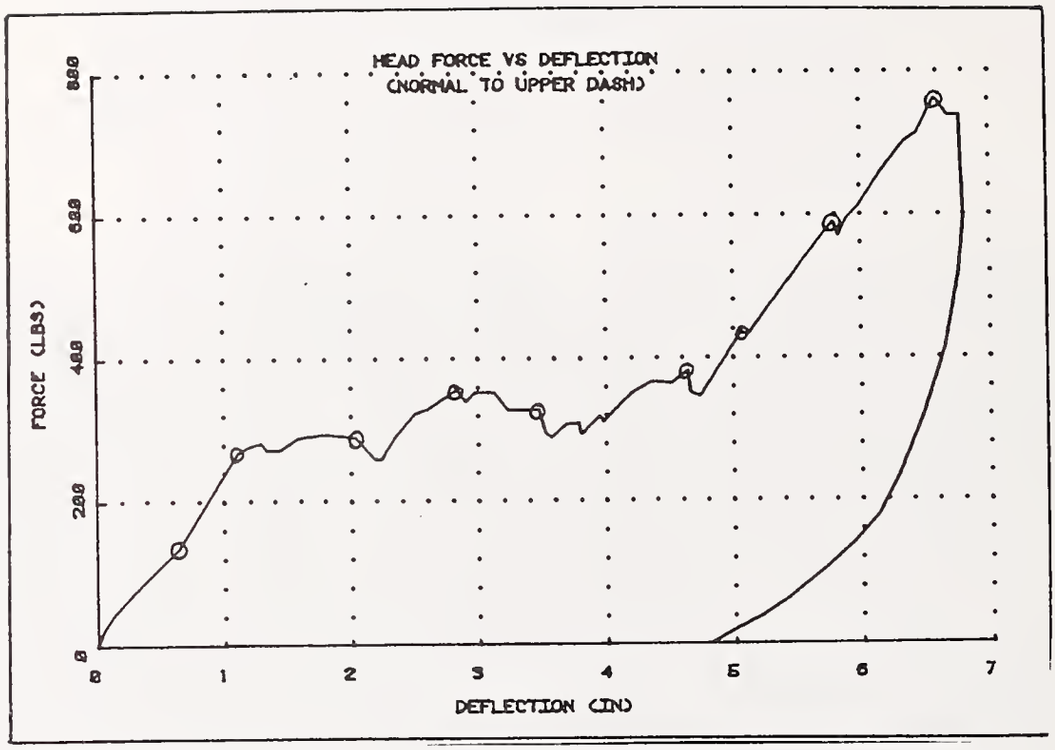

Test: Head (static) Date: September 11, 1984

Vehicle: Ford Pinto

Options: Metal dash with foam crash pad on top,

heat control and radio missing

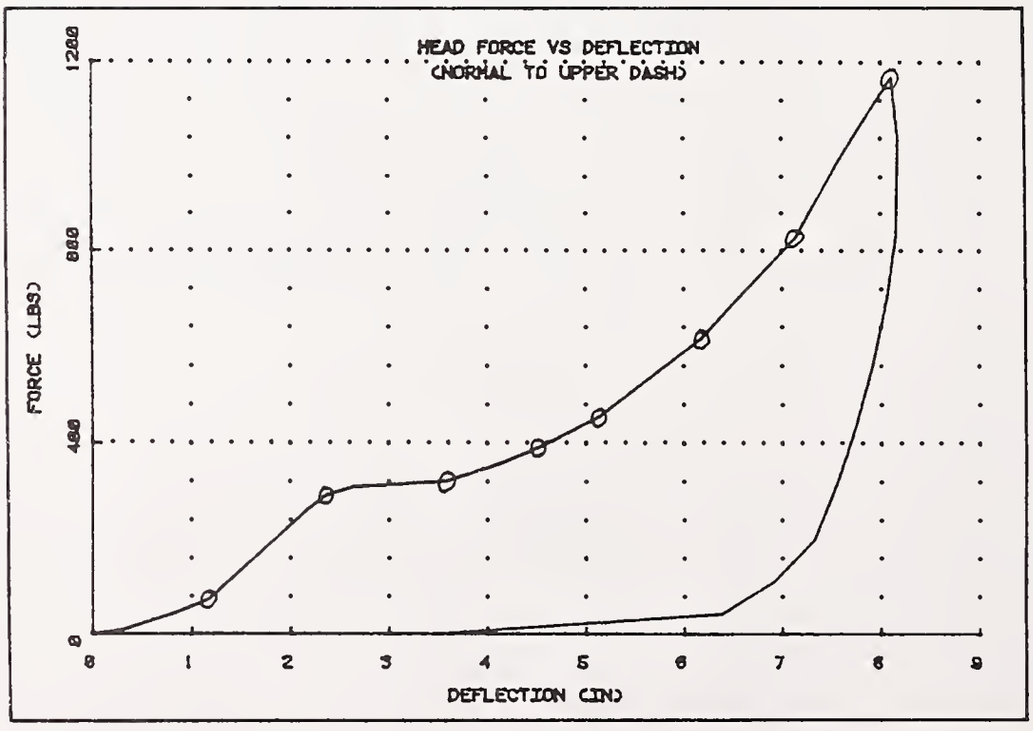

FIGURE 4-12. FORD LTD VS. FORD PINTO HEAD FORCE-DEFLECTION COMPARISON

Shown in Figures 4-13 and 4-14 are overplots of the dynamic femur and torso instrument panel data. As with the static data, these overplots are included to illustrate the range of the data across all the vehicles. Dynamic data shown are filtered at a corner frequency of 100 Hz.

The dynamic data generally show an inertial effect upon impact characterized by a quicker rise in force level compared to the static data which had a more gradual rise in force level. The torso data tends to show a continuously increasing force level while the femur data tends to level out after the initial rise and then rises again at bottoming.

Figures 4-15 through 4-22 contain a selection of force-deflection data comparisons for several of the vehicles tested. Contained in each figure is an overplot of the dynamic and static data for either the femur or torso test. There are several characteristics of the data that do not correlate between the static and dynamic tests consistently across all the vehicles tested. There may be several reasons for these inconsistences such as the material of the instrument panel, material failure modes, etc. that may only be identifiable through further in-depth study of the instrument panel construction.

There are several cases where the static and dynamic force levels are nearly the same, such as the Monza torso, Volare torso and the Omni femur tests. However, there are others such as the Volare femur, Omni torso and Pinto torso tests that show considerable difference between the static and dynamic data. Generally, where there are differences the dynamic data shows higher force level that the static, as would be expected due to loading rate sensitivity. However, for the LTD and Chevette femur tests, the static data is somewhat higher. The reasons for this type of difference are not readily apparent.

In all dynamic tests, care was taken to duplicate test conditions of the static tests. That is, undamaged instrument panels were used and were secured to the cowl in a manner consistent with the original panel. Components inside the dash were duplicated as closely as possible if they were thought to influence measurements. Nevertheless, damage induced by previous tests, internal components or instrument panel attachment brackets and missing or poorly connected components (i.e., instrument cluster, radio, speaker, etc.) may be the source of some data inconsistencies. It is also thought that differences in material failure modes may

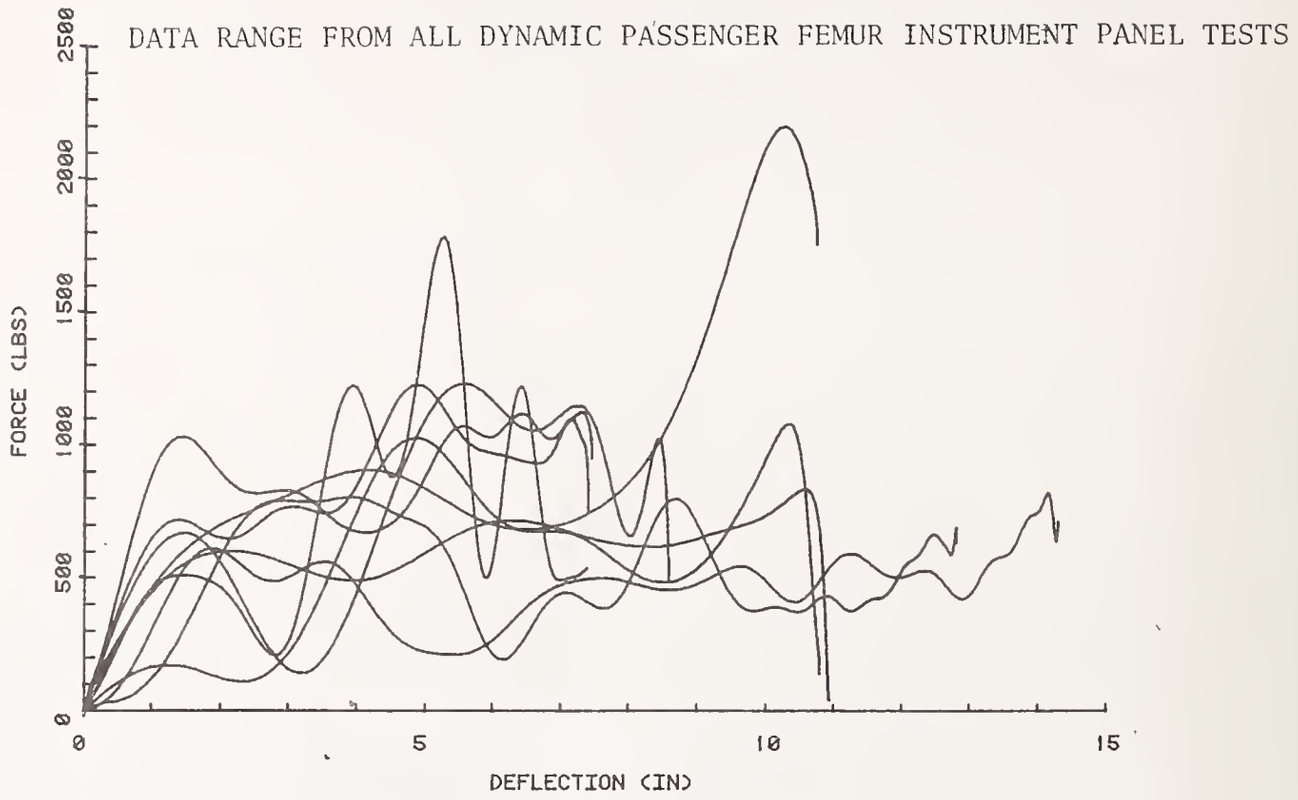

FIGURE 4-13. DYNAMIC FEMUR TEST DATA RANGE

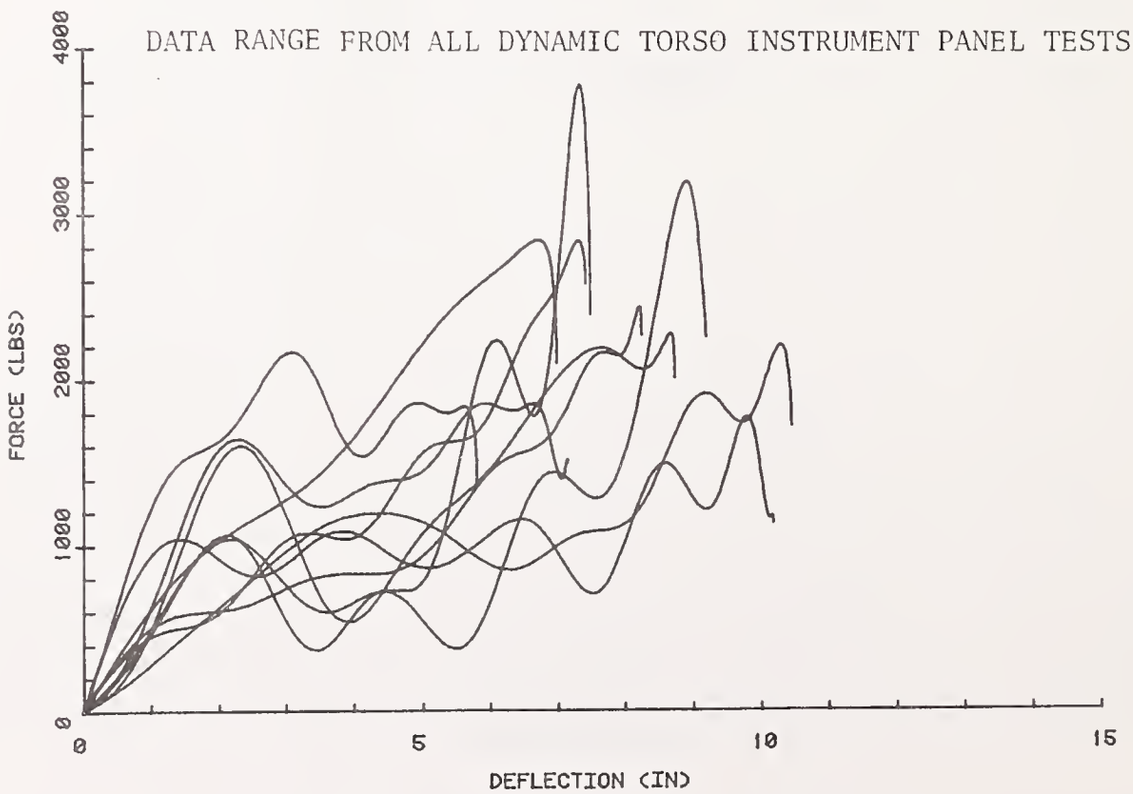

FIGURE 4-14. DYNAMIC TORSO TEST DATA RANGE

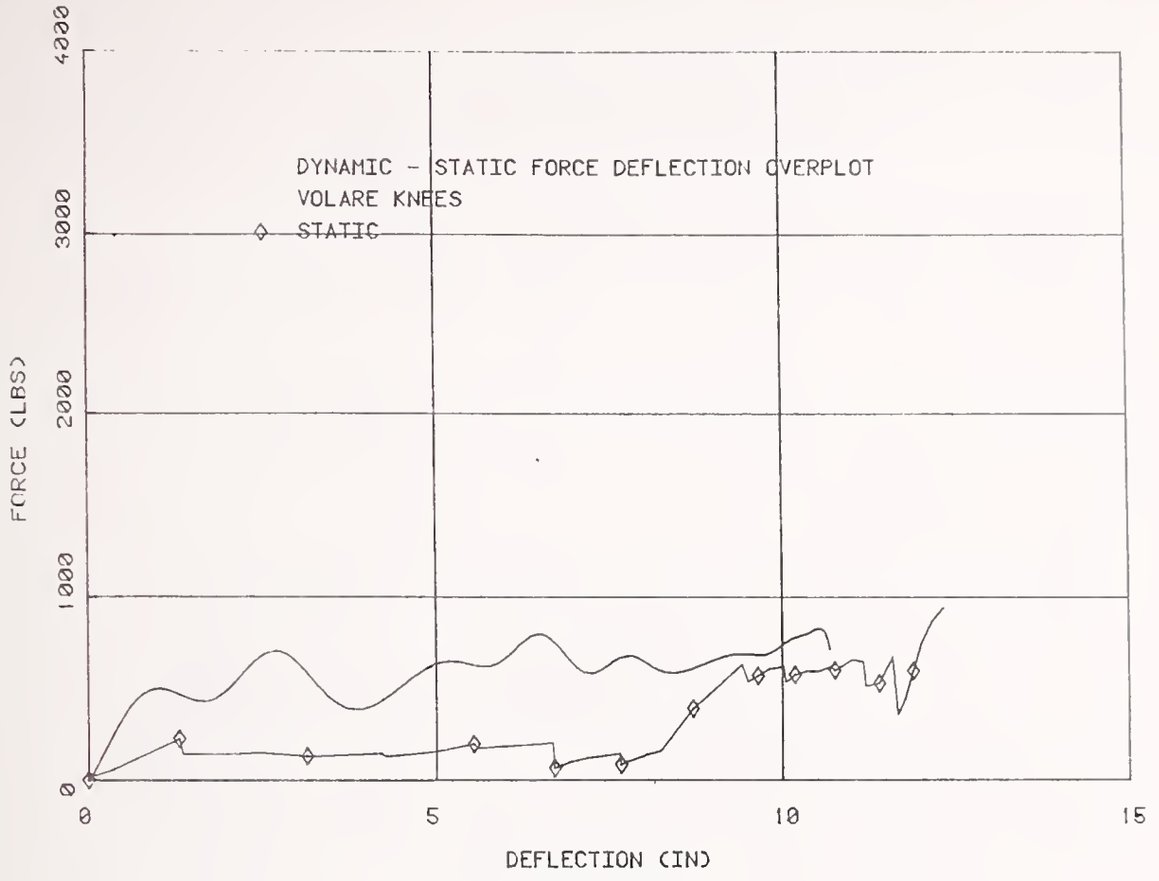

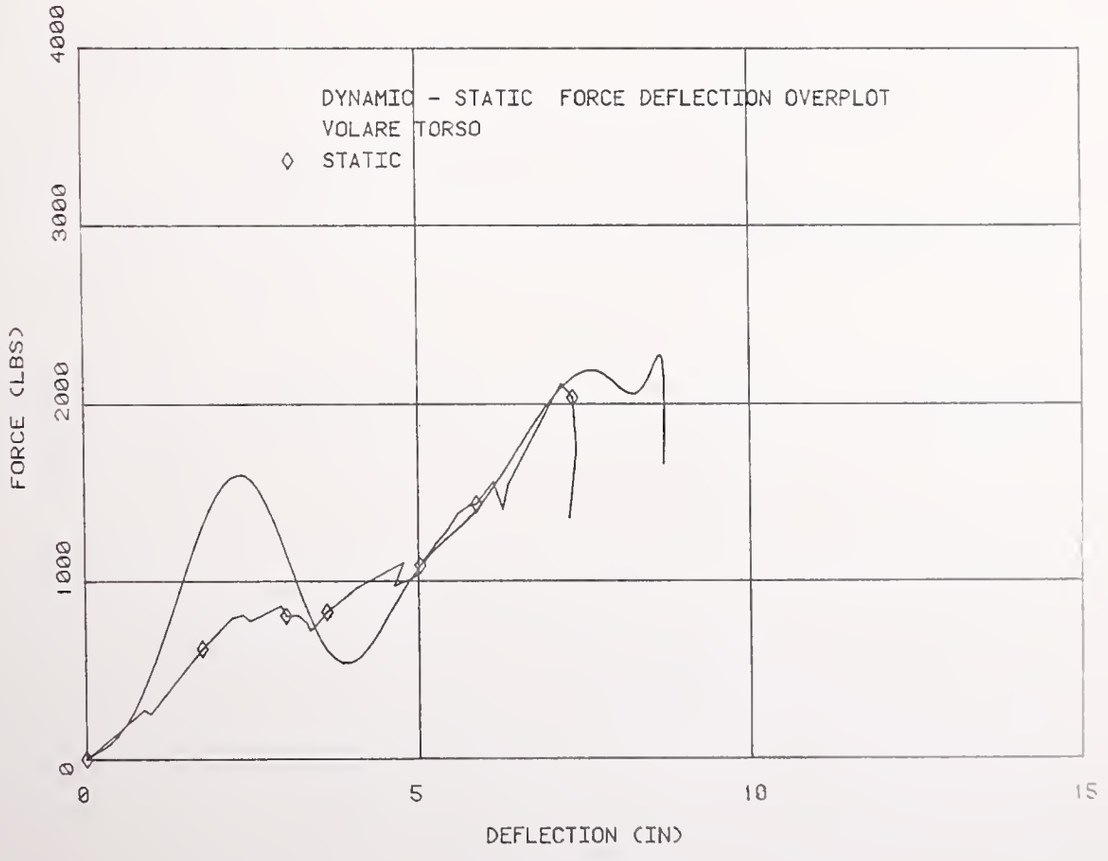

FIGURE 4-15. VOLARE DYNAMIC/STATIC DATA COMPARISON

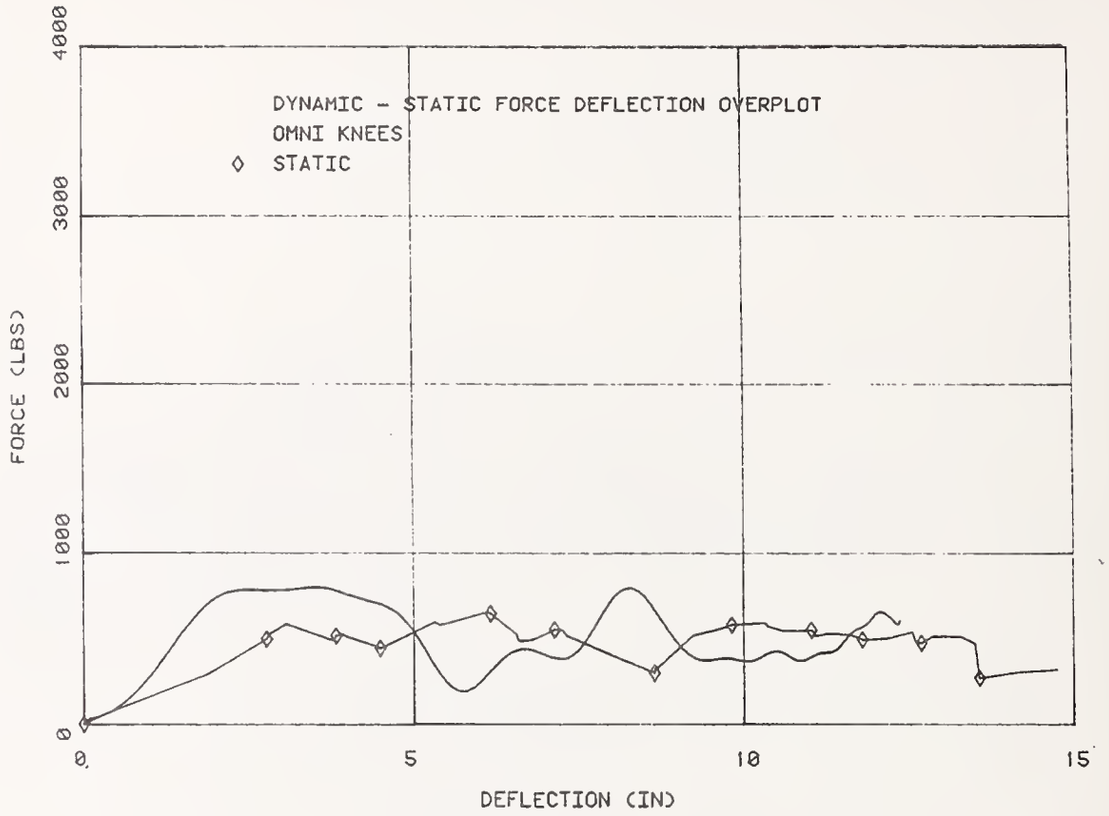

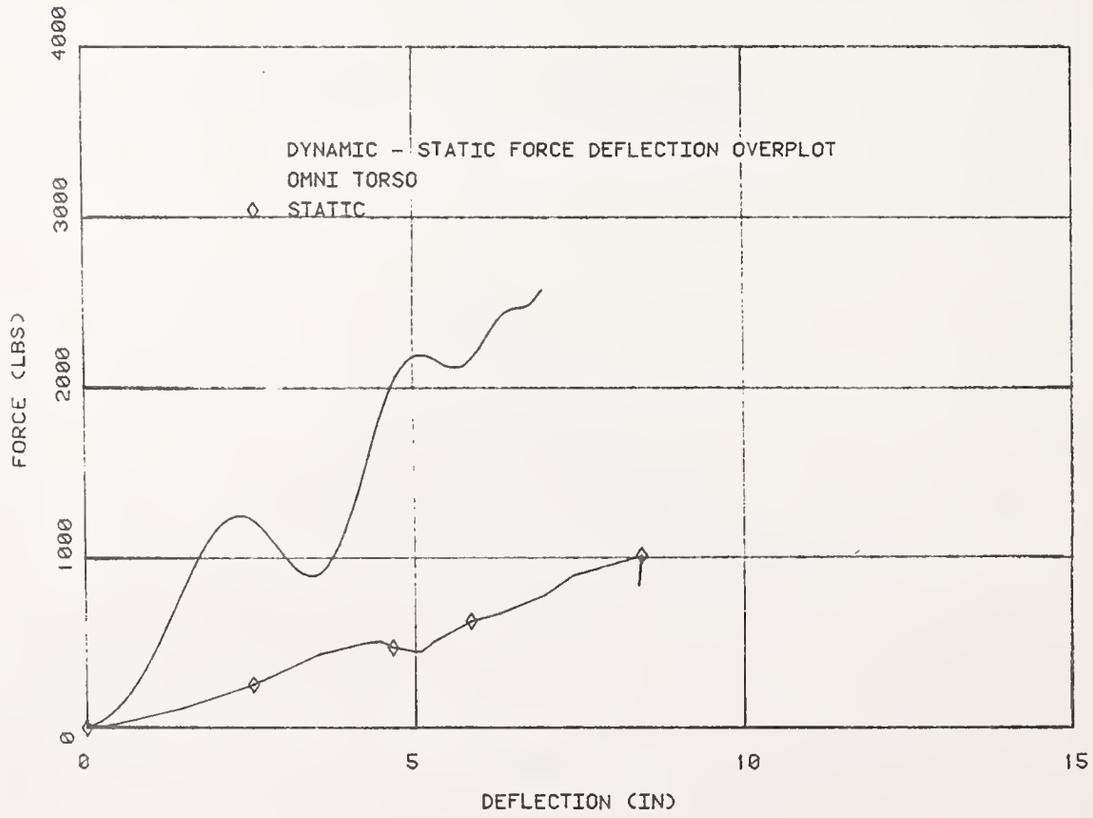

FIGURE 4-16. OMNI DYNAMIC/STATIC DATA COMPARISON

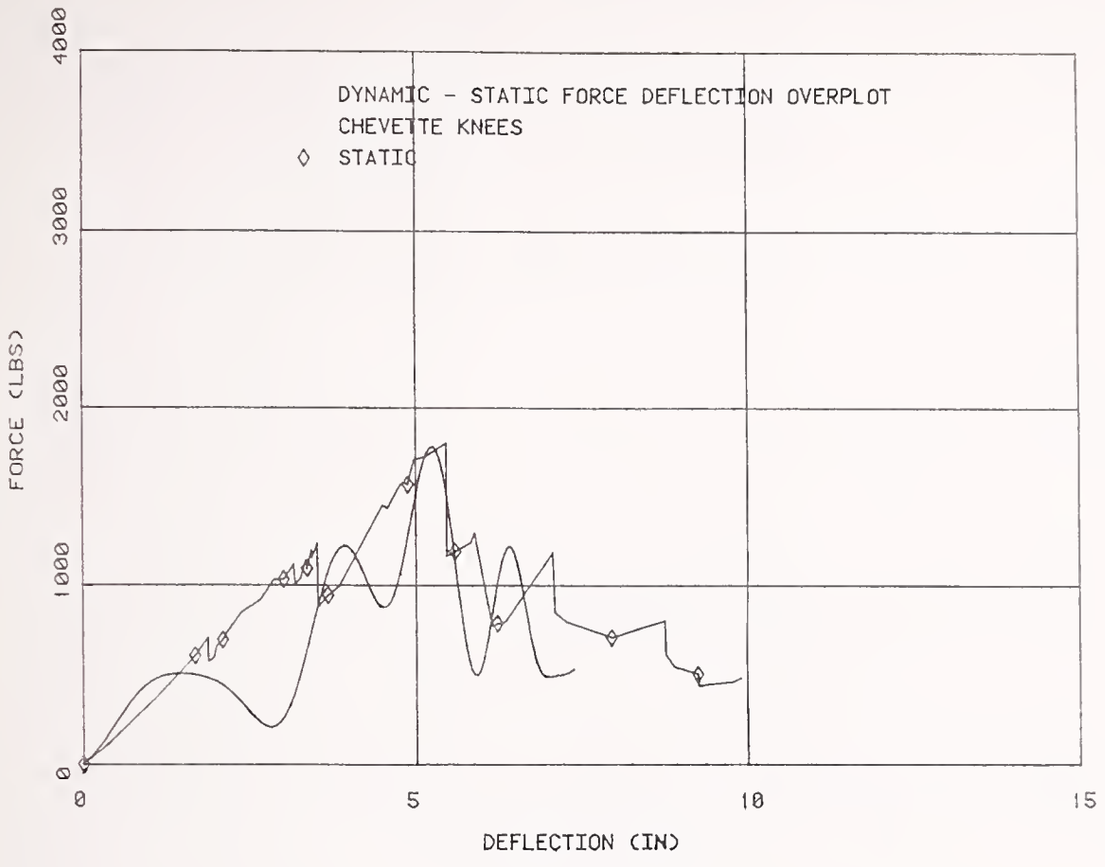

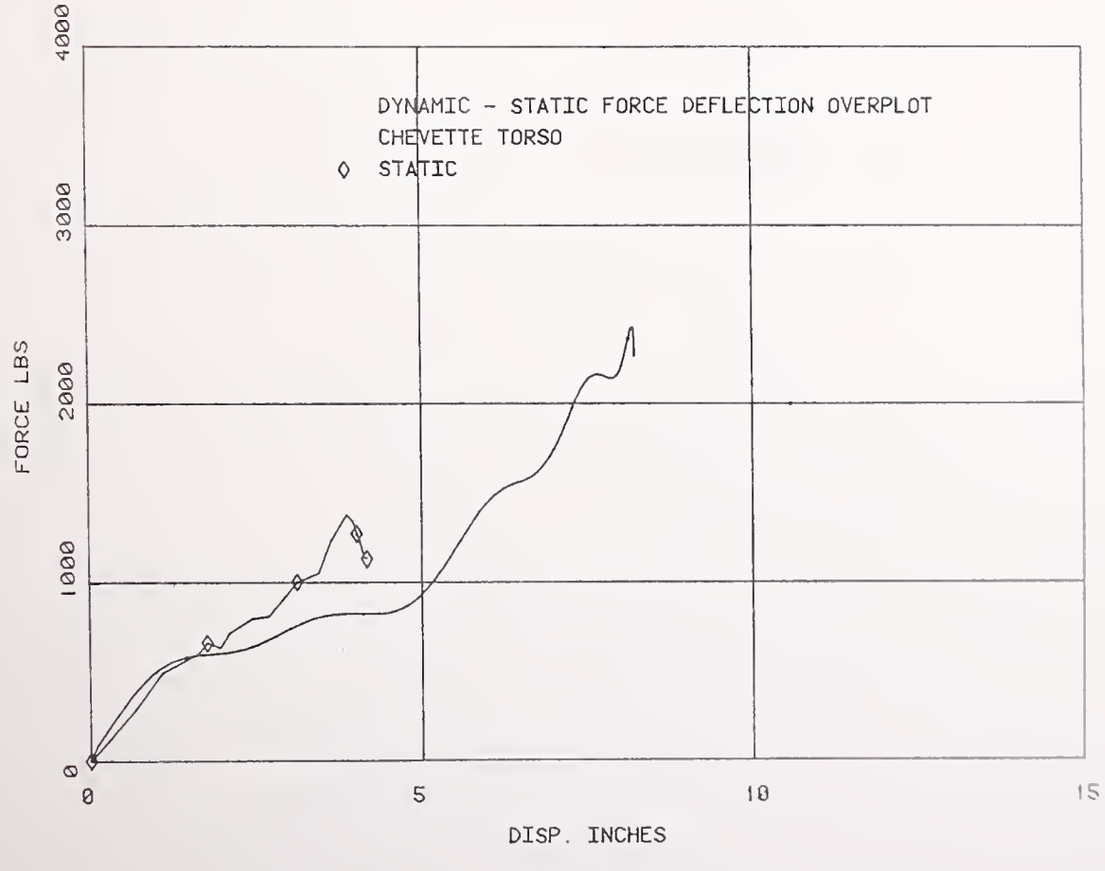

FIGURE 4-17. CHEVETTE DYNAMIC/STATIC DATA COMPARISON

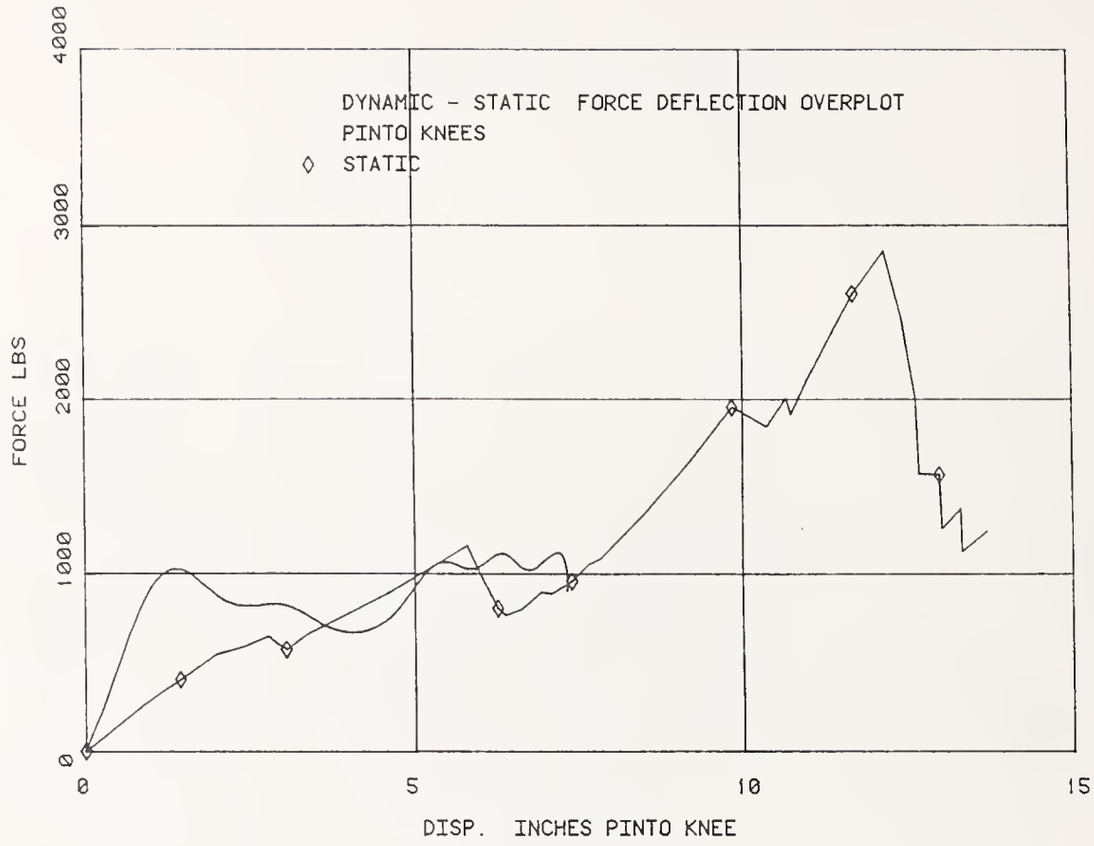

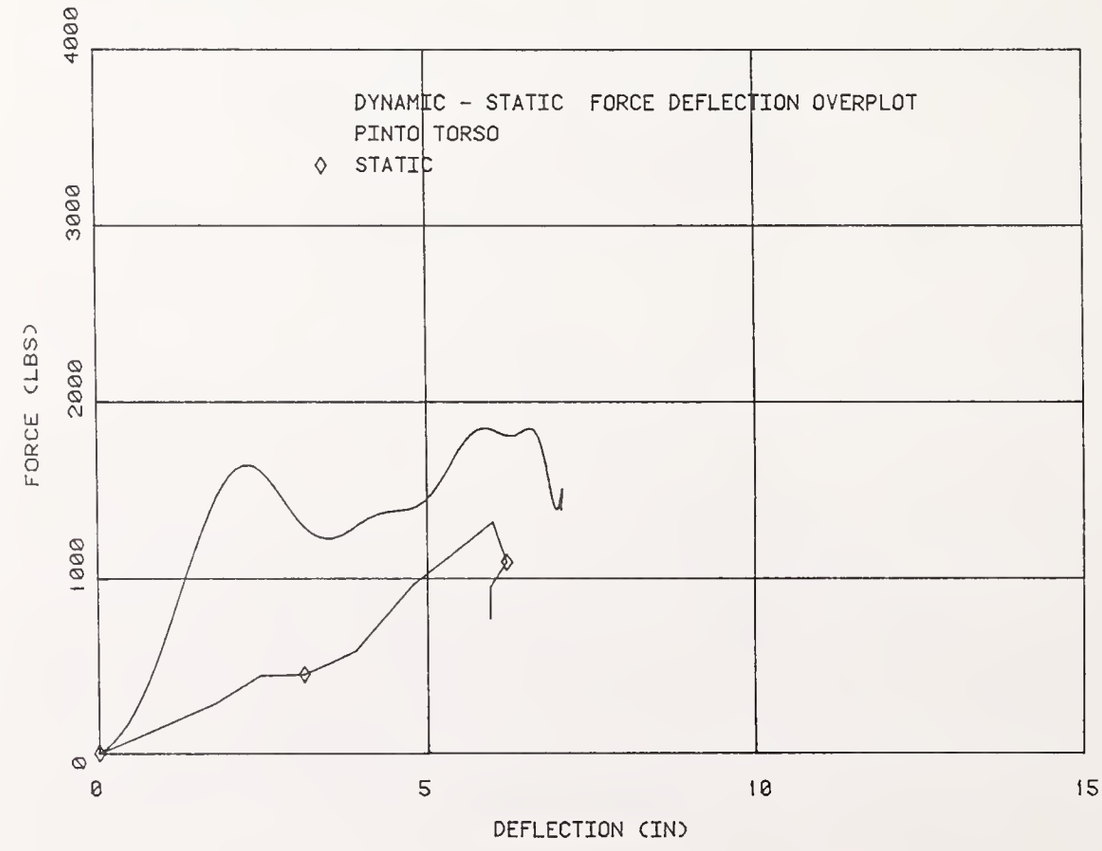

FIGURE 4-18. PINTO DYNAMIC/STATIC DATA COMPARISON

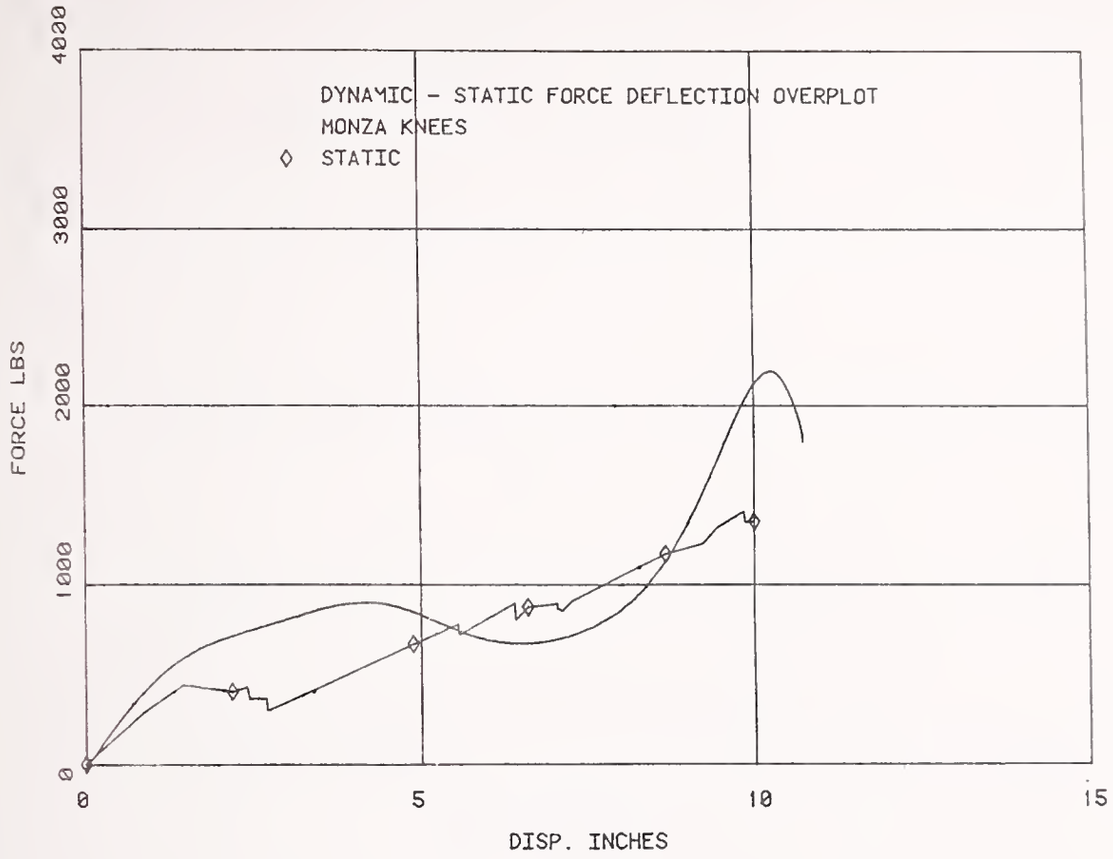

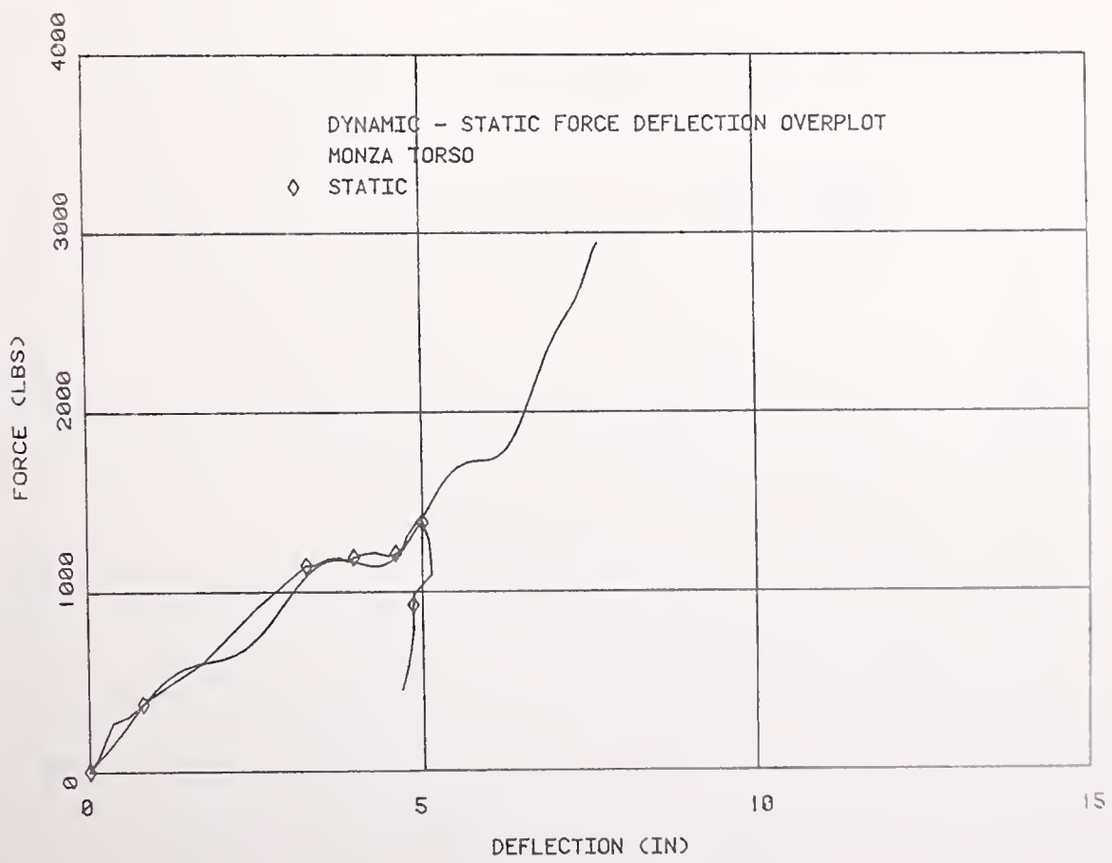

FIGURE 4-19. MONZA DYNAMIC/STATIC DATA COMPARISON

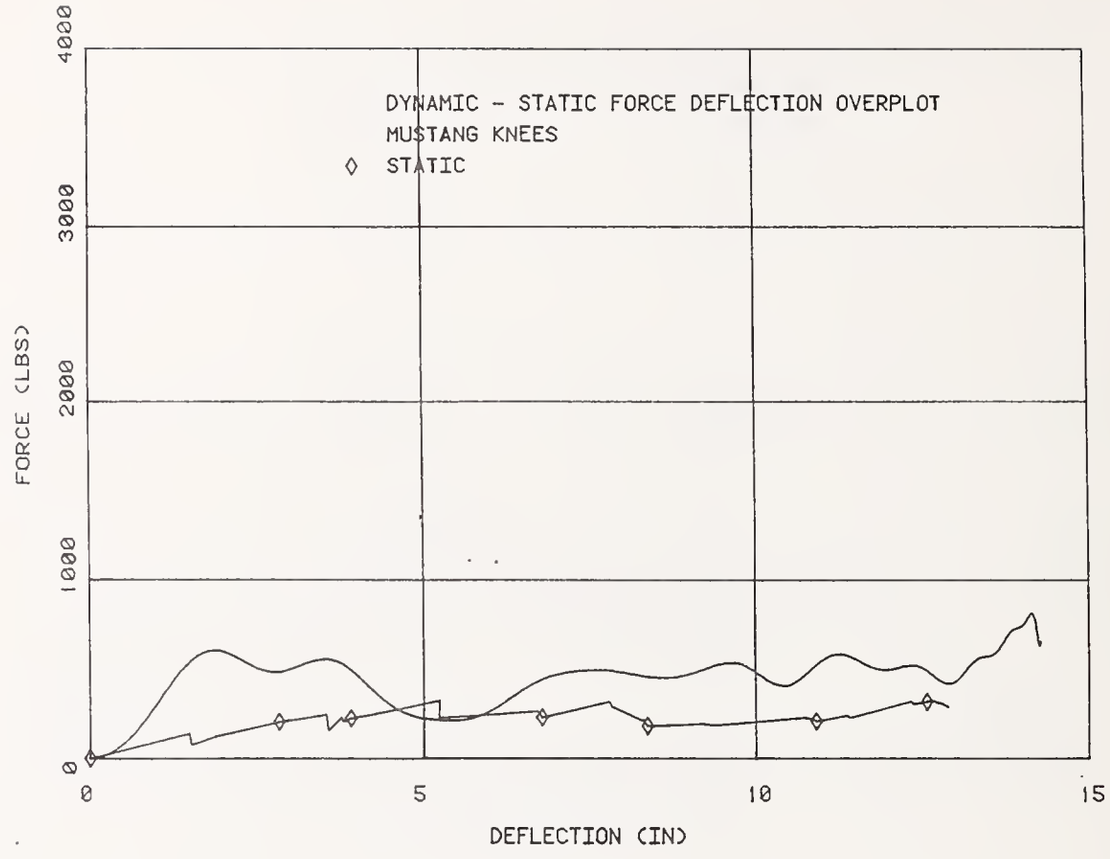

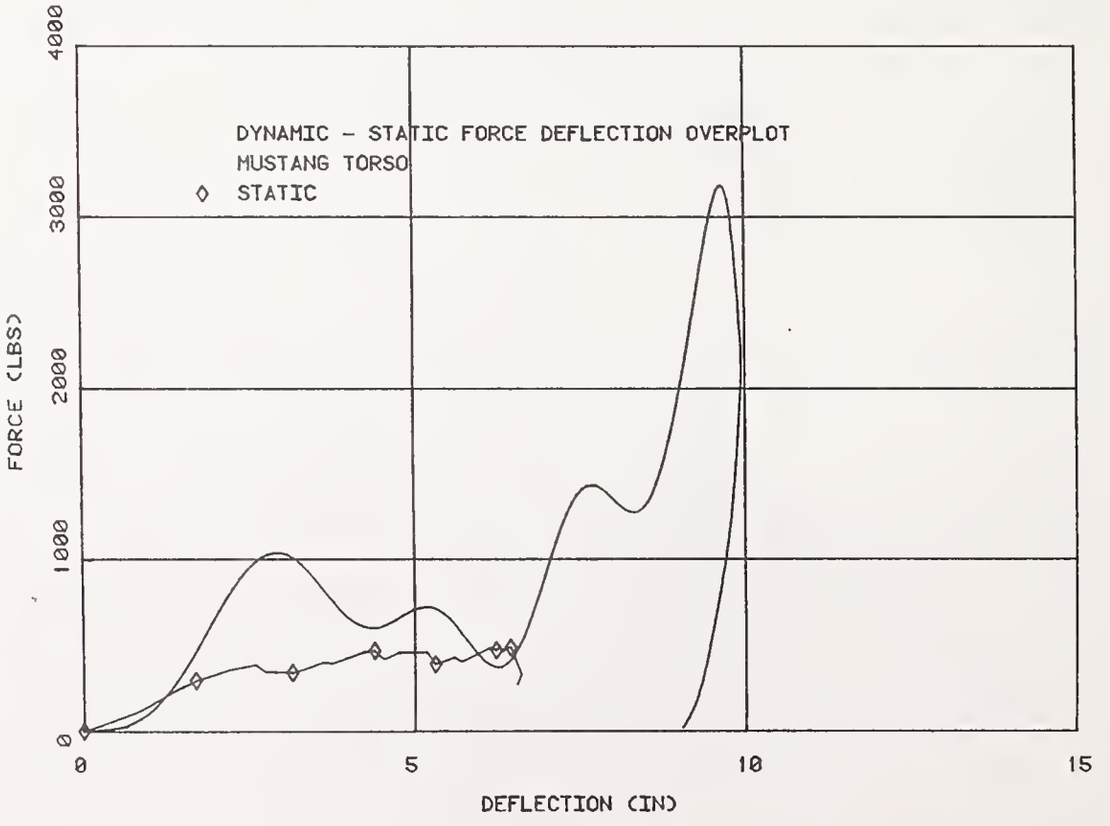

FIGURE 4-20. MUSTANG DYNAMIC/STATIC DATA COMPARISON

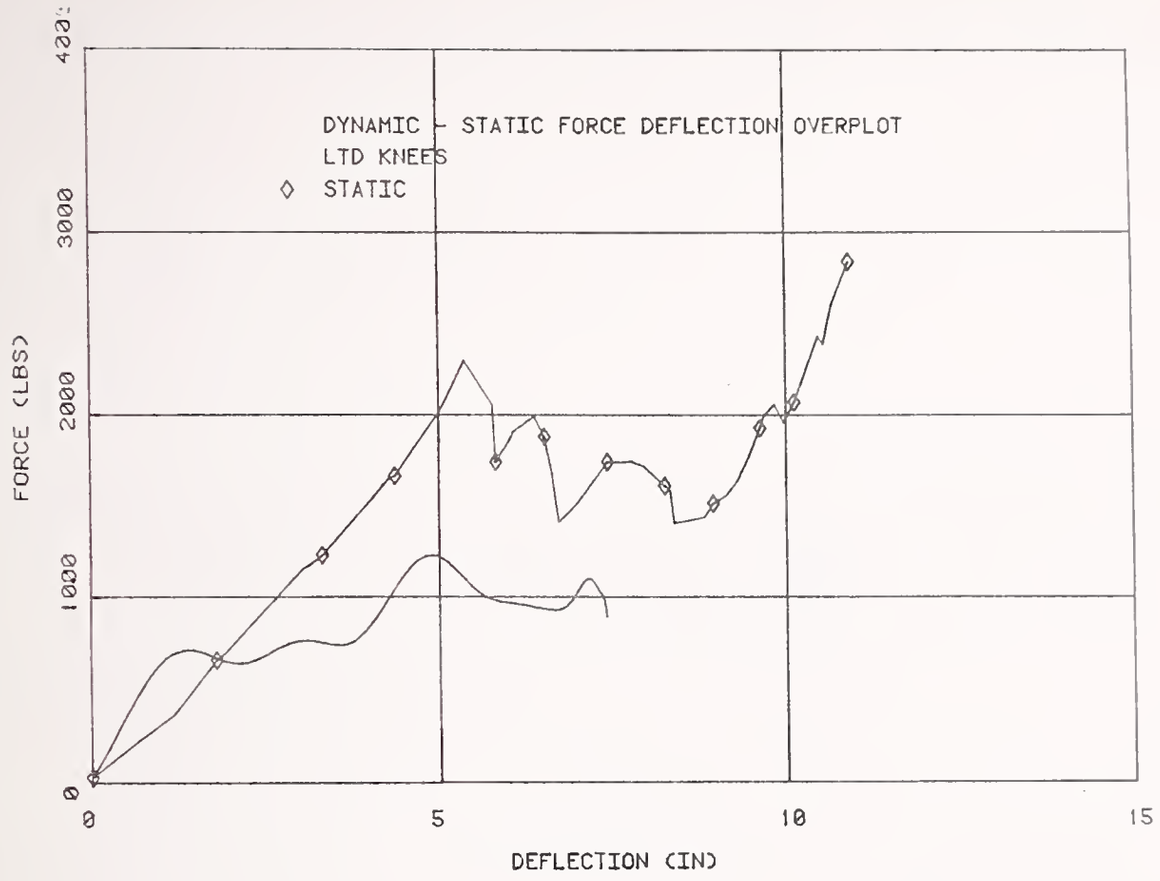

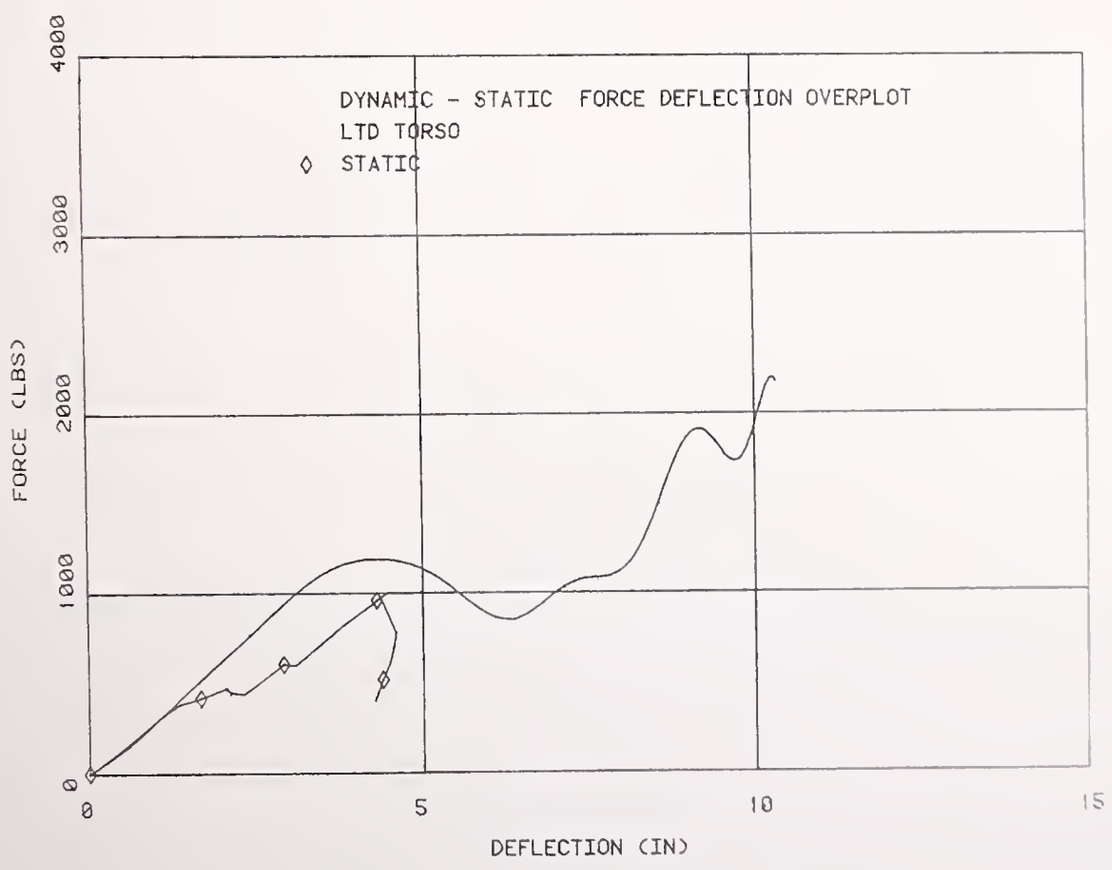

FIGURE 4-21. LTD DYNAMIC/STATIC DATA COMPARISON

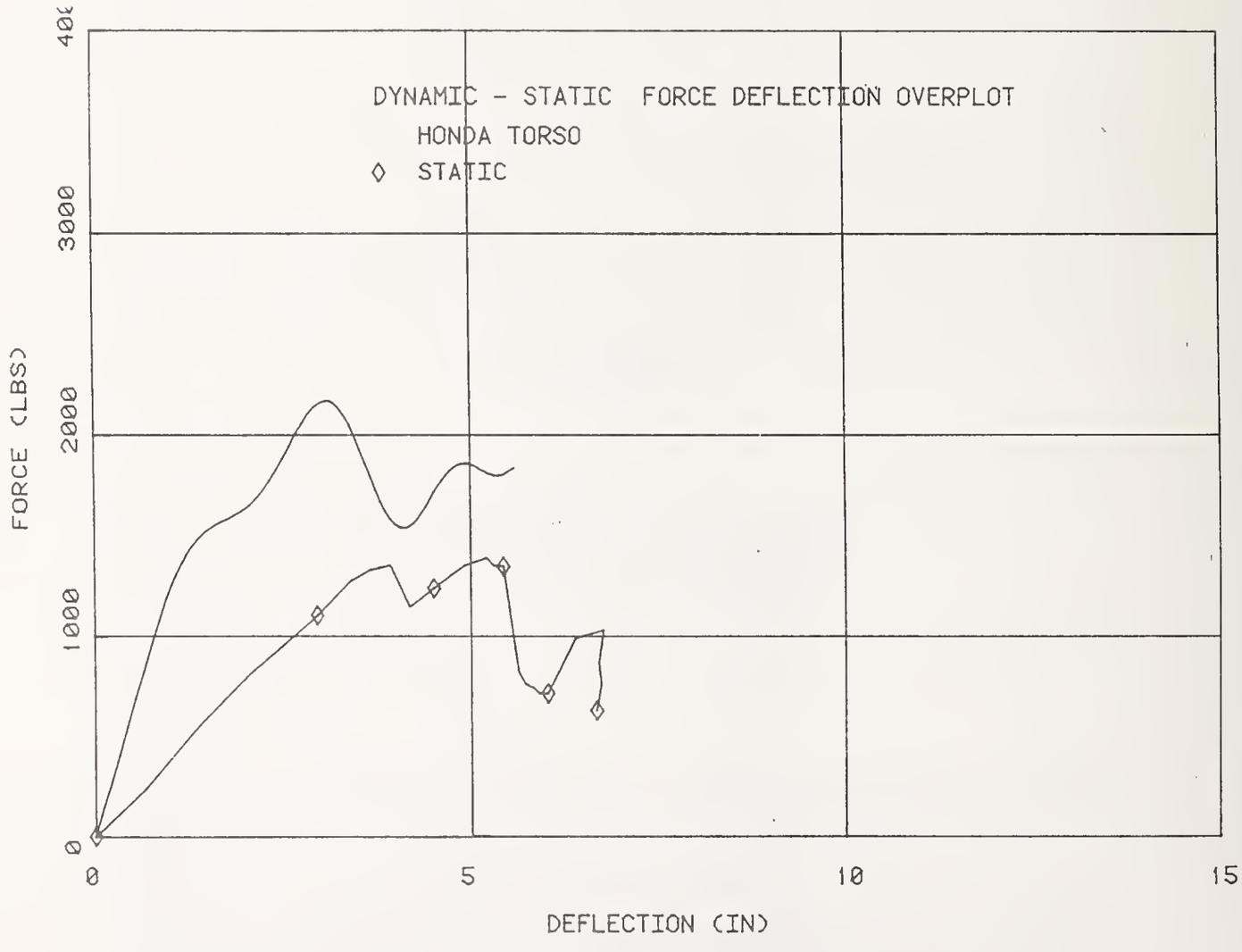

FIGURE 4-22. HONDA DYNAMIC/STATIC DATA COMPARISON

well be a principal source of such differences between static and dynamic data. This is an area that should be investigated further.

It can be noted, however, that the dynamic femur data for the Chevette shows the same general characteristics of the static data, which had no rise in force due to bottoming. This contrasts with the Mustang torso test which had considerable bottoming forces in the dynamic test and more in the static test. For the Mustang test, the higher force level in the dynamic data are primarily due to a greater penetration compared to the static test.

Average viscous damping factors for those tests in which the absorbed energy was larger in the dynamic tests as compared to the static tests was also calculated. This was done by assuming the absorbed energy difference was attributed to an average viscous damping coefficient. The value of the coefficient was calculated by:

$$\overline{C} = \frac{E_D - E_S}{\overline{V}}$$

Where:

E_D and E_S are the absorbed energy at a common deflection representing the lesser of the maximum deflection of the dynamic and static test data, respectively.

$\overline{V}$ is the average velocity of the impactor over the common deflection.

$\overline{C}$ is the average viscous damping coefficient.

A summary of the average damping coefficient computed by this means is provided in Table 4-3. Note that in those cases where the absorbed energy in the static test was larger than that in the dynamic test, a meaningful damping factor is not available and is therefore not provided in the table.

TABLE 4-3. AVERAGE INSTRUMENT PANEL DAMPING COEFFICIENTS

Vehicle	Damping Coefficient (lb-sec/in) Femur Test	Torso Test
Chevette	N/A(1)	N/A(1)
Monza	0.62	0.345
Mustang	1.01	0.69
Pinto	0.64	2.51
Omni	0.16	2.94
Volare	1.55	0.57
Civic	N/A(2)	2.60
LTD	N/A(2)	0.66
Celebrity	1.19	N/A(1)
LeSabre	N/A(1)	1.51
LeSabre (driver side)	1.34	

(1) If the energy absorbed in the static test exceeds that absorbed in the dynami test for equal deflections, then the technique used to calculate average damping results in a negative factor. In this instance, the computed value was omitted. The dynamic to static effect was further investigated with simulated mild steel panel and these results are presented in the following reference:

Griffith, D.G., "Design and Procedure Verification of Dynamic Instrument Pane Testing", Contract No. DTRS-57-84-C-00003, MGA Report No. G85A12-V-1, January 1986.

(2) Test data not available.

4.3 STATIC WINDSHIELD TESTS

The initial windshield tests conducted under Technical Task Directive Number 7 consisted of static horizontal tests on the vehicles indicated in the test matrix of Table 3-1. The data from these tests are included on the standard data forms in Appendix C. It was believed that the results from these tests were not representative of typical dynamic force-deflection properties of windshields. Shown in Figure 4-23 is the force-deflection data for the Honda Civic which is typical of the static data for all the vehicles. The force rose up to its peak force in less than two inches before the windshield broke and then dropped off. The force then remained fairly constant as the headform continued moving. Shown in Figures 4-24A and B are photographs of a typical static windshield test. As can be seen in photos, there is a great deal of disbonding around the perimeter of the windshield, which is not usually seen in dynamic windshield impacts. This appeared to be caused by the development of a vertical crack in the windshield which initiated disbonding at the header area. Windshield separation then continued at low head force levels without the characteristic "spider-web" pattern generally associated with windshield impacts.

In an effort to determine the force-deflection relationship for a dynamic impact, a pneumatic impactor was designed and built and used to conduct further tests on windshields. The results from these tests are discussed in the next section.

4.4 DYNAMIC WINDSHIELD TESTS

Dynamic windshield tests were conducted on the initial group of eight vehicles as well as the second group of ten vehicles. The first eight vehicles were tested with a test procedure consisting of a horizontal impact while the second set of tests consisted of impacts which were perpendicular to the windshield. The reason for the change to the normal impacts for the production tests was the nature of the data collected during the horizontal tests. Figure 4-25 is a deceleration time history for the Volare horizontal windshield test, which is typical of all the horizontal tests. The initial portion of the time history, where the deceleration is negative, represents the acceleration of the impact device up to speed. The impact occurred just before 0.05 seconds as indicated on the plot. However, just following the impact, there is a negative deceleration spike.

Windshield DOT #: 20 M 355 Ambient temperature during test: 66°

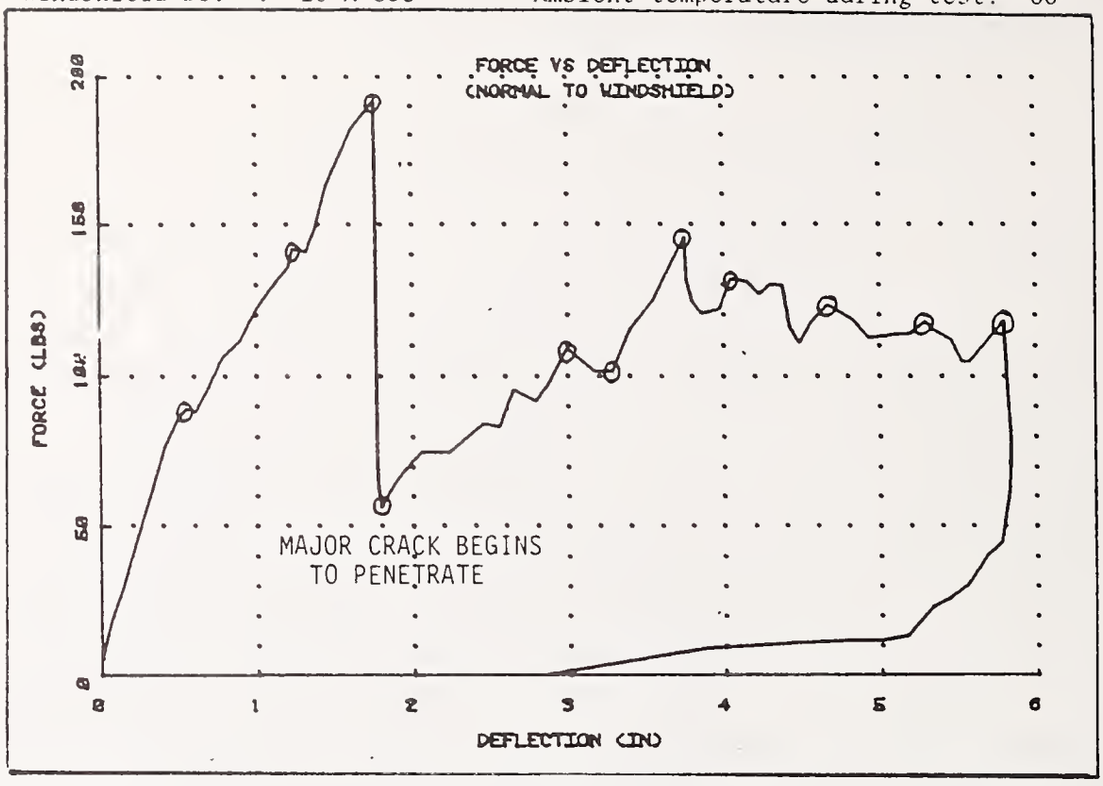

FIGURE 4-23. HONDA CIVIC STATIC WINDSHIELD FORCE-DEFLECTION

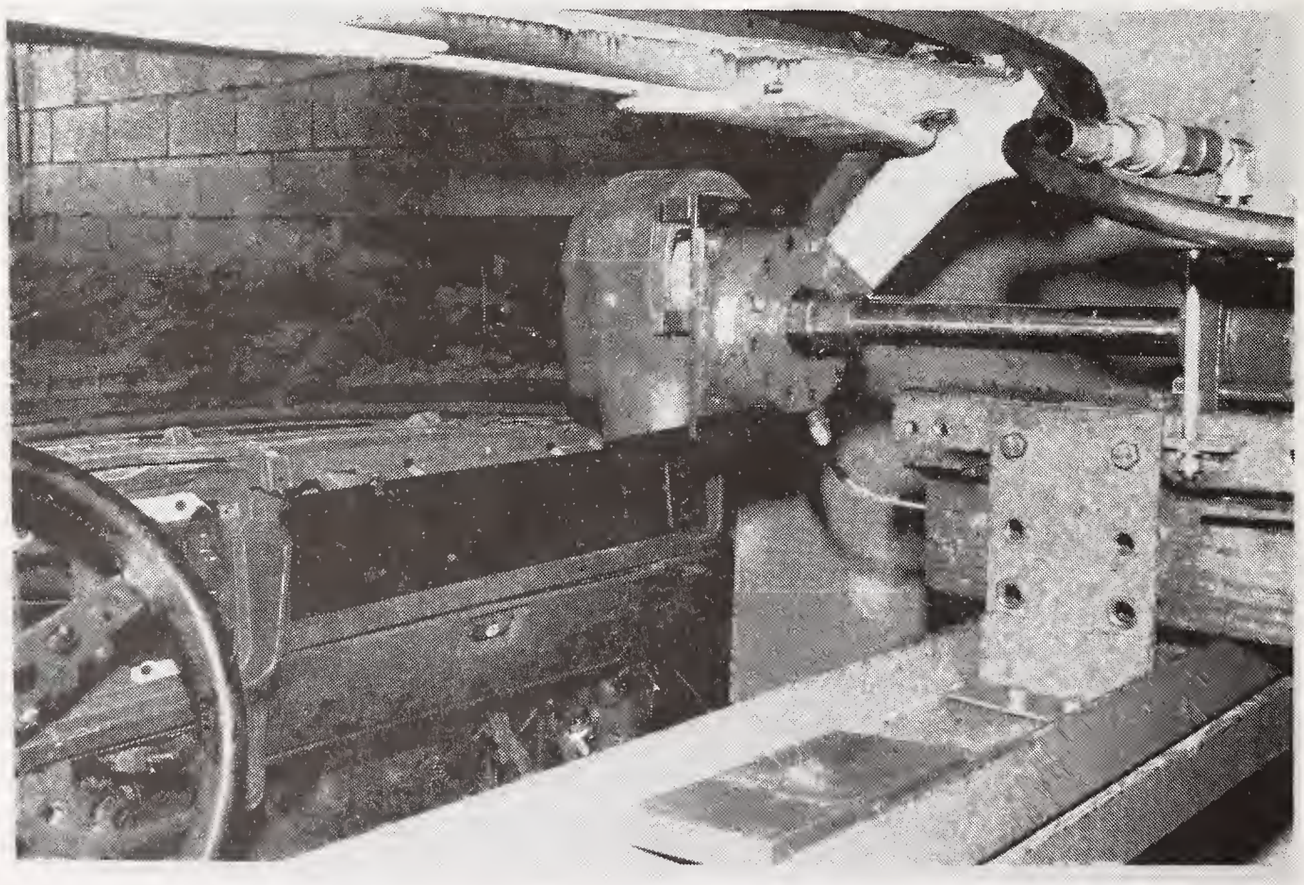

FIGURE 4-24A. TYPICAL STATIC WINDSHIELD TEST (INTERIOR VIEW)

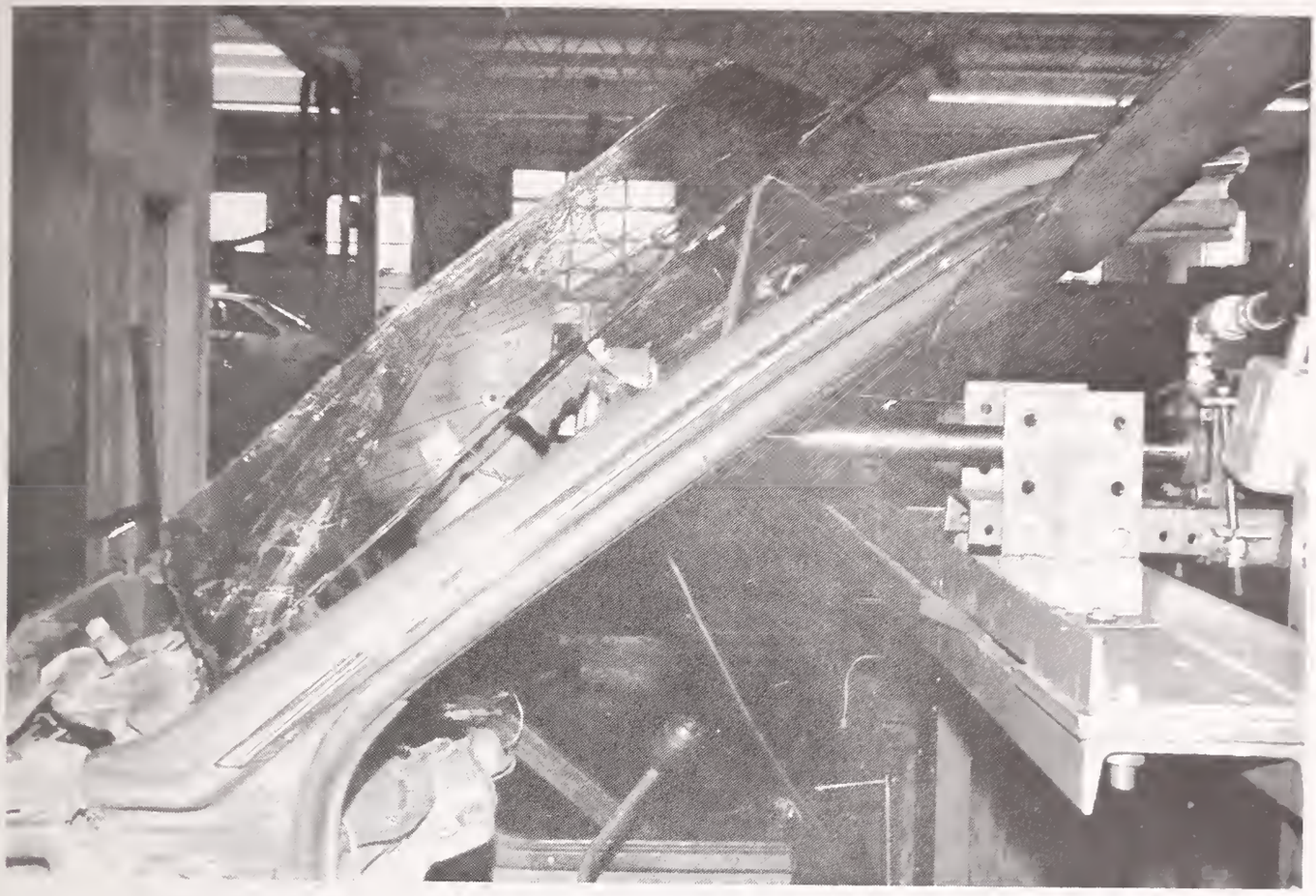

FIGURE 4-24B. TYPICAL STATIC WINDSHIELD TEST (EXTERIOR VIEW)

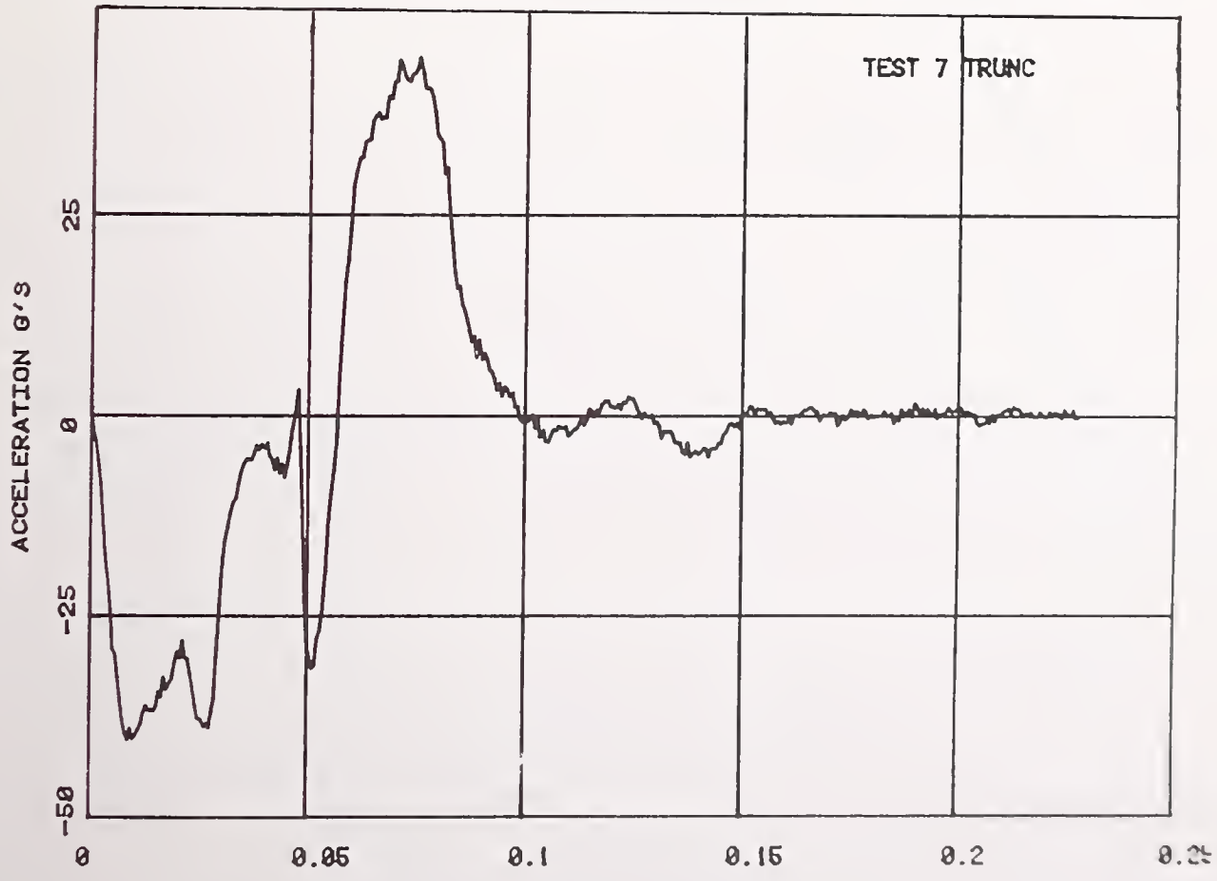

FIGURE 4-25. TYPICAL HORIZONTAL WINDSHIELD TEST DATA

Analysis of these test data resulted in two possible explanations for the negative deceleration spike which was in the opposite direction from the inertial spike typically expected during dynamic windshield impacts. First, it was hypothesized that rotation of the headform may have occurred early in the impact due to the non-axial force applied. Second, it was believed that the plate attaching the headform to the impactor shaft lacked sufficient rigidity resulting in a coupled tow mass system. As a result, the test set-up was changed to a perpendicular impact with a more rigid headform mounting plate for the remainder of the windshield tests.

Since a negative inertial spike would result if the acceleration time history was processed from the time of impact, the data was truncated and integrated from the point just after the negative deceleration spike, as indicated in Figure 4-25. The force deflection plots for the horizontal impacts calculated using this truncated data are presented in Figure 4-26 through 4-29. While the truncating procedure results in a calculated peak deflection that doesn't correspond to the measured value, these plots are believed suitable for comparing the peak penetration levels for the various windshields. Shown in Figure 4-30 is a photo of typical post-test damage to the windshield.

The data from the perpendicular windshield tests are included in Appendix D on the standard forms. Enclosed in Figure 4-31 is an acceleration time plot for the Cordoba normal windshield test, and the resulting force-deflection plot. The acceleration plot, typical of the normal tests, shows the event from the time of impact, and has been filtered at a corner frequency of 300 Hz. This data shows a positive inertial spike, as expected, in contrast to the results seen in the previous horizontal impact tests. Consequently, elimination of the potential for headform rotation and stiffening the headform mounting plate corrected the problem. Shown in Figure 4-32 is a photograph of a typical post test condition of a windshield.

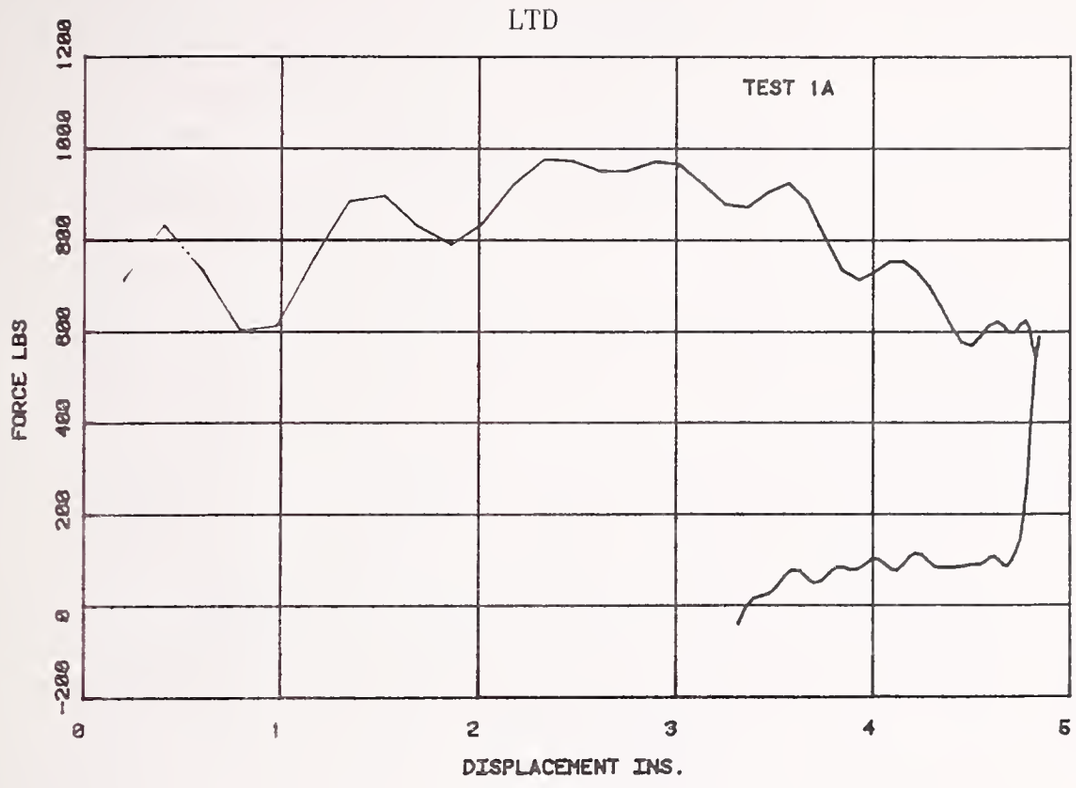

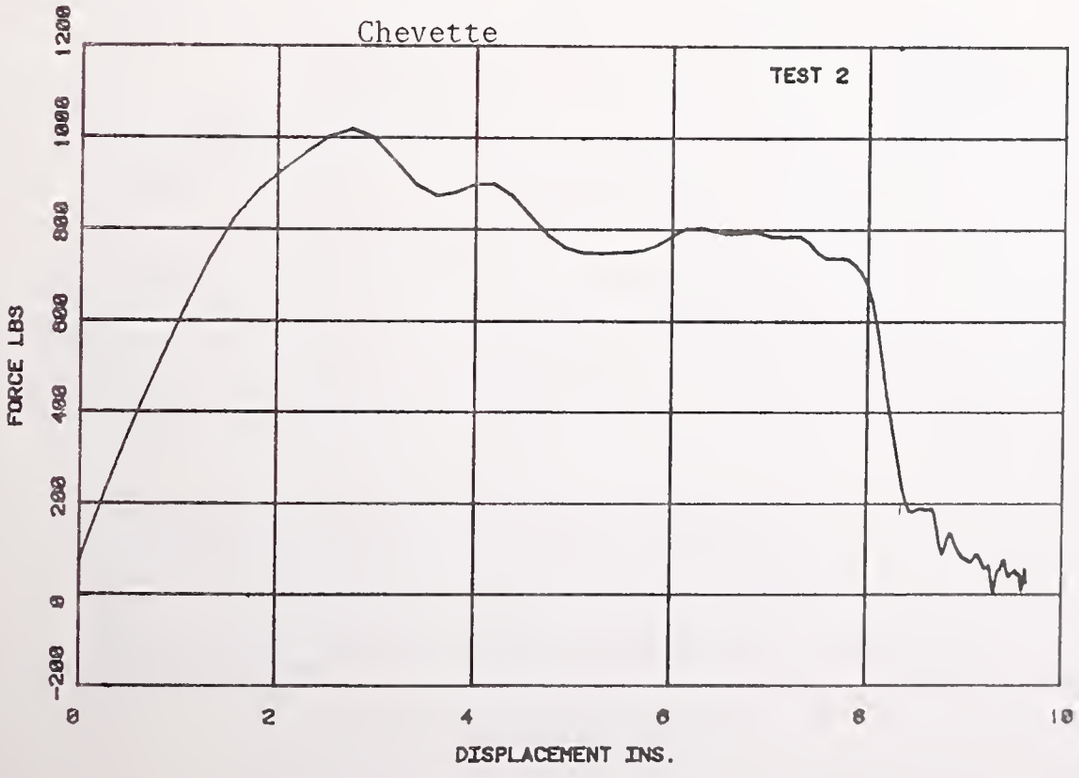

FIGURE 4-26. HORIZONTAL WINDSHIELD DATA (LTD, CHEVETTE)

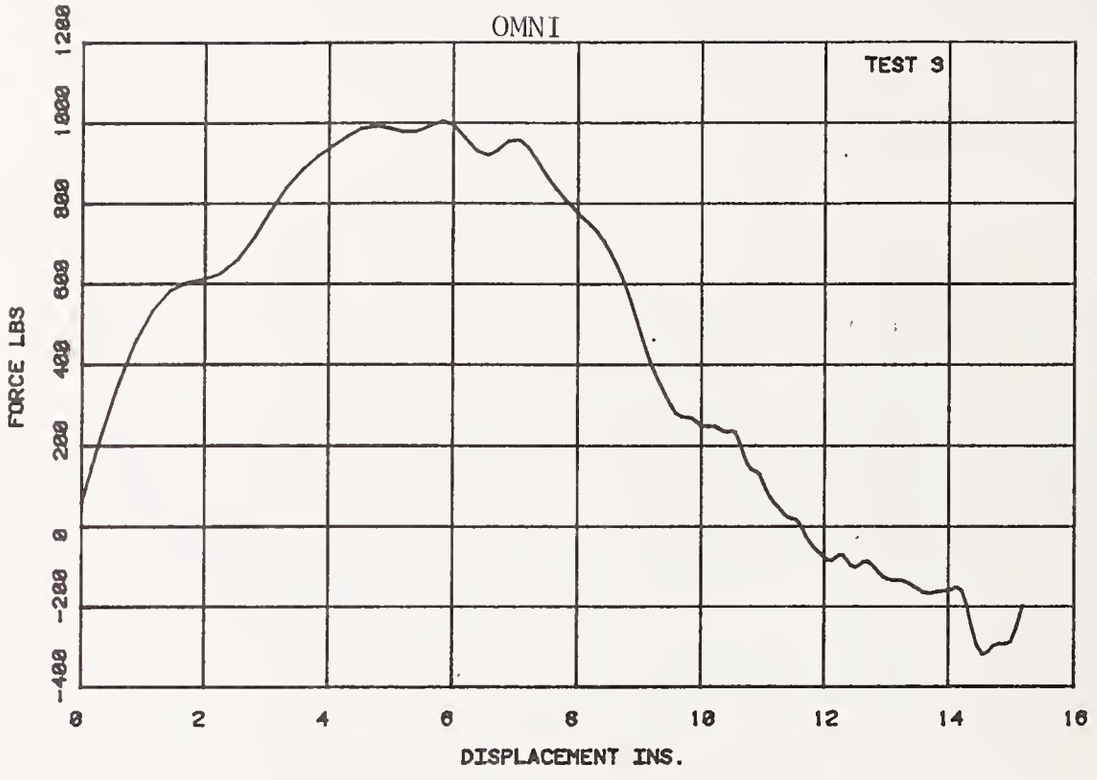

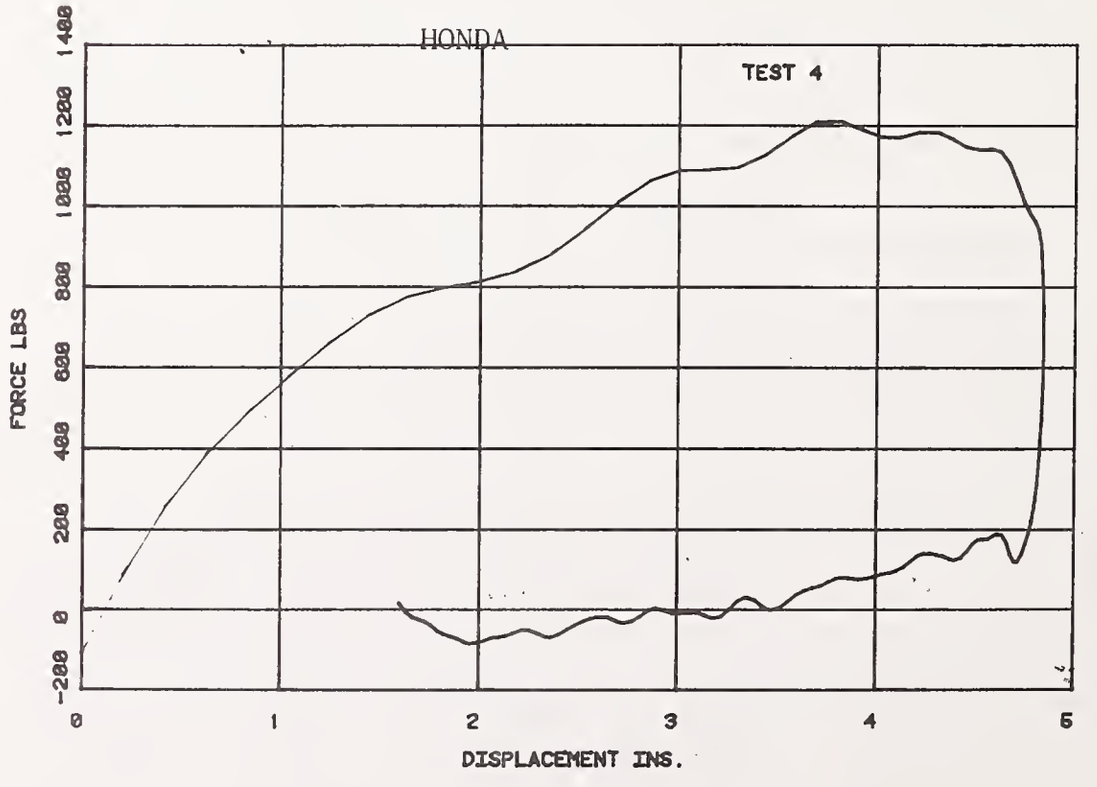

FIGURE 4-27. HORIZONTAL WINDSHIELD DATA (OMNI, HONDA)

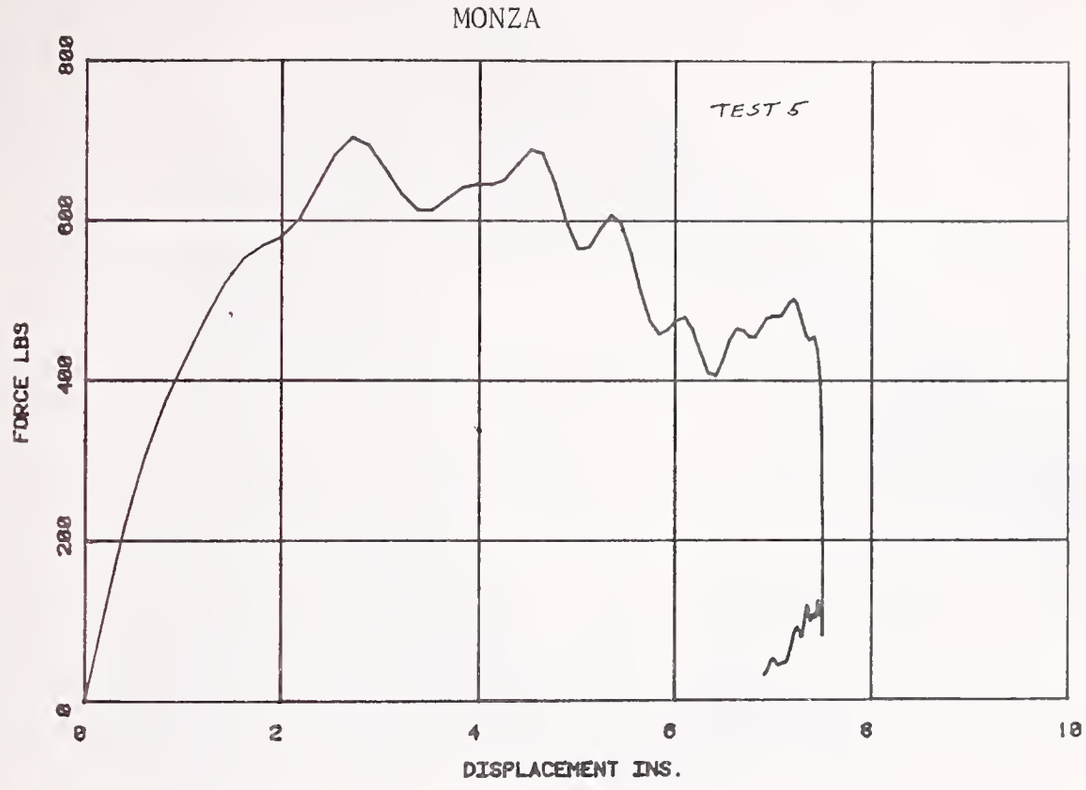

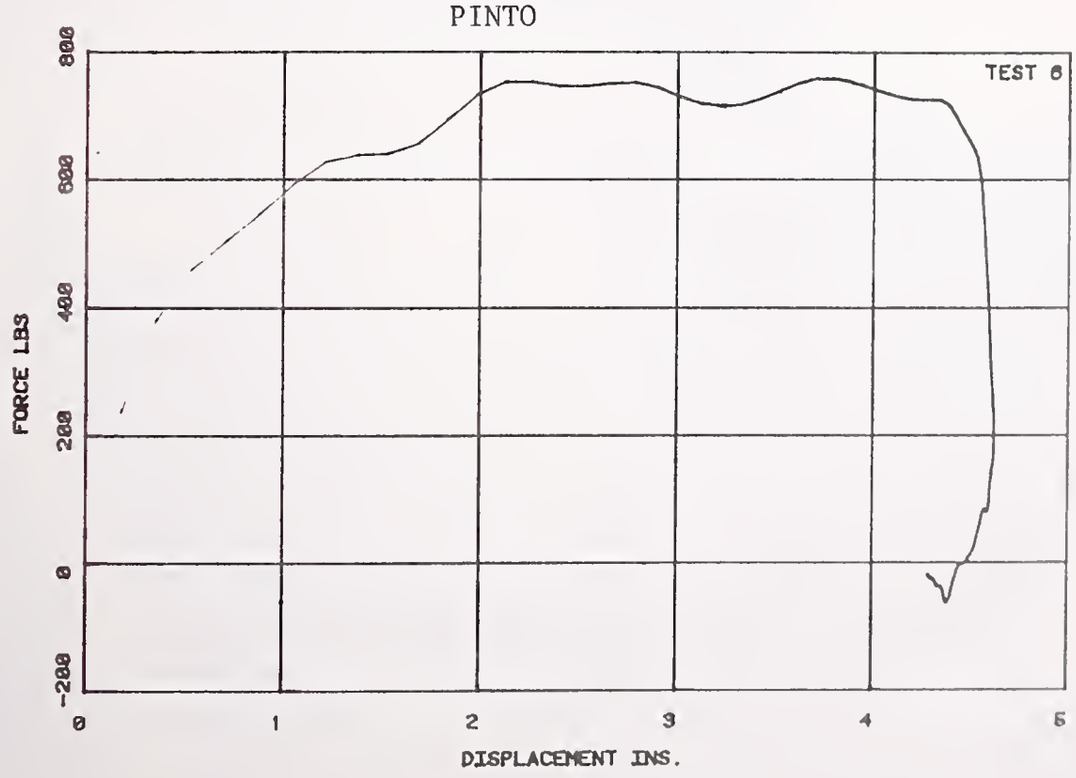

FIGURE 4-28. HORIZONTAL WINDSHIELD DATA (MONZA, PINTO)

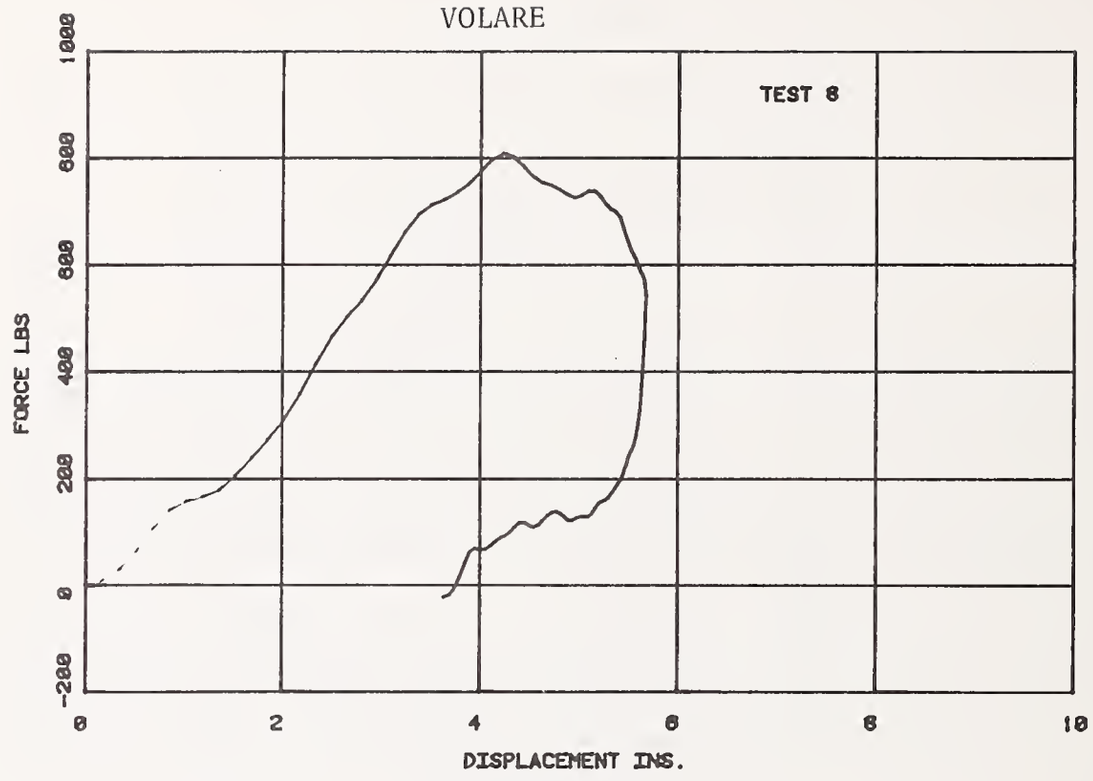

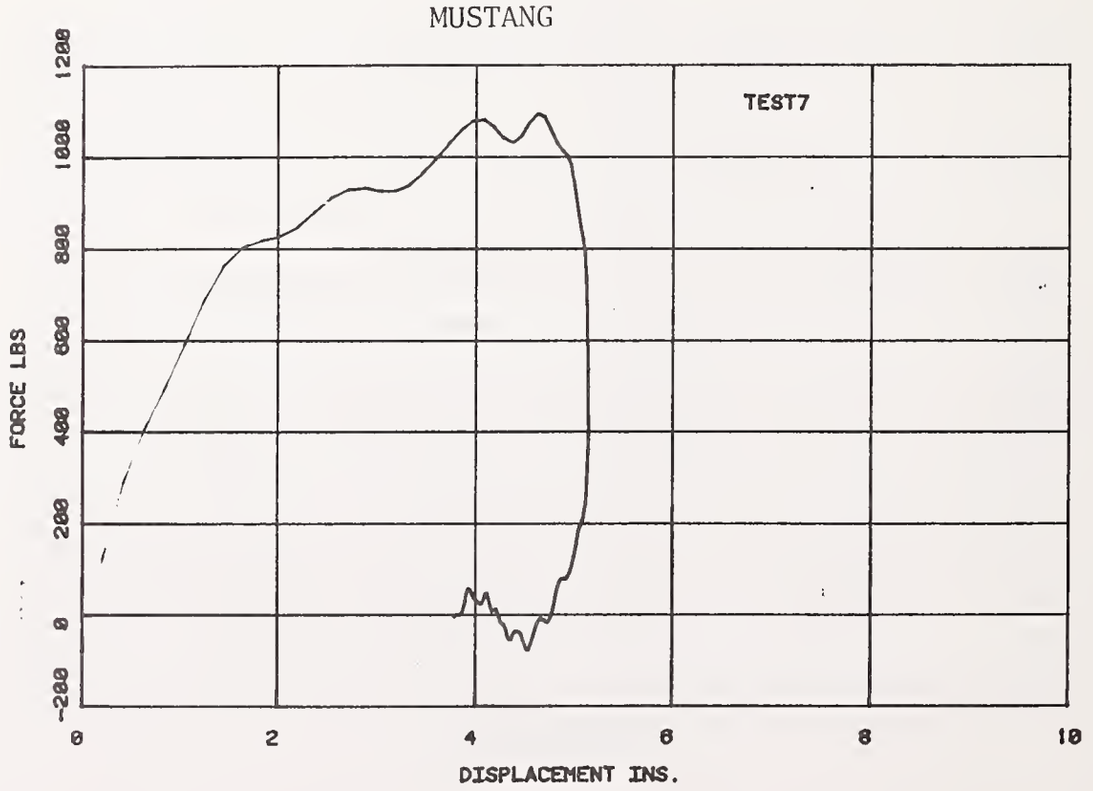

FIGURE 4-29. HORIZONTAL WINDSHIELD DATA (VOLARE, MUSTANG)

FIGURE 4-30. TYPICAL DYNAMIC HORIZONTAL WINDSHIELD DAMAGE

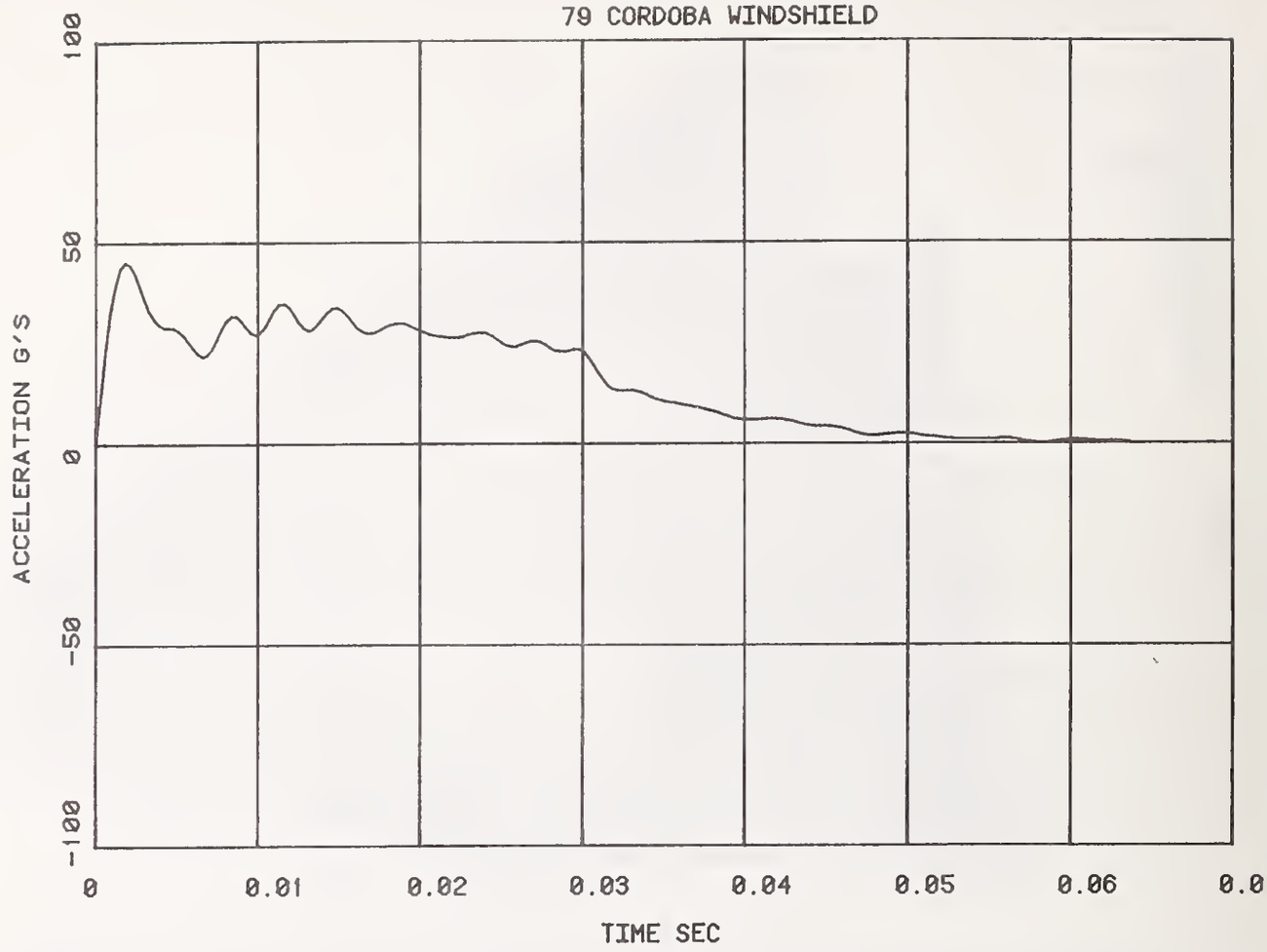

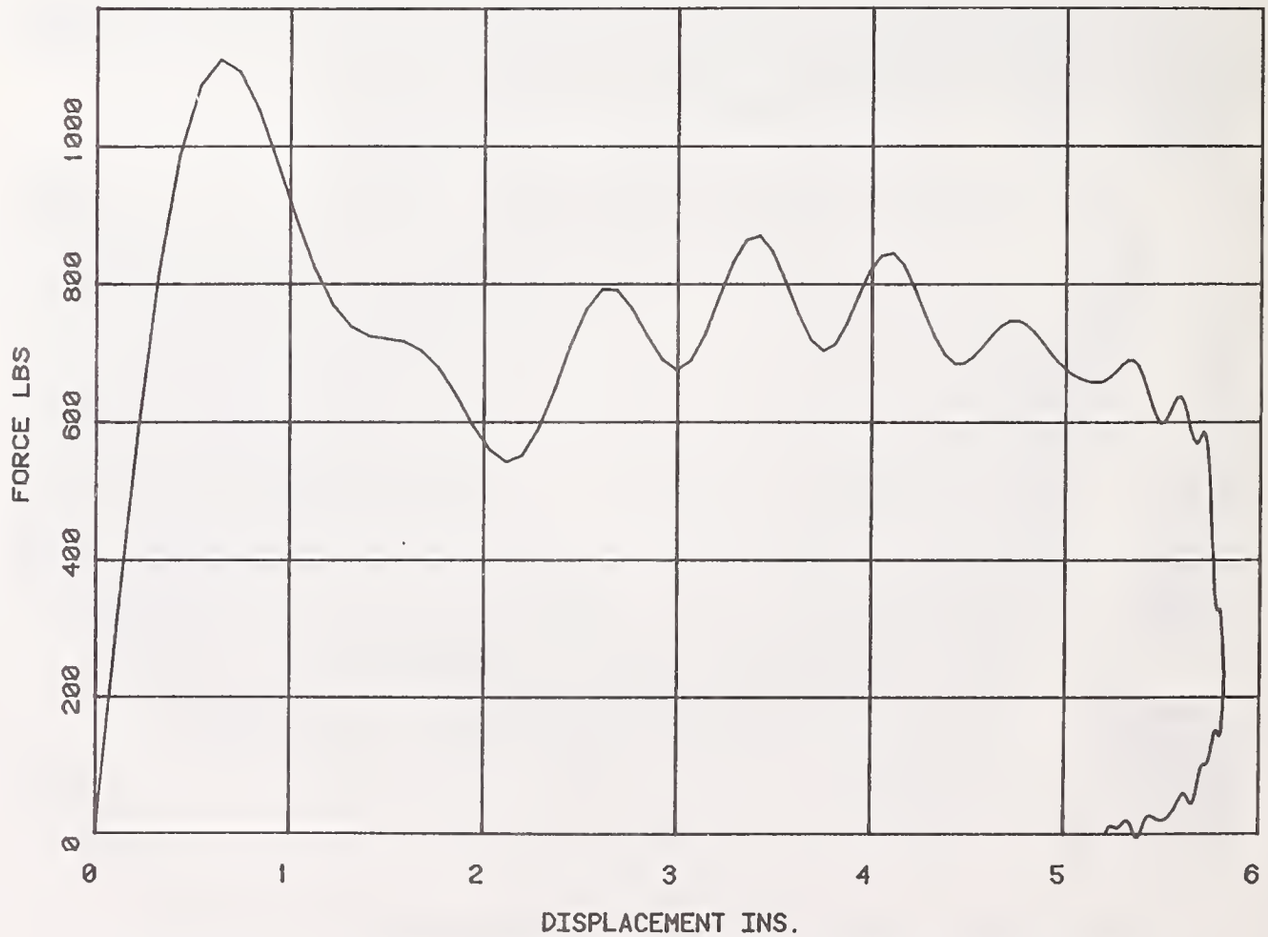

FIGURE 4-31. DYNAMIC WINDSHIELD TEST DATA AND FORCE-DEFLECTION

FIGURE 4-32. POST TEST CONDITION OF BUICK LESABRE WINDSHIELD

There were two tests that did not produce the typical windshield damage pattern. The Volkswagen Rabbit windshield is installed with a rubber gasket mount. During this test, the windshield was forced completely out of the gasket. A post test photo is included in Figure 4-33 and the force-deflection data in Figure 4-34. The second test that did not show typical results was the Pontiac LeMans. During this test, a great deal more penetration of the headform through the windshield occurred, as shown in Figure 4-35. The data for this test is in Figure 4-36

The test results from the normal windshield tests are summarized in Table 4-4 which includes the impact speed, peak force and peak deflection.

4.5 PARAMETRIC INSTRUMENT PANEL TEST RESULTS

This section deals with results obtained from the parametric tests conducted on four of the initial eight vehicles tested. To aid in interpreting the results, overplots have been made showing the individual parametric test results and the results from the corresponding standard tests. The full set of plots are presented in Appendix E. From a general overview of these plots it becomes apparent that general statements cannot be made for all instrument panels but each test must be considered individually.

The first series of tests involved the offsetting of the point of force application two to three inches laterally toward the center of the instrument panel keeping the angle of application as near as possible to the angle used in the baseline test. In these tests, a strong similarity between the baseline and offset results is seen for the passenger side femur tests. The similarity manifests itself in either a similar force range or a similar force-deflection pattern.

Figure 4-37 shows the results of the offset test conducted on the Ford LTD instrument panel. This was the only exception to this general pattern. Upon examination of all the available information concerning this test, no simple explanation could be found. It is believed that the lack of the windshield, heater controls, and radio caused the instrument panel to be weaker by removing some of the resistance to intrusion provided by these components. A further supporting factor for this conclusions is seen in Figure 4-38. This figure shows

FIGURE 4-33. VOLKSWAGEN RABBIT WINDSHIELD - POST TEST

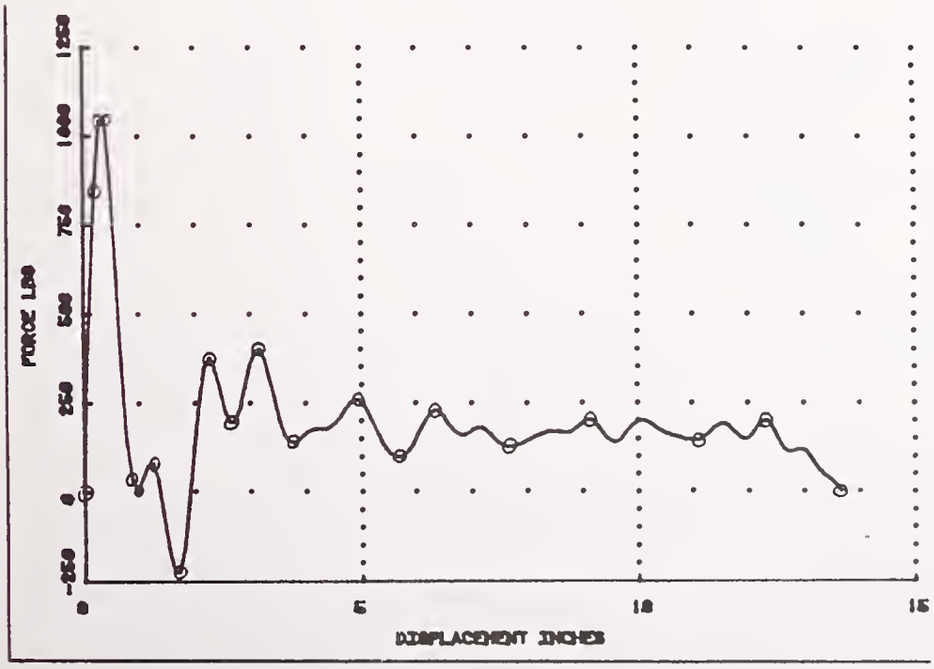

FIGURE 4-34. VOLKSWAGEN RABBIT WINDSHIELD DATA

FIGURE 4-35. PONTIAC LEMANS WINDSHIELD - POST TEST

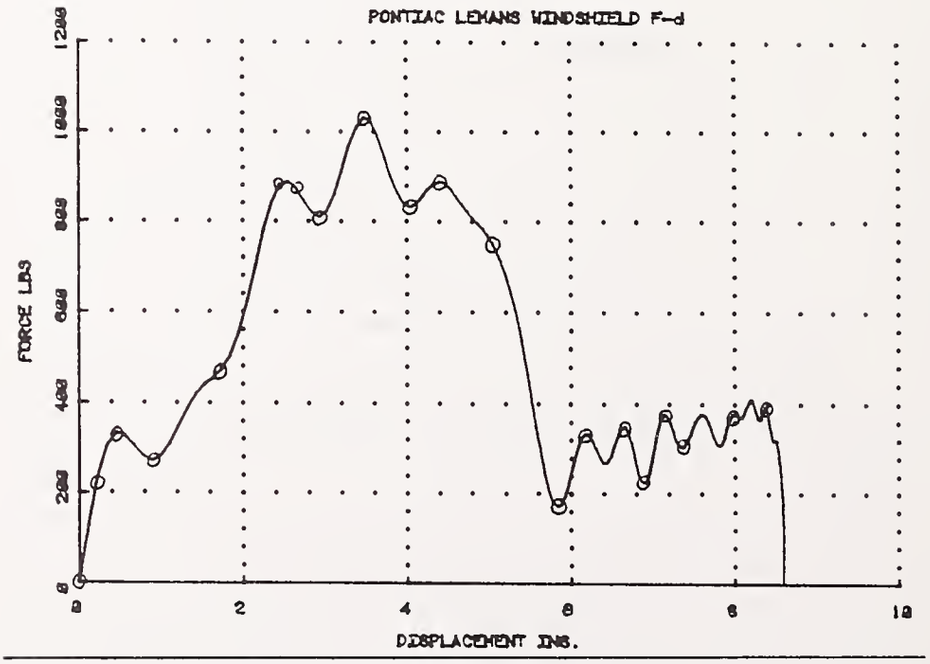

FIGURE 4-36. PONTIAC LEMANS WINDSHIELD DATA

TABLE 4-4. PERPENDICULAR IMPACT WINDSHIELD TEST RESULTS

Vehicle	Velocity (mph)	Peak Force (lbs)	Maximum Headform Penetration
Celebrity	16.9	960 @ 2.4"	5.7"
Datsun	19.9	950 @ 3.8"	6.9"
LeMans	21.6	1,032 @ 3.5"	8.6"
Nova	19.3	760 @ 5.2"	6.9"
Granada	15.6	720 @ 2.2"	2.9"
Cordoba	20.6	1,120 @ 0.6"	5.8"
LeSabre	14.9	620 @ 4.2"	4.9"
Rabbit	19.2	1,050 @ 0.4"	windshield separated
Firebird	26.0	1,225 @ 5.4"	8.2"

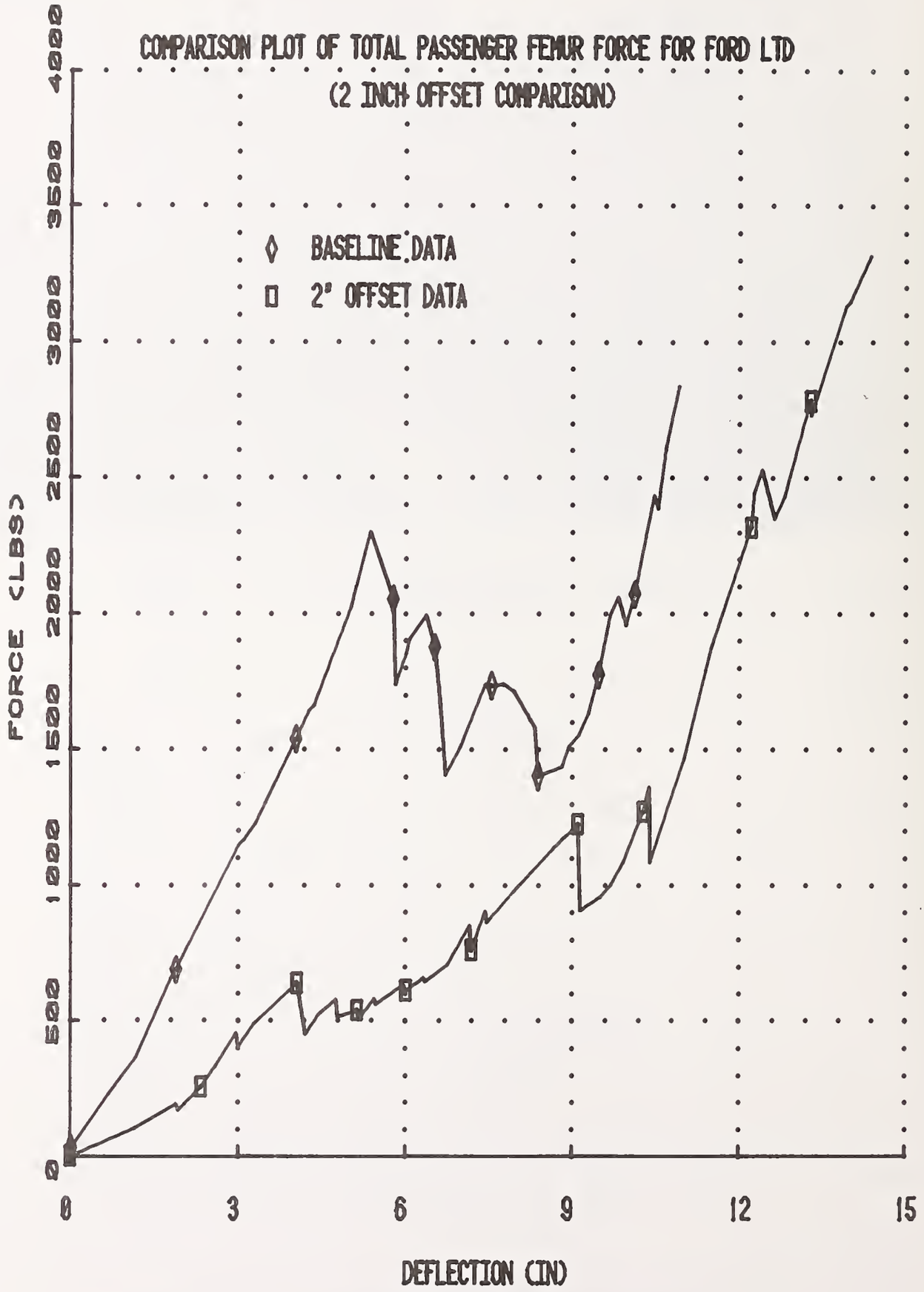

FIGURE 4-37. PARAMETRIC FEMUR TEST COMPARISON (LTD)

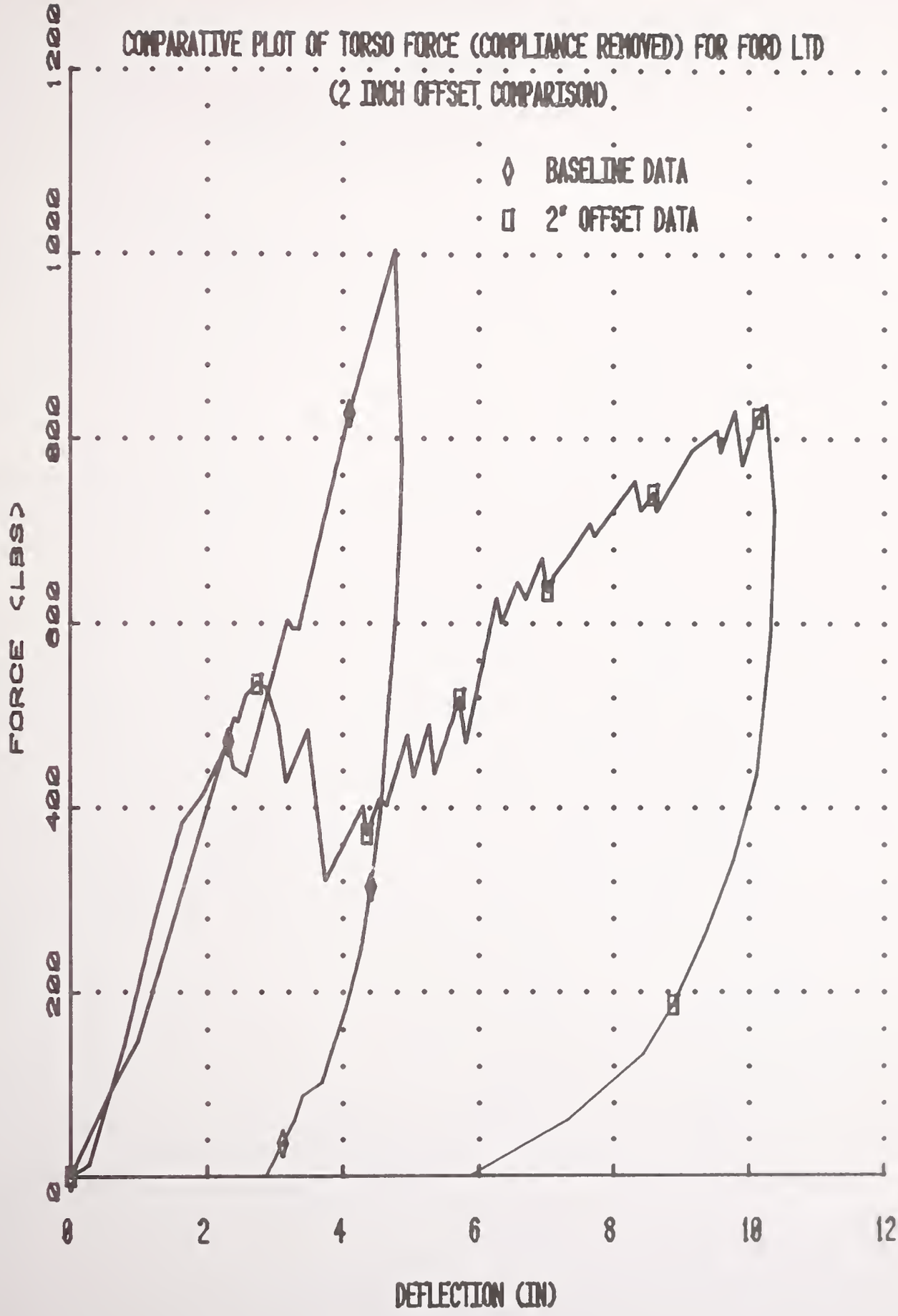

FIGURE 4-38. PARAMETRIC TORSO TEST COMPARISON (LTD)

the results for the torso test conducted on the LTD instrument panel. Up until a deflection of approximately 3 inches, the force levels were very similar. The radical divergence in force levels is, for the most part, due to the lack of a windshield. Normally the instrument panel would have pushed up against the windshield at approximatley 3 inches of deflection (such was the case for the baseline test).

A further example of the individuality of the instrument panels is given by the torso test conducted on the Plymouth Volare (see Figure 4-39). In this test the entire instrument panel was dislodged from its support and attachment mechanisms. Investigation into the cause for this led back to the femur test. Although the femur test overplot showed a similar low level of force, photographs showed that a substantial amount of damage was caused in the offset test thus weakening the instrument panel to the point where the attachments failed. The remaining two tests (the Chevy Monza and the Honda Civic) show some similarity between the baseline and offset tests.

This dependence of one test's results upon the previous test damage is also seen in the offset head tests. An example of this is shown in the overplot for the Plymouth Volare offset head test (Figure 4-40). In this test, the instrument panel attachments also failed. The most immediate explanation for this is that the torso test weakened the anchor points to the extent that the force of the head test was enough to break the instrument panel free from its mounting. The Ford LTD offset head test also exemplifies how previous damage affects a subsequent test. In this case, the instrument panel did not break free, but there was a sufficient amount of damage during the torso test to reduce the overall strength (see Figure 4-41).

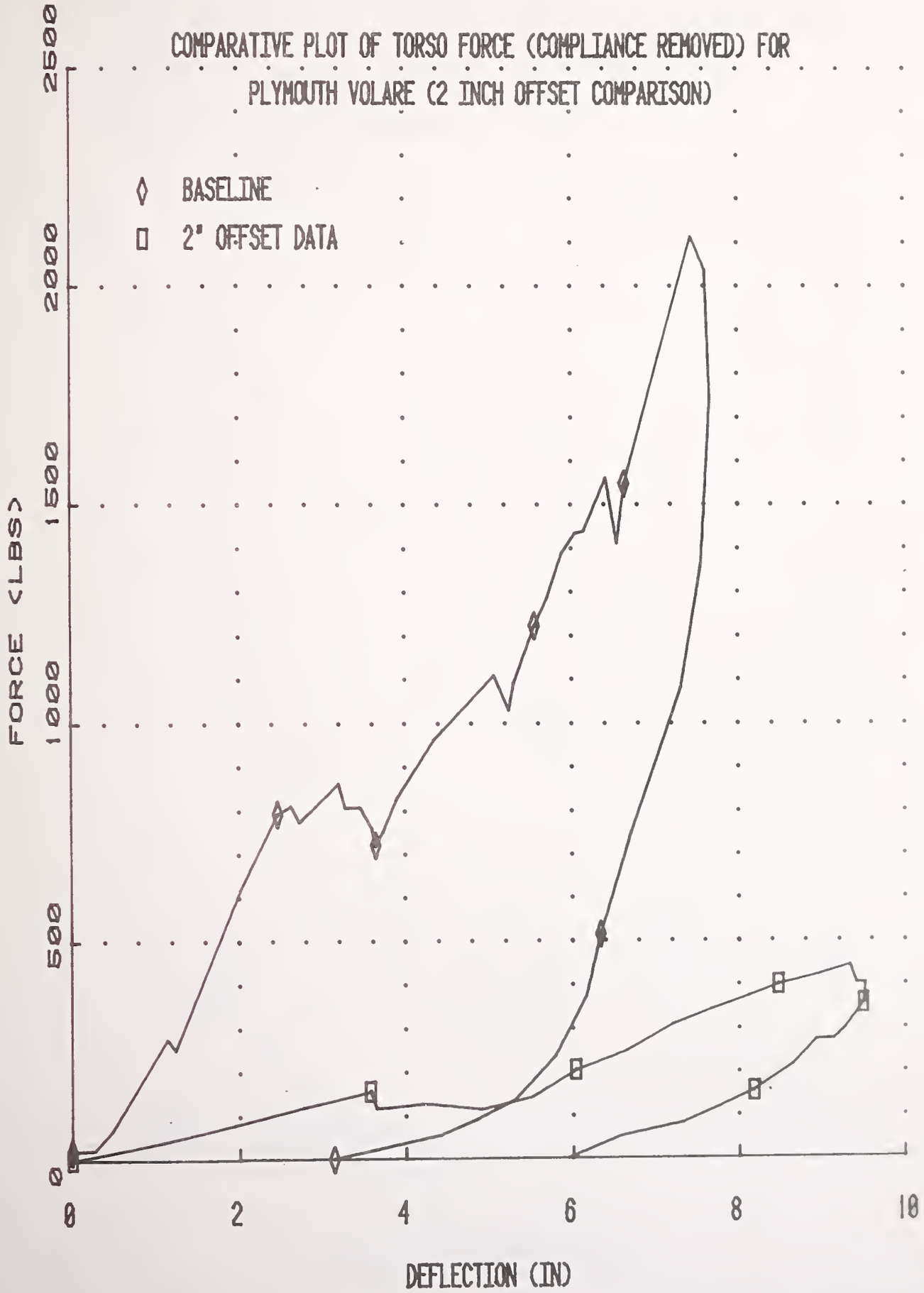

FIGURE 4-39. PARAMETRIC TORSO TEST COMPARISON (VOLARE)

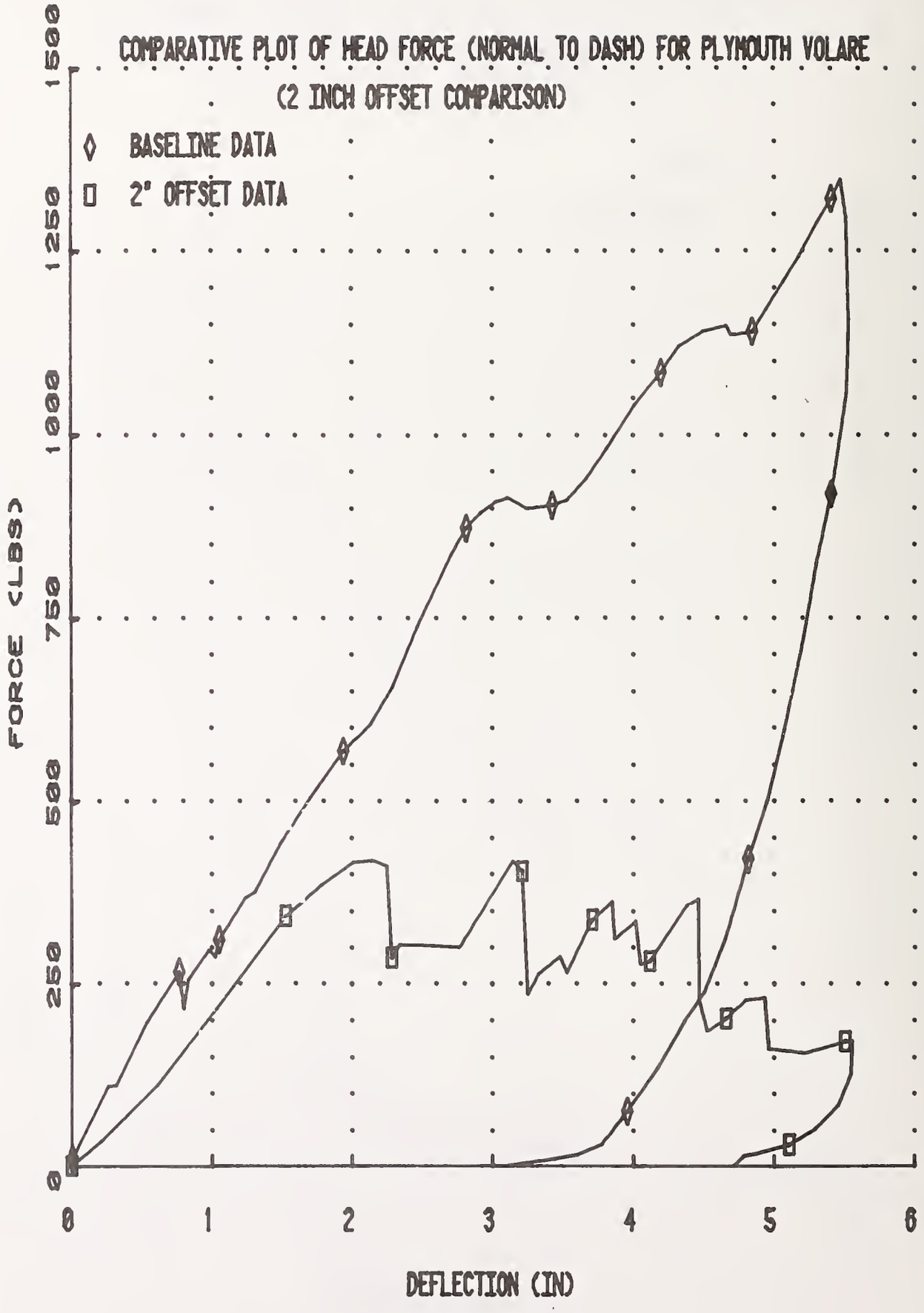

FIGURE 4-40. PARAMETRIC HEAD TEST COMPARISON (VOLARE)

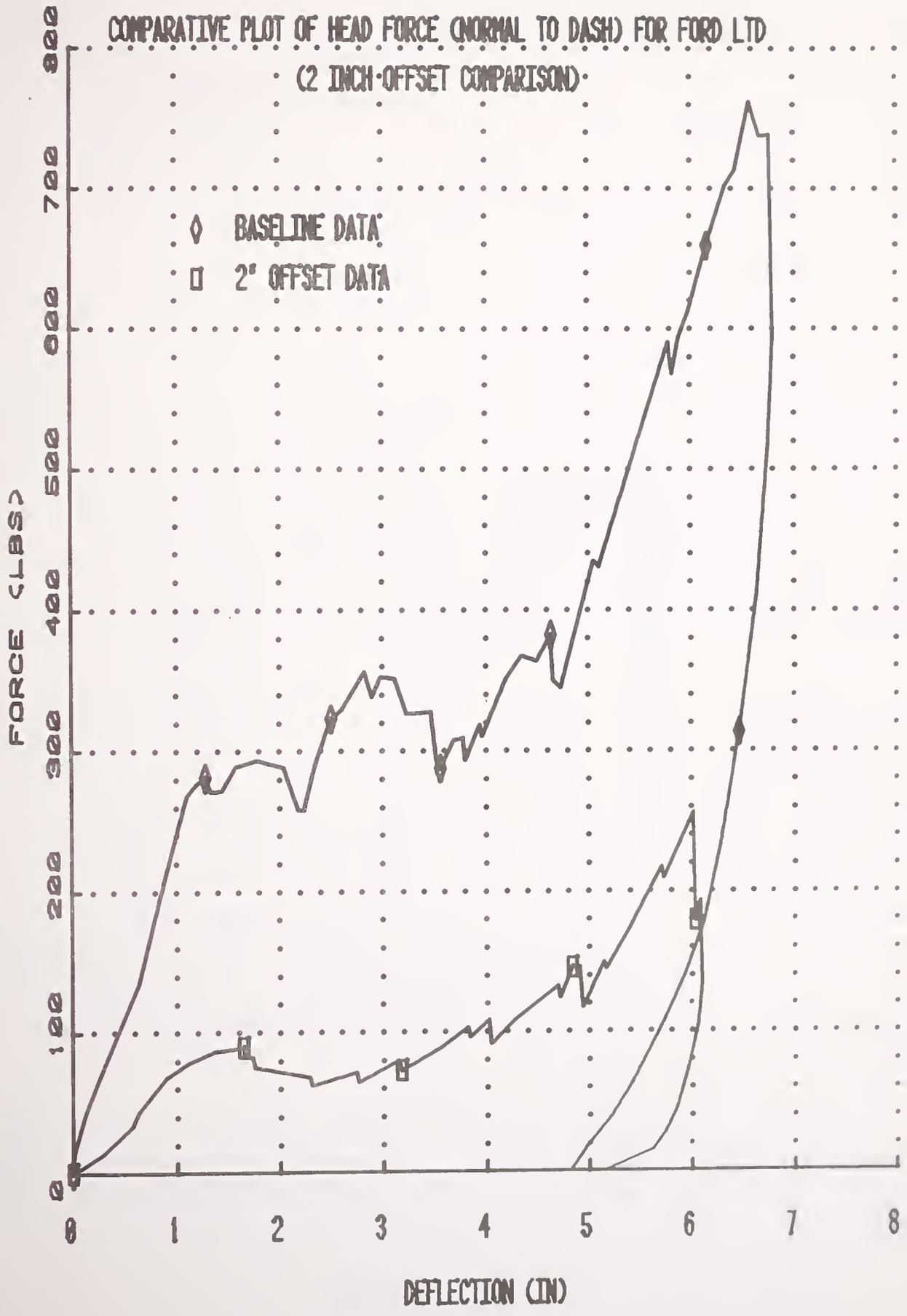

FIGURE 4-41. PARAMETRIC HEAD TEST COMPARISON (LTD)

The second series of tests involved modifying the angle of force application with the lateral position of contact approximately as in the baseline tests. The results of the femur tests for this set of tests show some similarity to the offset tests in that substantial differences in results exist in some cases. Figure 4-42 shows the results from the femur tests on the Plymouth Volare instrument panel. In the baseline test, only the lower section of the glove box was pushed in while the angled test the entire glove box area was deformed. This accounts for the larger force experienced during the angle test. Additional energy was needed to displace a major portion of the instrument panel instead of just working to break the glove box door.

The torso tests in the second series appear to follow a general pattern. In all of the angle torso test, the results show that the instrument panel is less resistant to deformation than in the normal (baseline) tests. It is believed that the angles at which the force was applied caused a rotational moment on and rotational deformation of the instrument panel around the upper attachment points. This indicated that an instrument panel resists compression better in a straight crushing mode than when a rotation mode is added (see Figure 4-43).

A general overview of the angle test overplots also show that each instrument panel responds differently and to a different degree to the addition of the inducing bending force. Two examples of the angle of force causing a greater amount of damage are represented in Figures 4-44 and 4-45. Both of these figures are actually results from the angle head tests. Figure 4-44 shows the results of the Plymouth Volare angle head test. In this test, the dash fell away from its anchors. This is most likely due to the extensive damage caused by the angle torso test. Figure 4-45 shows the results from the angle head test for the Ford LTD. In this case, the instrument panel was damaged by the torso test enough that the instrument panel provided very little resistance when the head test was conducted.

Generally the results from this parametric study have shown that each instrument panel responds differently to a given set of conditions. Loading history, location of contact, and loading direction can all have a substantial effect on the force-deflection characteristics of an instrument panel.

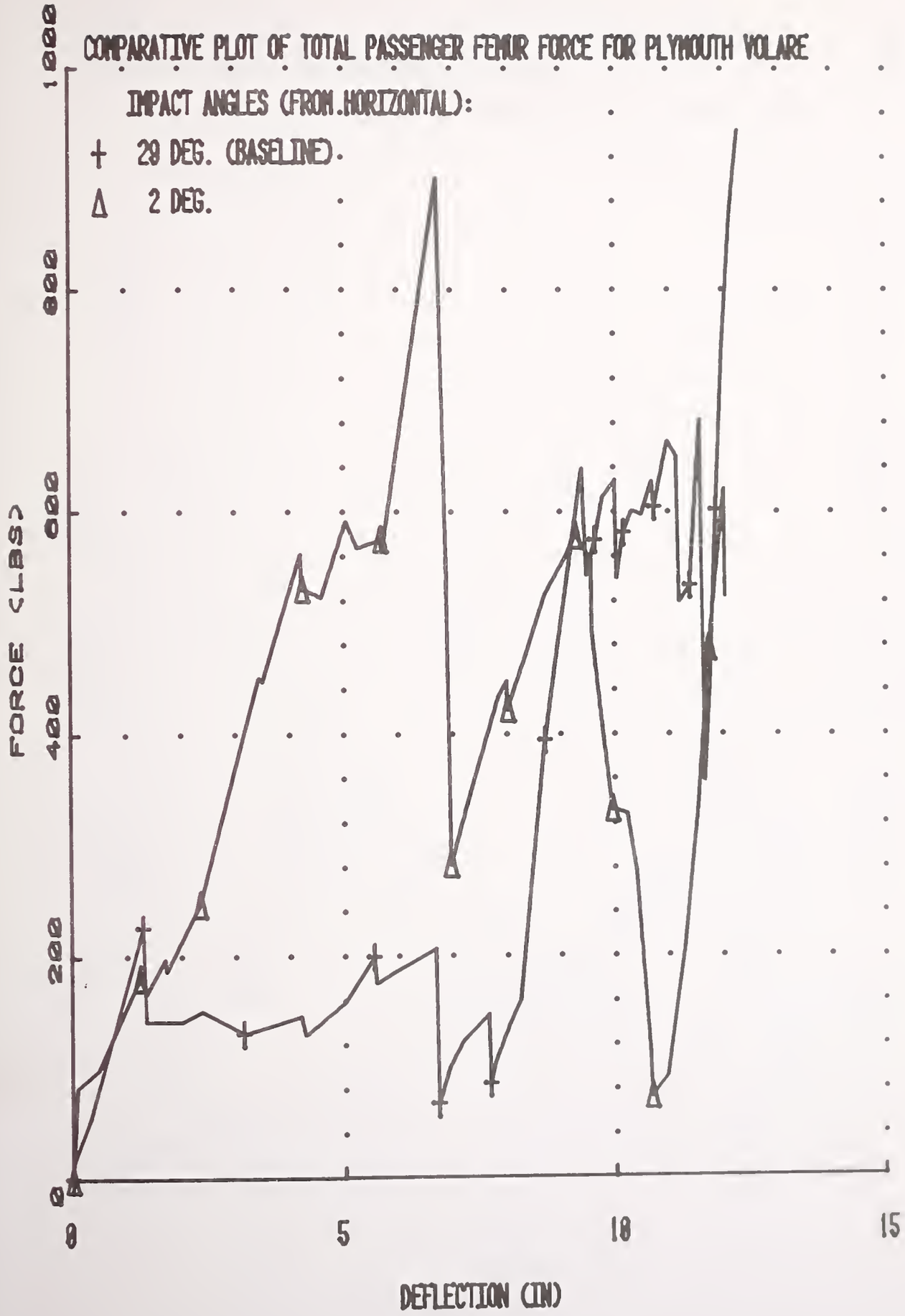

FIGURE 4-42. PARAMETRIC FEMUR TEST COMPARISON (VOLARE)

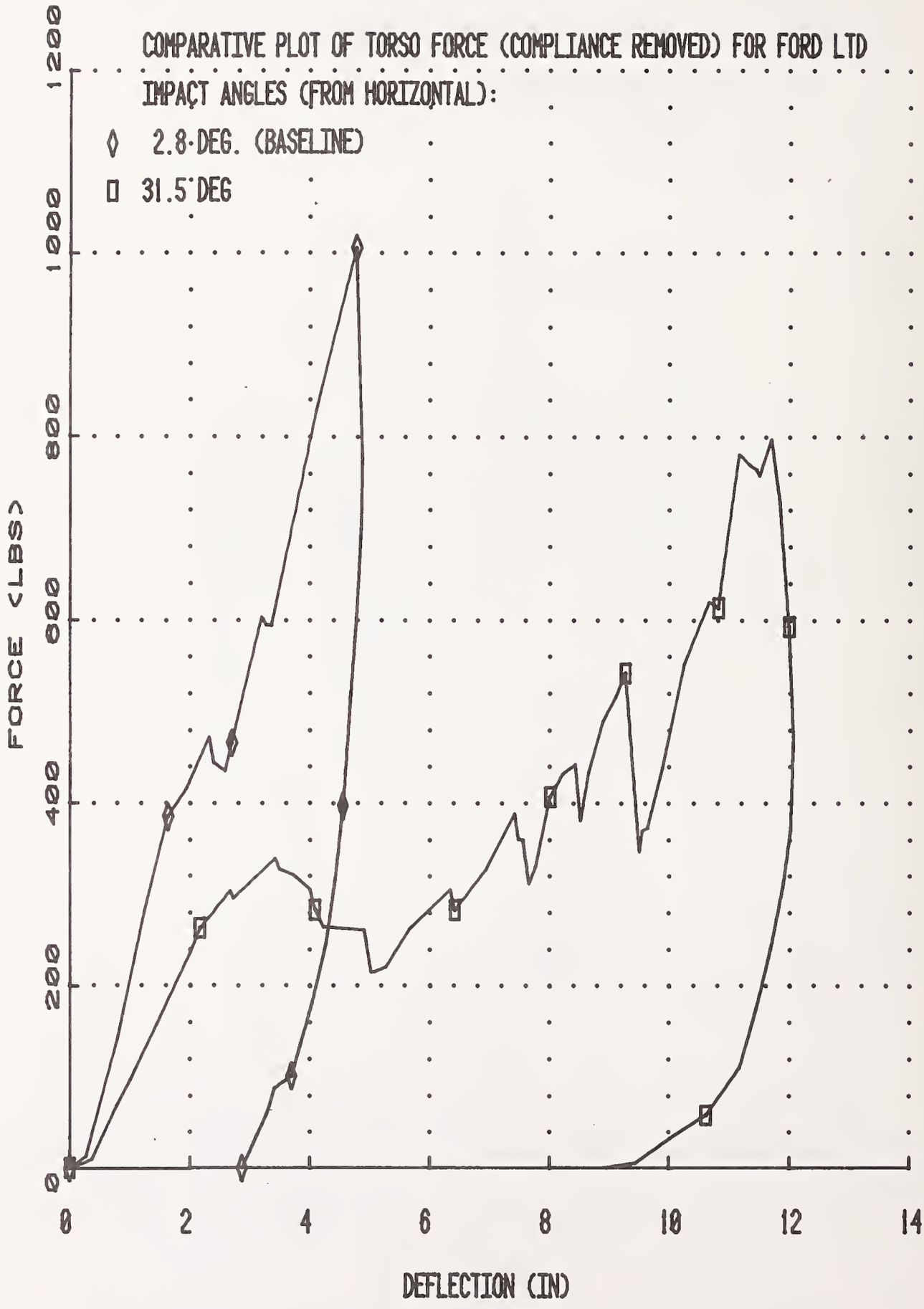

FIGURE 4-43. PARAMETRIC TORSO TEST COMPARISON (LTD)

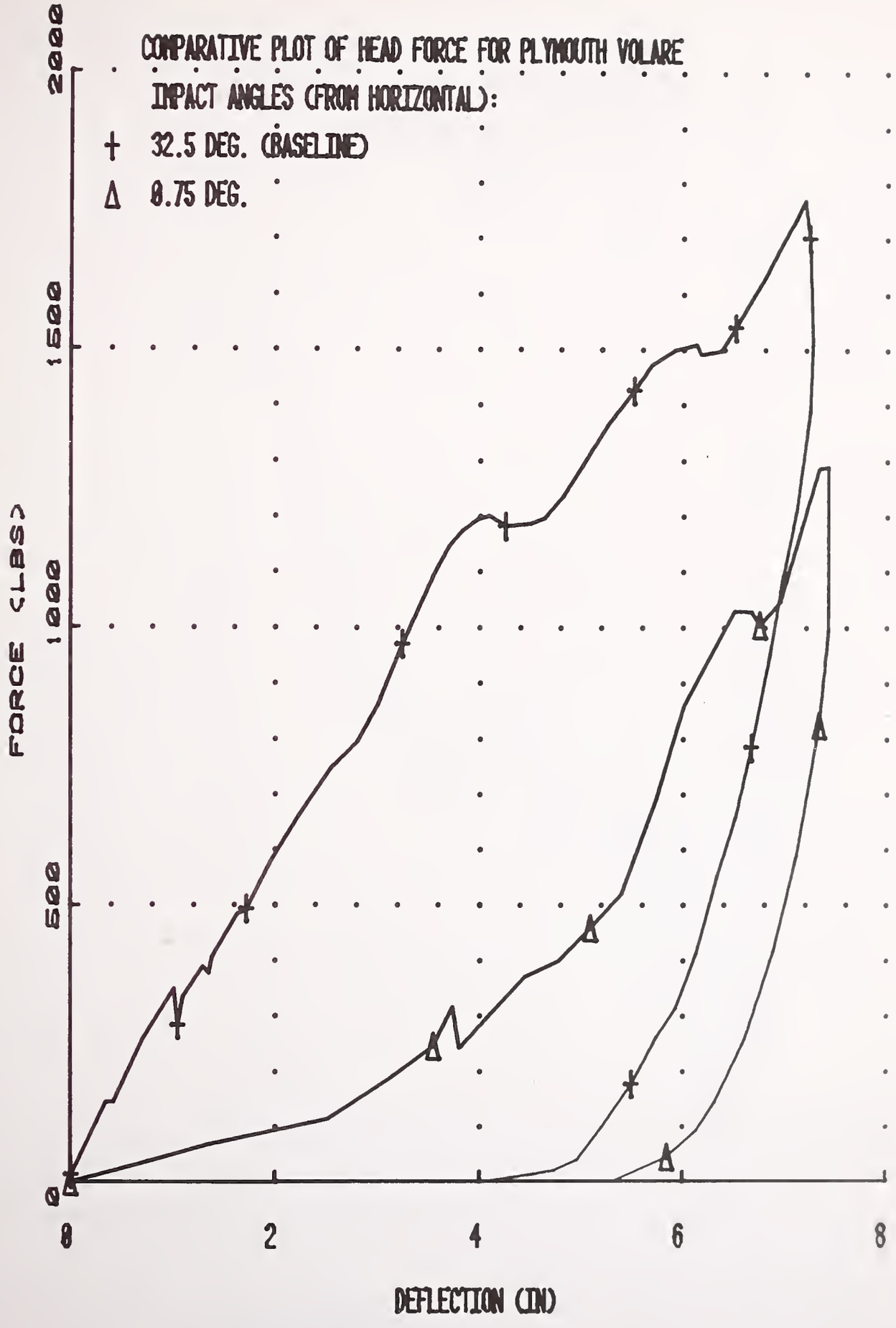

FIGURE 4-44. PARAMETRIC HEAD TEST COMPARISON (VOLARE)

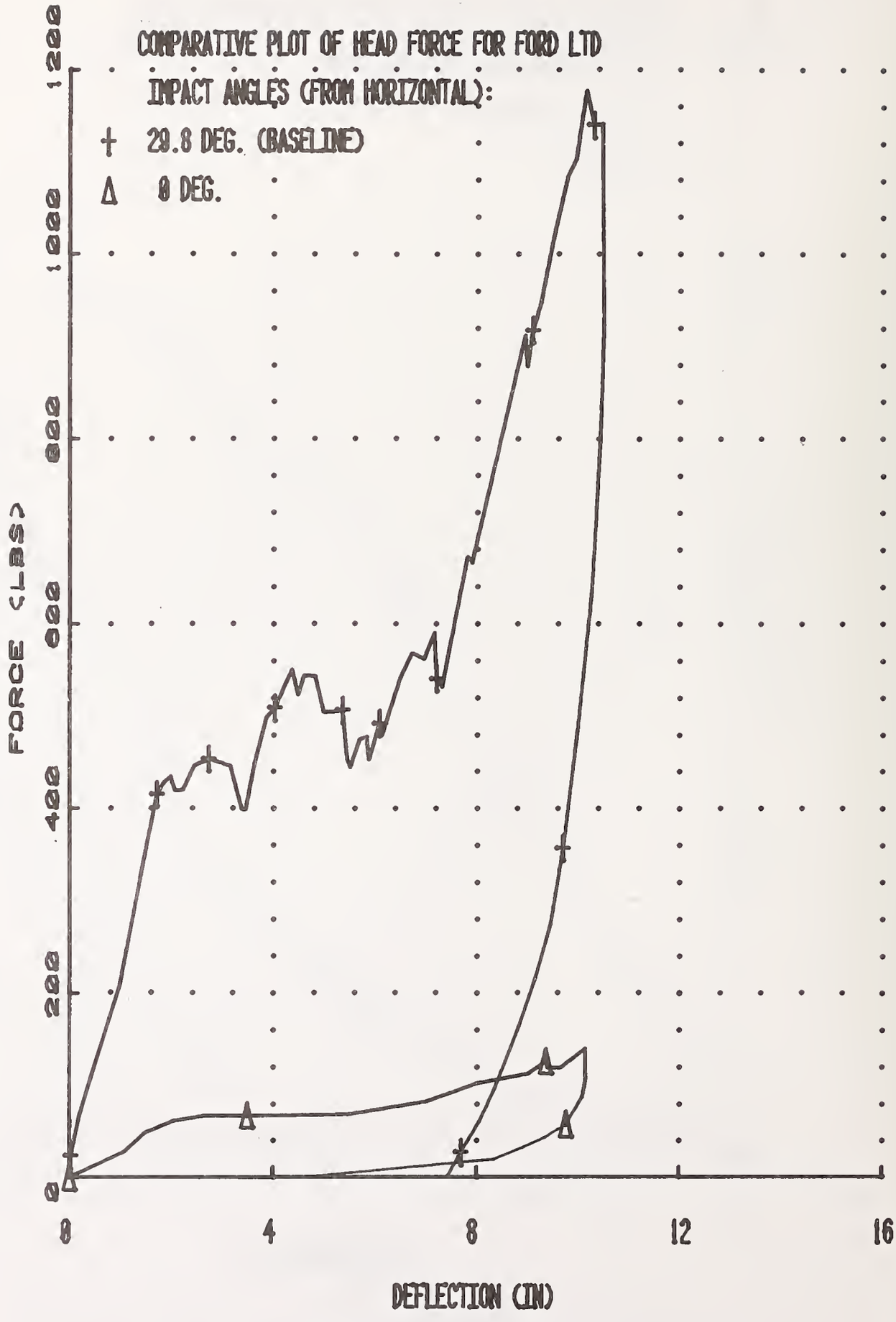

FIGURE 4-45. PARAMETRIC HEAD TEST COMPARISON (LTD)

4.6 INSTRUMENT PANEL FRICTION TEST

As noted in the description of the instrument panel test procedure, both normal loads and tangential loads were measured as a function of time as the femurs, pre-loaded to various initial normal force levels, were rotated about a pivot point causing a scrubbing along the instrument panel surface. Both loads were digitized and stored on a microcomputer as functions of time. The recorded tangential load was processed to refer the force to the interface between the knee and instrument panel surface. The adjusted tangential force was then divided by normal force at corresponding times to obtain friction coefficient as a function of time. Friction tests were run on only the Chevrolet Celebrity.

Data was taken at three values of initial force - 160, 300, and 400 pounds. Note that the actual normal force varied during the collection of data as a result of the changing geometry and instrument panel characteristics. Plots of friction coefficients vs. time for these three cases are shown in Figures 4-46, 4-47,and 4-48. In all cases, the friction coefficient gradually rises over time to an approximate steady-state level. This initial rise results from the gradual build up of tangential forces due to stretching of the fabric covering the knees and elastic motion of the instrument panel as a whole as it adjusts its position to react the tangential loads. Once a steady-state is reached the calculated friction coefficient remains relatively constant within a range of about 0.8 to 1.0 for all three initial loads. Thus, for the tests conducted, results indicate that the effective friction coefficient is independent of normal load (and therefore deflection). However it should be noted that high values of initial normal force, and therefore large instrument panel deflections (where plowing effects would be expected) were not considered in this limited testing effort.

4.7 WINDSHIELD PARAMETRIC TESTS

As previously noted in Table 3-2, nine dynamic impact tests were conducted on Citation windshield to investigate the effects of test variables. Of these, two tests were conducted on Securiflex windshields and one was conducted on a previously tested standard windshield. The remainder were undamaged, standard windshields. Additional variables investigated included impact speed, impact angle, pre-stress, and impact location relative to the windshield edge. A tabulation of the test conditions, impact velocity, and maximum penetration of the headform is provided in Table 4-5.

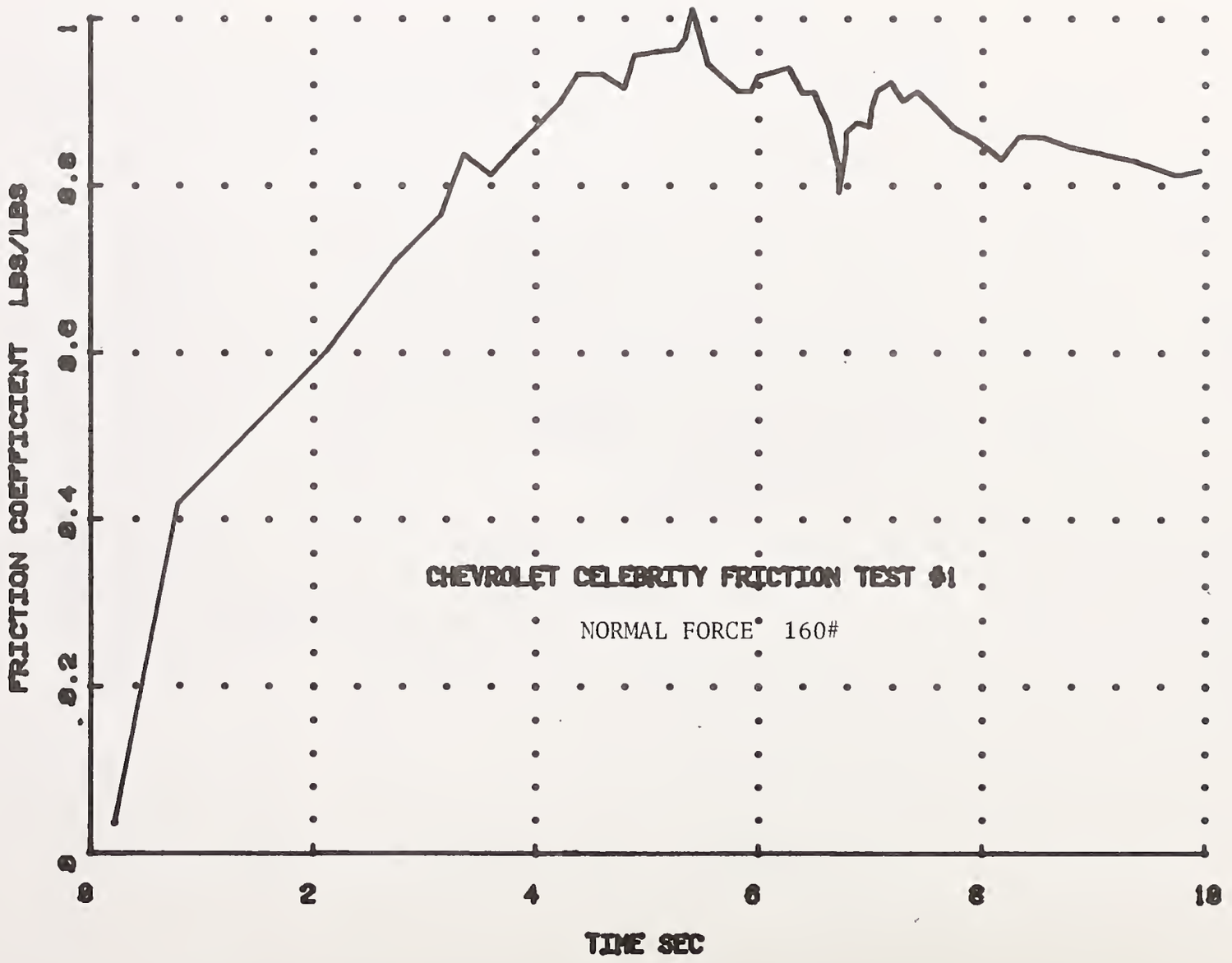

FIGURE 4-46. CELEBRITY FRICTION DATA AT NORMAL LOAD OF 160 LBS.

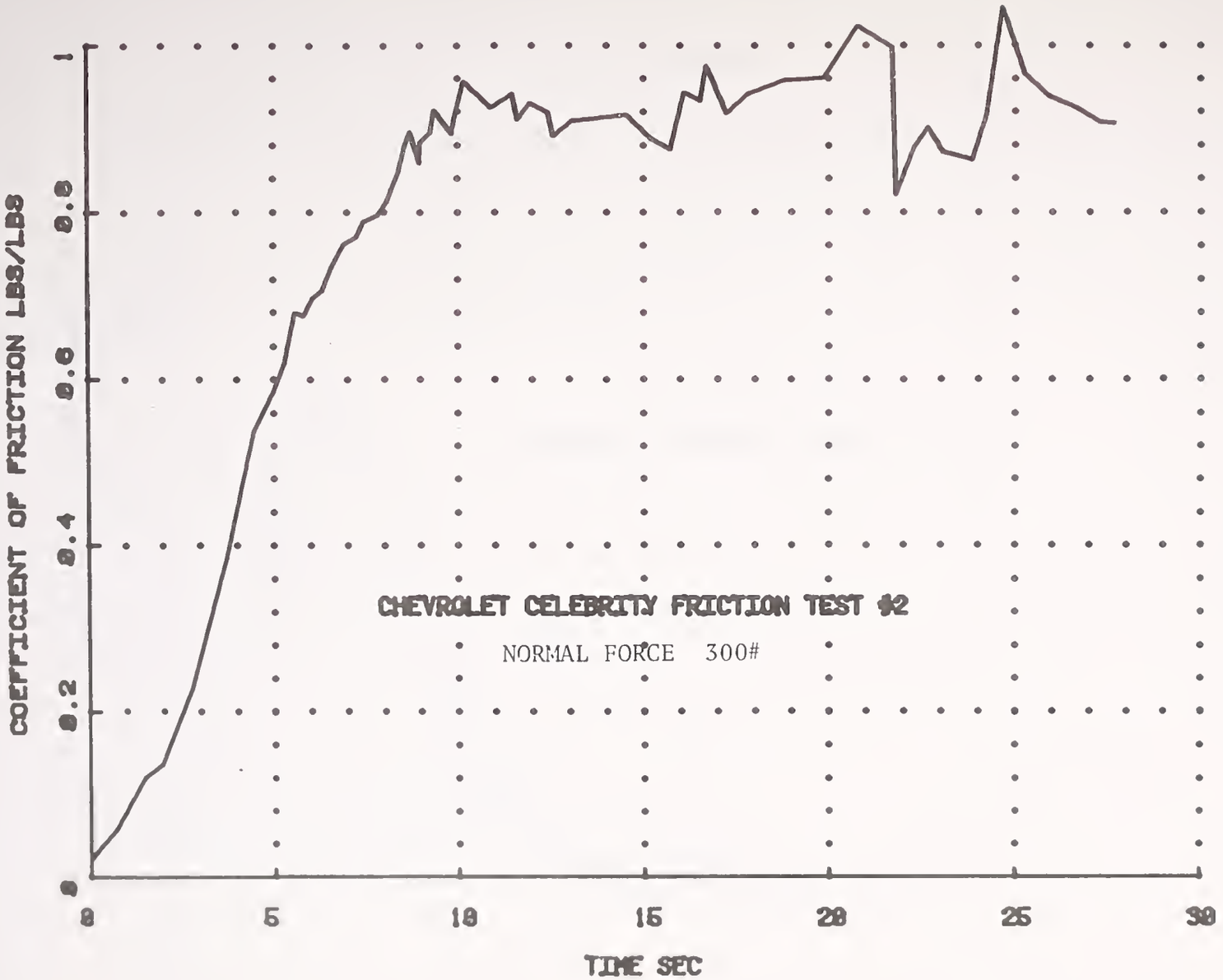

FIGURE 4-47. CELEBRITY FRICTION DATA AT NORMAL LOAD OF 300 LBS.

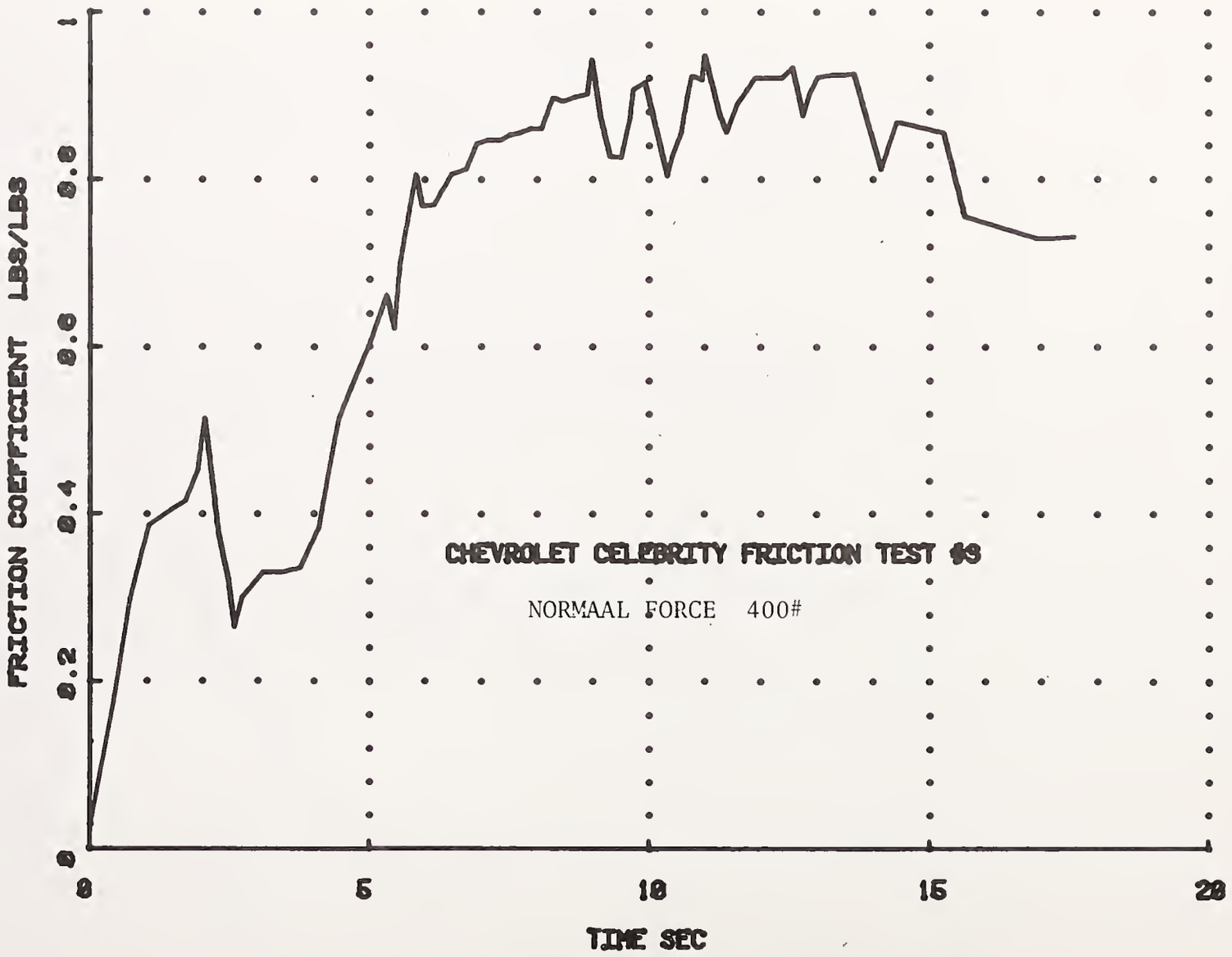

FIGURE 4-48. CELEBRITY FRICTION DATA AT NORMAL LOAD OF 400 LBS.

TABLE 4-5. SUMMARY OF PARAMETRIC WINDSHIELD TESTS

Test No.	Test Conditions	Impact Velocity (mph)	Maximum Penetration (in)
A	horizontal, securiflex	21.2	7.8
B	horizontal	13.2*	4.3
B2	horizontal, damaged other side	20.5	11.9
E2	normal, securiflex	18.9	5.4
F	normal	20.8	7.5
G	normal, edge effect	20.7	7.0
H1	normal	19.0	5.9
H2	nomral	20.8*	8.8
J	normal, pre-stress	19.9	8.2

*Impactor malfunction

The nominal impact speed for all tests except test H2 was intended to be 20 mph. The target test speed for test H2 was 25 mph. Unfortunately, malfunctions in the pneumatic impactor system used for the tests occurred in that test, reducing the impact velocity to 20.8 mph from the desired 25 mph, and in test B reducing the impact speed to 13.2 mph from the desired 20 mph. In addition to these dynamic tests, static tests were conducted in the horizontal and normal (to the windshield) directions.

Data collected in the dynamic tests consisted of headform acceleration readings which were subsequently integrated to obtain a displacement time history, multipled by the impactor mass to produce force time history and cross-plotted to produce a force-displacement curve for the event. All accelerations were digitially filtered at a corner frequency of 300 Hz prior to processing.

As a result of the pneumatic impactor system malfunction in test H2, a clear comparison of the effects of impact velocity of the force-deflection characteristic could not be obtained. However, a repeatability band encompassing three tests (tests F, H1, and H2) at nearly the same impact velocity is shown in Figure 4-49. In all three tests, the inertial spike occurs over the first inch of deflection, but substantial differences in the inertial spike peak, ranging from about 250 lbs. to about 700 lbs. are seen. The peak force due to penetration occurs at between 3 and 5 inches at values ranging from 800 to 1,000 lbs. Maximum penetration ranges from 5.9 to 8.8 inches. This rather substantial difference in maximum penetration apparently reflects differences in force levels observed in the inertial spike and other parts of the curve as the maximum absorbed energy for the three tests ranges from 3,618 to 4,359 in lbs. This is consistent with differences in impact speeds.

The effects of moving the impact location closer to the edge of the windshield is shown in Figure 4-50. With the impact location closer to the edge, a force-deflection curve resulted that is within the repeatability band illustrated in the previous figure with two exceptions. The initial rise in force subsequent to the inertial spike is higher near the edge and the peak force achieved is also higher. These differences are not, however, substantial.

The effect of pre-stressing the windshield glass is shown in Figure 4-51. In this case, the inertial spike appears to be reduced in magnitude and the initial stiffness of the force-deflection curve resulting from penetration appears to be increased. The maximum force level is not affected.

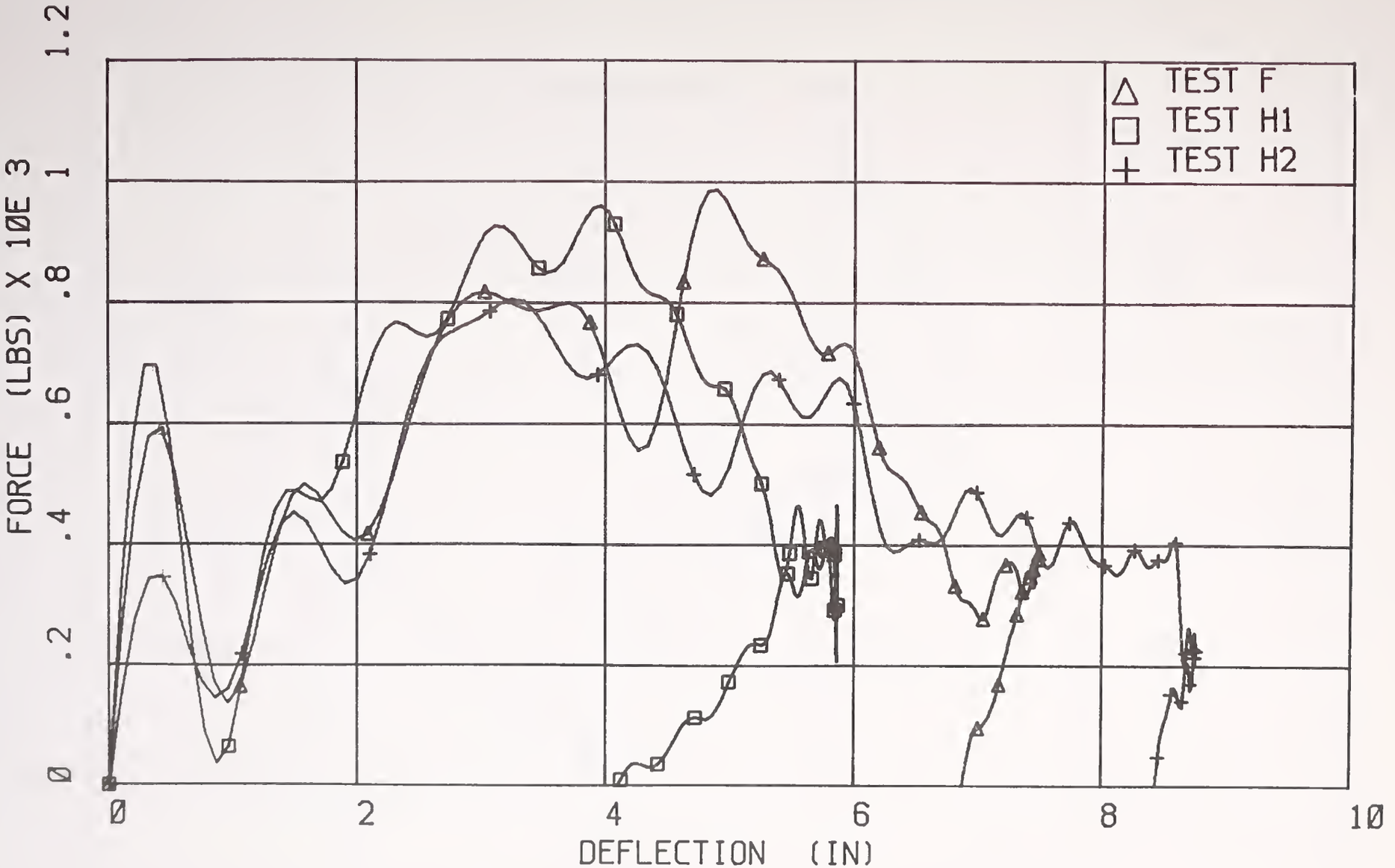

FIGURE 4-49. WINDSHIELD FORCE-DEFLECTION REPEATABILITY

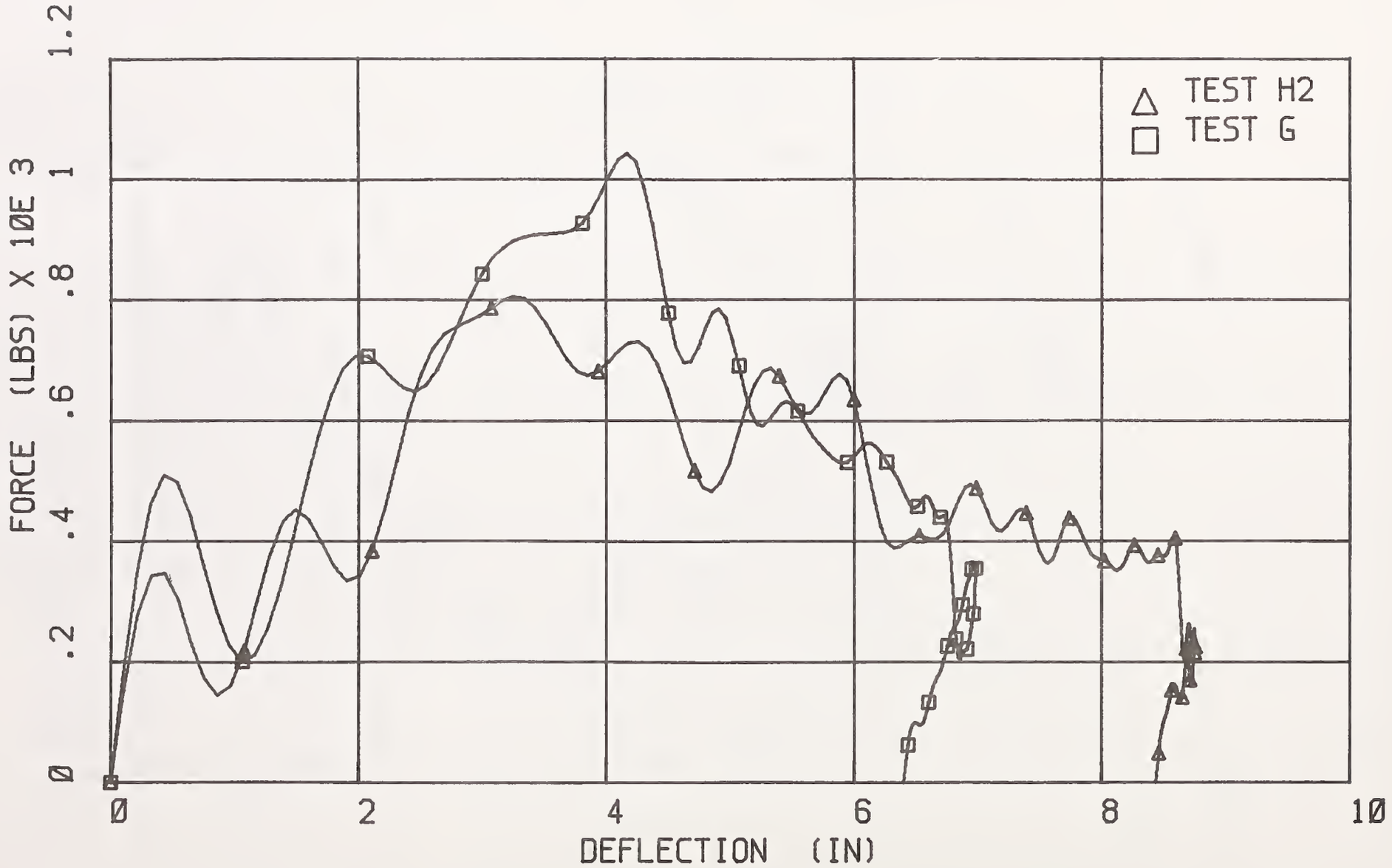

FIGURE 4-50. EFFECT ON IMPACT LOCATION

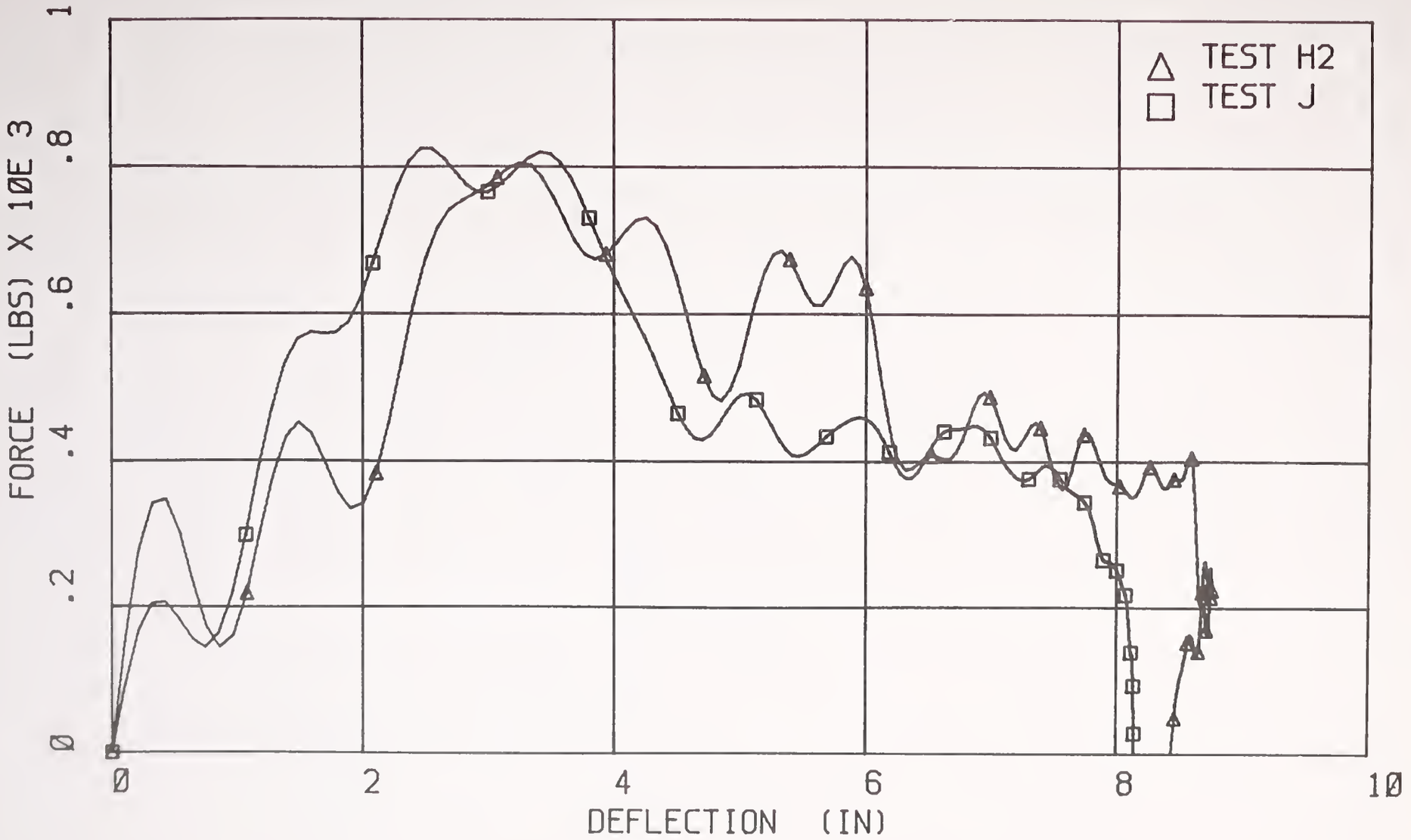

FIGURE 4-51. EFFECT OF PRE-STRESS

The effect of impact direction for standard (non-securiflex) windshields is illustrated in Figure 4-52. In this case, the inertial spike for the horizontal test is greater in magnitude than in the normal test but it is still within the repeatability band shown in Figure 4-49. The penetration force level for the horizontal test is noticeably diminished from the normal test results. The horizontal test penetration force level appears to be slightly in excess of 400 lbs. (on the average) which corresponds to the force level at extreme penetration for the normal test. However, the horizontal test impact speed was only 13.2 mph due to a malfunction in the impactor system and consequently the associated energy level and maximum penetration are small.

Due to the low energy level of this test, a second horizontal test was run on the opposite side of the same windshield in an attempt to obtain larger penetration levels. This test also provides an indication of the effect of a previously damaged windshield. A comparison of force-deflection data from these two tests on the same windshield is shown in Figure 4-53. As seen there, pre-existent damage results in a substantial change in force levels at the lower deflection levels. However, the saturation force level of between 100 and 500 lbs. is similar in both cases at larger deflection.

It should be noted that these two different test orientations appear to result in different characteristics in the force-deflection data. That is, the normal test results typically show an increasing then decreasing force bulge in the middle part of the curve followed by a force saturation level. This bulge is a result of deformation of the plastic interlayer without separation or tearing of the interlayer. As the interlayer begins to tear, the head starts to penetrate the interlayer and windshield at a force level that is approximately constant.

In the case of a horizontal impact, the characteristic bulge in the center of the force-deflection curve is much less evident. Apparently with this impact orientation, tearing of the plastic interlayer begins much sooner in the event resulting in a more constant force level during penetration.

Two Securiflex windshields were also tested dynamically in horizontal and normal orientations. These windshields have an additional plastic layer on the inside surface of the glass in order to reduce facial lacerations during accidents. A comparison of normal test force-deflection data for this and a standard windshield are shown in Figure 4-54. As is seen there, the Securiflex

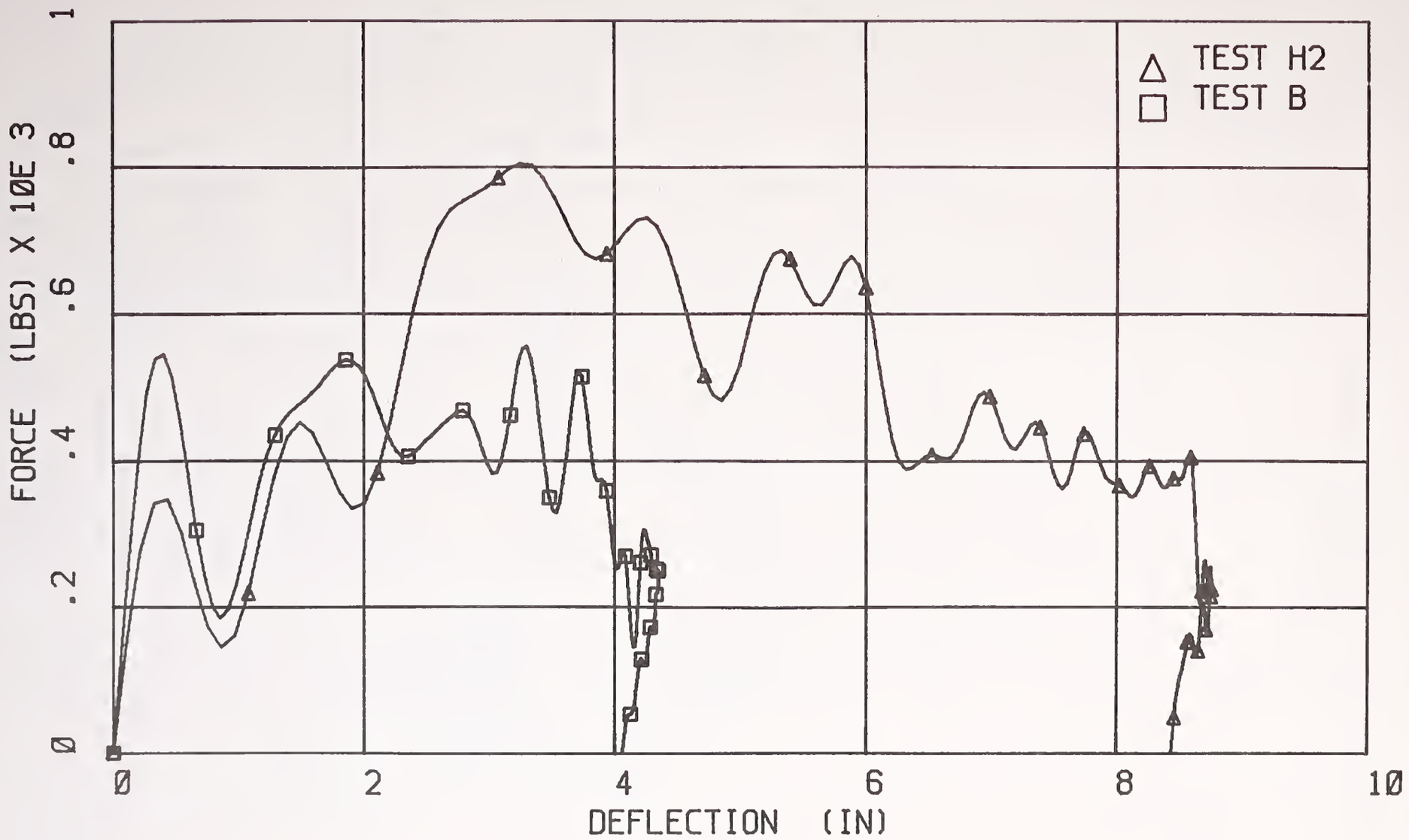

FIGURE 4-52. EFFECT OF IMPACT DIRECTION

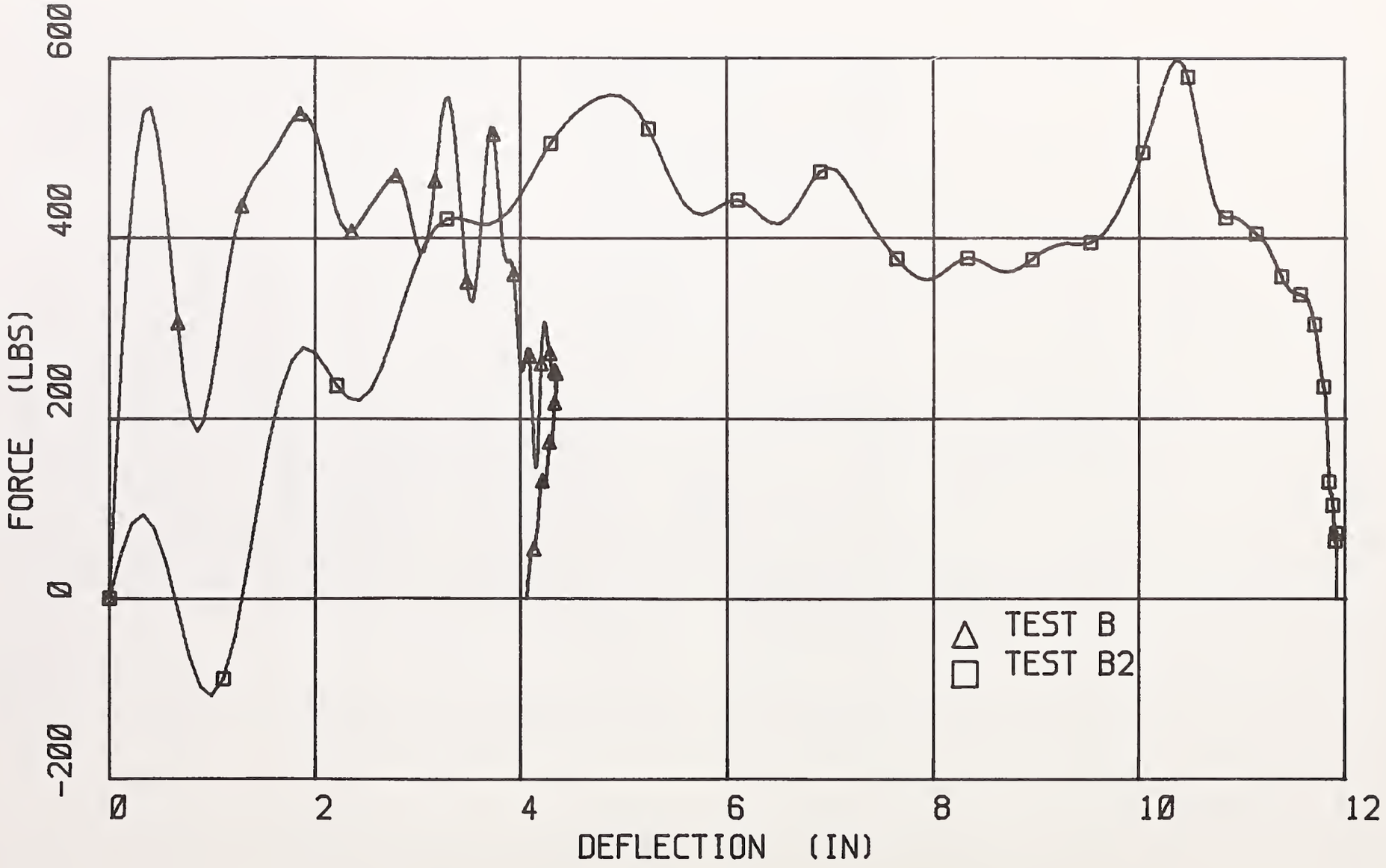

FIGURE 4-53. EFFECTS ON MULTIPLE IMPACTS

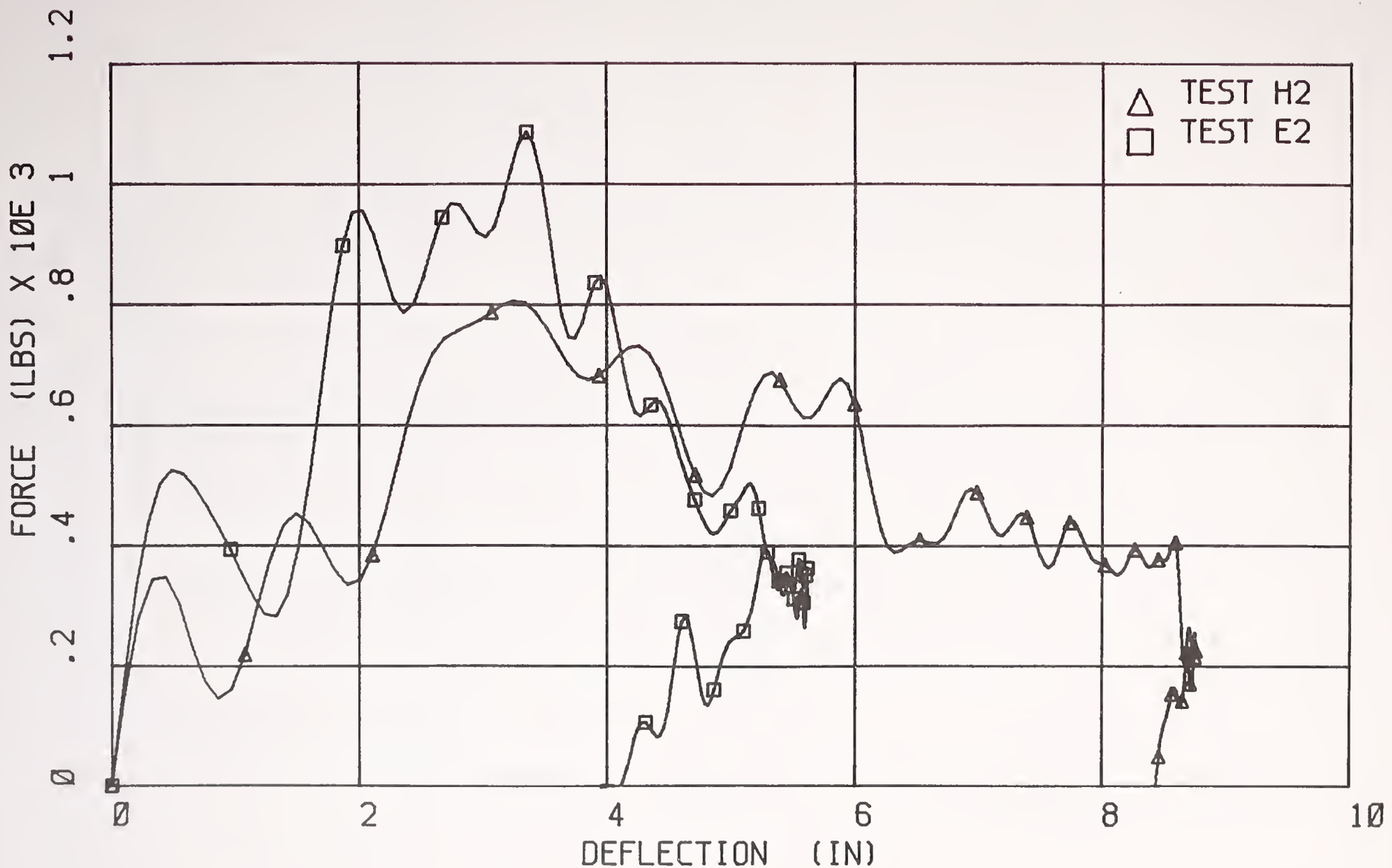

FIGURE 4-54. NORMAL TEST RESULTS FOR SECURIFLEX AND STANDARD WINDSHIELDS

windshield exhibits a different force-deflection pattern with an inertial spike that appears longer in duration (or deflection) followed by a steep rise to a higher force level that is more rapid and higher than is seen with standard windshields. Figure 4-55 which compares horizontal impact test results for the two types of windshields also shows the same trends. The Securiflex windshield's inertial spike is wider and is followed by a quick rise to a higher force level than is seen in the standard windshield test.

By comparing results from horizontal and normal tests, it is possible to obtain an estimate of friction and/or plowing effects experienced during windshield impacts. The approach used for this comparison is based on that developed by MCR Technology, Incorporated*, as is summarized in Figure 4-56. This procedure was carried out for the Securiflex windshield and for a standard windshield. Shown in Figure 4-57 are overplots of the normal and horizontal (at the same value of normal deflection) force-deflection characteristics for the two windshield types. Note that for the standard windshield, test B2, the repeat on a previously impacted windshield was used because the impact velocity for the test B was too low to provide a meaningful comparison. While it is clear that the initial portion of this test data is not representative of the behavior of previously unbroken glass, the penetration portion of the curve is believed to be appropriate for this evaluation of slowing effects at larger deformations.

Application of the MCR procedure to the data shown in Figure 4-57 yields the relationship between the friction coefficients and deflection. The relationships for the two windshield types are shown in Figure 4-58. As seen in this figure, it appears that the Securiflex windshield initially has a friction coefficient lower than that of the standard windshield. At higher values of penetration, however, the Securiflex windshield produces a considerably higher friction coefficient, and thus a higher tangential force, than does the standard windshield.

*Schwartz, R. and Forrest, S.M., "Design and Development of Modified Production Vehicle for Enhanced Crashworthiness and Fuel Economy - Phase II," Contact No. DTNH22-81-C-07085, March 1984.

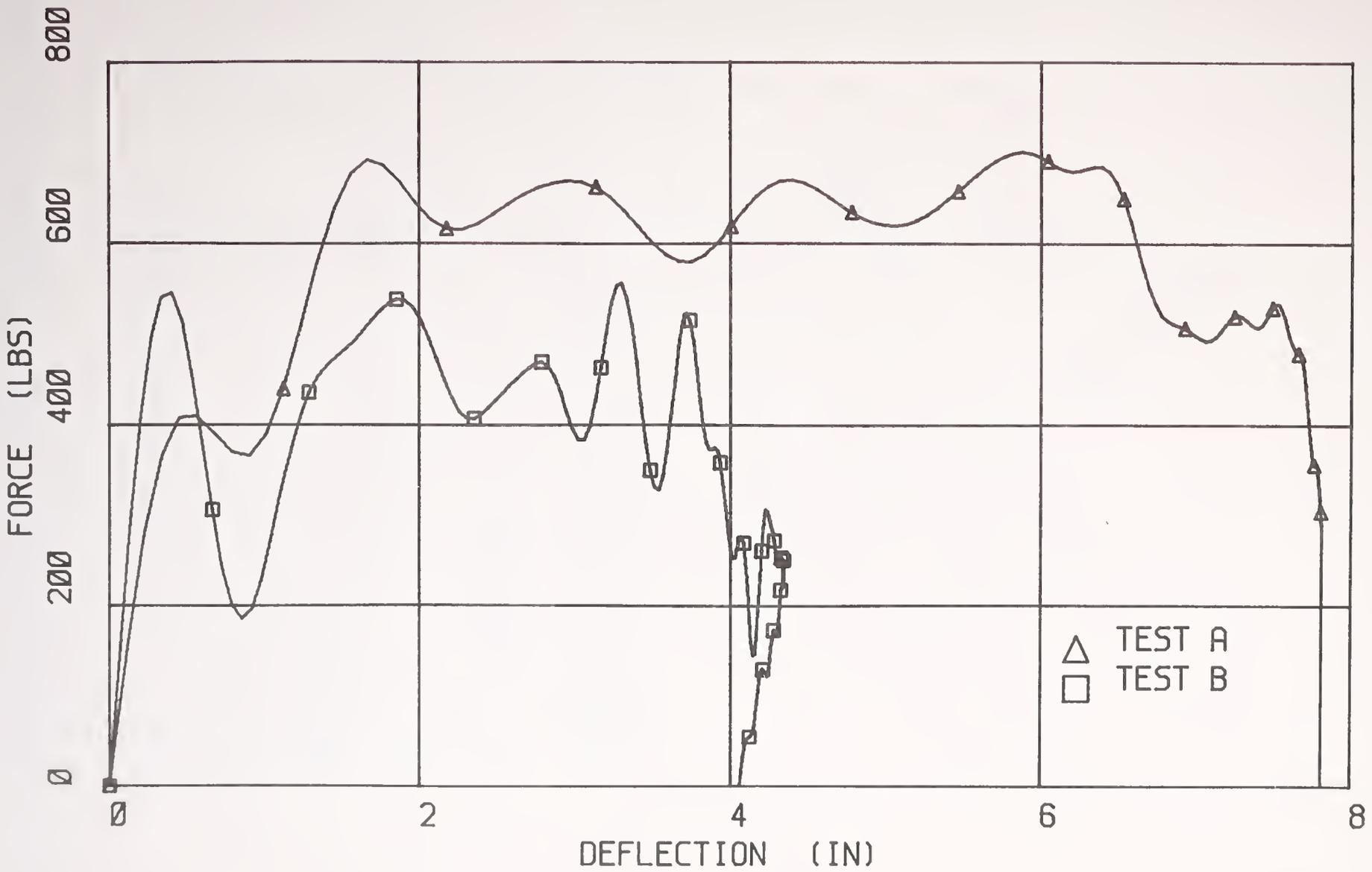

FIGURE 4-55. HORIZONTAL TEST RESULTS FOR SECURIFLEX AND STANDARD WINDSHIELDS

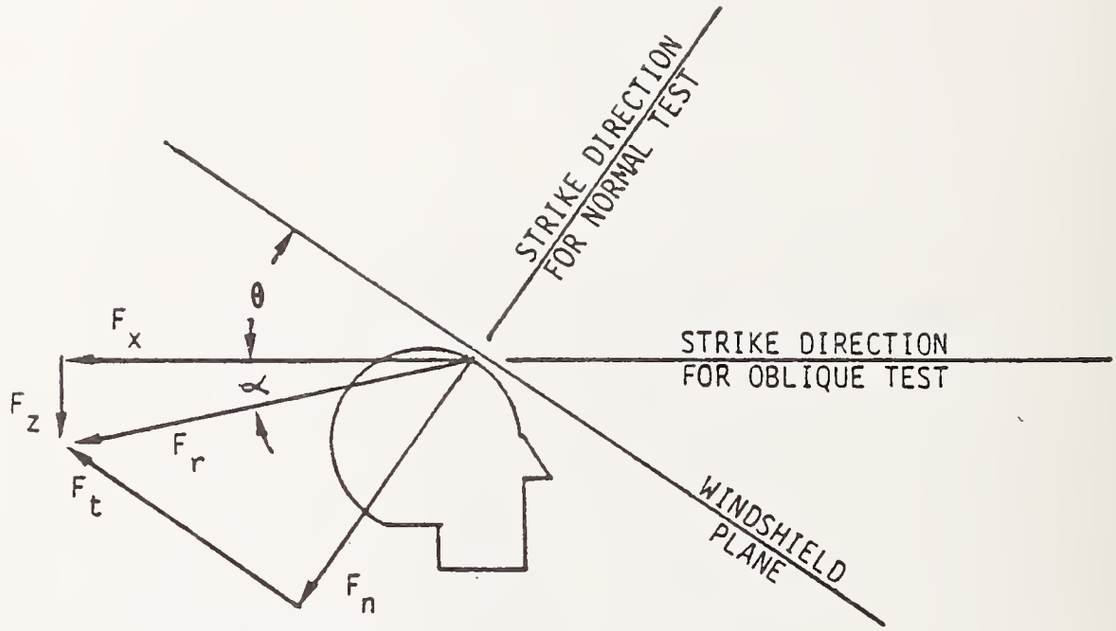

F_n = PENDULUM FORCE FROM NORMAL IMPACT TEST

F_x = PENDULUM FORCE FROM OBLIQUE IMPACT TEST (AT SAME VALUE OF NORMAL DEFLECTION AS F_n)

$$F_z = \left(\frac{F_n}{\sin\theta} - F_x\right) \tan\theta$$

$$\alpha = \tan^{-1} \frac{F_z}{F_x}$$

$$F_r = \sqrt{F_x^2 + F_z^2}$$

$$F_t = F_r \cos(\theta + \alpha)$$

$$\mu = \frac{F_t}{F_n}$$

FIGURE 4-56. COMPUTATION OF APPARENT FRICTION COEFFICIENT FROM RESULTS OF NORMAL AND OBLIQUE WINDSHIELD PENDULUM TESTS

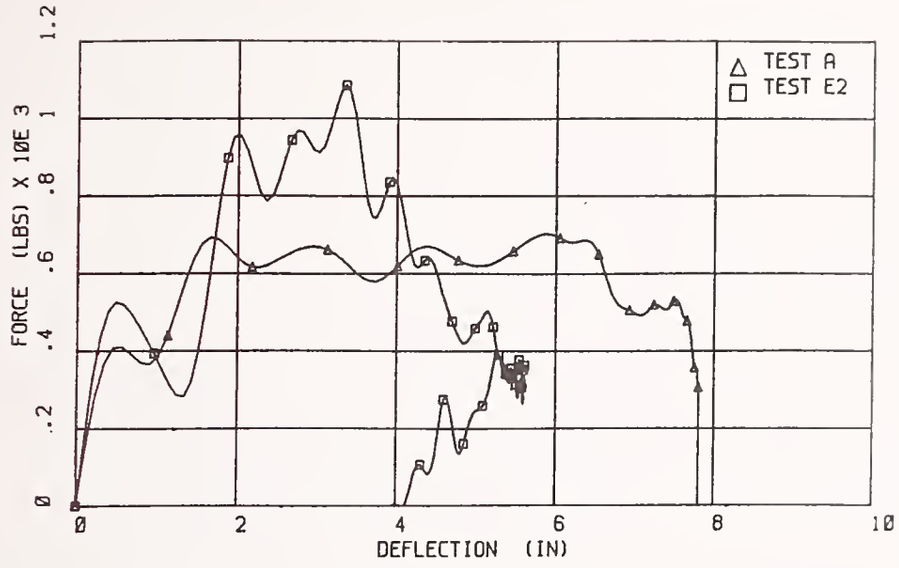

A) SECURIFLEX WINDSHIELD

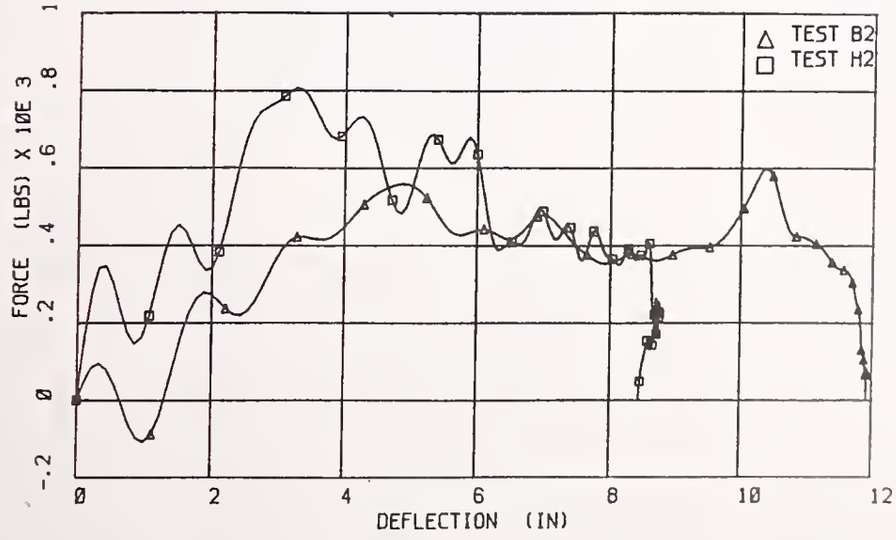

B) STANDARD WINDSHIELD

FIGURE 4-57. COMPARISON OF NORMALIZED HORIZONTAL AND NORMAL TEST RESULTS FOR STANDARD AND SECURIFLEX WINDSHIELDS

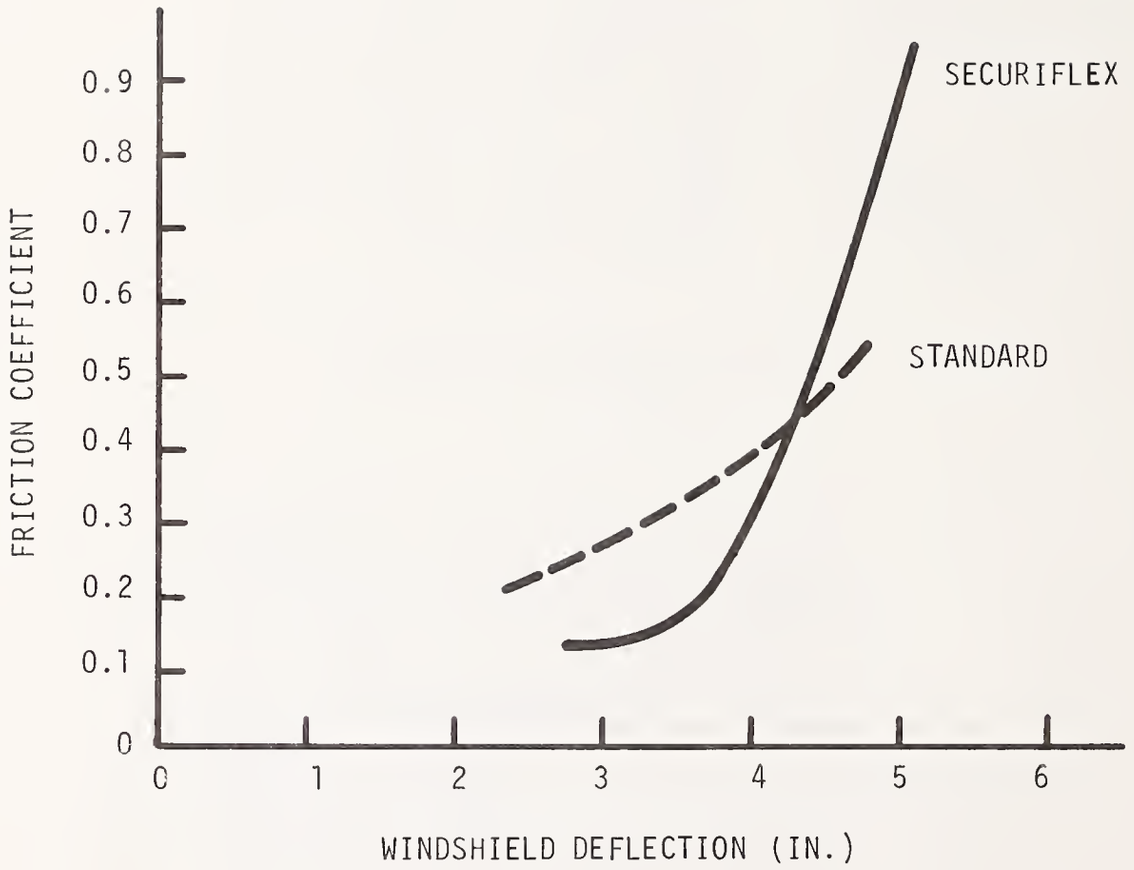

FIGURE 4-58. COMPARISON OF WINDSHIELD FRICTION COEFFICIENTS